Mechanisms of S-Nitrosation and S-Glutathiolation and Expression and Purification of Human Calbindin D_{28k}

Limei Tao

A Thesis

in

The Department

of

Chemistry and Biochemistry

Presented in Partial Fulfillment of the Requirements
for the Degree of Doctor of Philosophy at
Concordia University
Montreal, Quebec, Canada

April 12, 2004

Your file Votre référence
ISBN: 0-612-96941-X
Our file Notre référence
ISBN: 0-612-96941-X

Abstract

Mechanisms of S-Nitrosation and S-Glutathiolation and Expression and Purification of Human Calbindin D_{28k}

Limei Tao, Ph.D.

Concordia University, 2004

How nitric oxide (NO) reacts with free thiols to form S-nitrosothiols (RSNOs) *in vivo* is a question of much debate. The effects of different chelators and added metals ions on NO and O_2 consumption, and S-nitrosocysteine (CysNO) formation in cysteine solutions were studied using amperometric (NO and O_2 electrodes) measurements and UV-vis absorption. The results support a free radical mechanism for CysNO formation that involves $Cys^{\bullet}$ generation by reaction with $^{\bullet}NO_2$ at higher NO concentrations and with copper ions at lower NO concentrations.

The mechanism of recombinant human brain calbindin D_{28k} (rHCaBP) S-nitrosation by CysNO or S-nitrosoglutathione (GSNO) was investigated in detail. First, an efficient rHCaBP expression and purification system was set up by subcloning the HCaBP gene into the pET15b vector and expressing the protein in BL21(DE3)pLysS host cells. A protein yield of >30 mg/L culture with >95% purity was obtained. UV-vis and circular dichroism absorption, intrinsic fluorescence and mass spectrometry measurements indicate that rHCaBP is S-nitrosated by CysNO. Of a total of five free cysteine residues 2.6 ± 0.05 and 4.4 ± 0.09 are S-nitrosated in Ca^{2+}-loaded and Ca^{2+}-free rHCaBP, respectively, as determined by the Saville assay. Intrinsic protein fluorescence

was demonstrated to be a sensitive probe of protein S-nitrosation due to efficient Förster energy transfer ($R_0 \sim 17$ Å) between tryptophan donors and RSNO acceptors.

Mass spectrometry and UV–vis absorption results support a mechanism for NO transfer from GSNO to rHCaBP that requires trace copper added as either Cu,Zn-superoxide dismutase (CuZnSOD) or $CuSO_4$. CuZnSOD is an efficient catalyst of rHCaBP S-nitrosation *via* a mechanism involving reduction of its active-site Cu^{II} by a number of the thiols in rHCaBP, giving rise to $Cys^{\bullet}$ radicals. The $Cu^{I}ZnSOD$ formed catalyzes the reductive cleavage of GSNO to release NO, which reacts with the $Cys^{\bullet}$ radical to yield the S-nitrosoprotein.

Since exposure of rHCaBP to either CysNO or GSNO also leads to rapid S-thiolation, the mechanism of protein S-glutathiolation was investigated in detail. rHCaBP, human CuZnSOD (HCuZnSOD), rabbit muscle glyceraldehyde-3-phosphate dehydrogenase (GAPDH), and bovine serum albumin (BSA) were found to be S-glutathiolated in decomposed GSNO solutions. Fresh GSNO, reduced glutathione (GSH) or oxidized glutathione (GSSG) are not efficient S-glutathiolating agents for the proteins examined here. Based on analysis by mass spectrometry and UV-vis absorption, GSNO decomposition in the dark at room temperature yields glutathione disulfide S-oxide [GS(O)SG], glutathione disulfide S-dioxide (GSO_2SG), and GSSG as products. A hydrolysis pathway yielding GSOH and nitroxyl HNO/NO^- as intermediates is proposed based on inhibition of GSNO breakdown by dimedone, and nitroxyl scavenging by metmyoglobin. Cys111, Cys187, Cys149 and Cys34 were tentatively identified as the S-glutathiolation sites in HCuZnSOD, rHCaBP, GAPDH and BSA, respectively.

Acknowledgements

First and foremost, I would like to thank my research supervisor Dr. English for her guidance, encouragement and support during my PhD program. I truly admire her insight and dedication to research. I enjoyed working in her lab very much.

I thank the members of my committee, Professors Justin Powlowski and Peter Bird for their help and patience during my three and a half years at Concordia.

I would like to thank the fantastic people in my lab, including Farida Mohamed, He Jiang, Mengwei Ye, Biao Shen, Dominic Cuerrier, Lekha Sleno and Mihai Ciortea. Special thanks to David Yong-Hoi Yeung for helping me get through the laborious task of protein expression and purification and for making the work enjoyable. I would particularly like to thank Jacqueline Montalibet who taught me valuable molecular biology "tricks". I would like to especially thank my friend and colleague Georgia Kremmydiotis, who led me to believe that everybody was born equal. Gratitude is also extended to June Man who made the first two years of my PhD study very enjoyable.

I am so grateful to my Mom, Dad and brother for all the love and support they have given me over the years. Without their blessing I could not have gone this far. Finally, I would like to thank my husband for his love and insight. I could not have done this without him.

Dedications

To my mother and father,

Chunling Lu and Shixiang Tao

For their love and support;

To my daughter,

Dongwen Wang

For giving me the greatest pleasure in life;

To my husband,

Xiaogang Wang

For the bright, simple and stable life we share

Table of Contents

List of Figures

List of Tables

List of Abbreviations

ACTH	adrenocorticotropic hormone
AMP	ampicillin
ANS	8-anilinonaphthalenesulfonic acid
*apo*rHCaBP	Ca^{2+}-free rHCaBP
BF4NO	nitrosonium tetrafluoroborate
BSA	bovine serum albumin
CaBP	calbindin D_{28k}
$Ca(OAc)_2$	calcium acetate
CD	circular dichroism
CuZnSOD	copper,zinc-superoxide dismutase
CysNO	S-nitrosocysteine
Dimedone	5,5-dimethyl-1,3-cyclohexanedione
DTNB	5,5'-dithiolbis(2-nitrobenzoic acid)
DTT	DL-dithiothreitol
DTPA	diethylenetriamine-N,N,N',N'',N''-pentaacetic acid
EDTA	ethylenediaminetetraacetic acid
EGTA	ethylene glycol bis(aminoethyl ether)-N,N,N',N'-tetraacetic acid
ESI-MS	electrospray ionization mass spectrometry
G25	G-type of dextran gel (Sephadex)
GAPDH	glyceraldehyde-3-phosphate dehydrogenase
GSH	glutathione; glycine N-(N-L-γ-glutamyl-L-cysteinyl)

GSNO	S-nitrosoglutathione; glycine N-(N-L--γ-glutamyl-S-nitroso-L-cysteinyl)
GSOH	glutathionesulfenic acid
GS(O)SG	glutathione disulfide S-oxide; glutathione thiosulfinate
GSO_2SG	glutathione disulfide S-dioxide; glutathione thiosulfonate
GSSG	glutathione disulfide; glycine N-(N-L--γ-glutamyl-L-cysteinyl) disulfide
HCaBP	human brain calbindin D28k
HCuZnSOD	human Cu,Zn-superoxide dismutase
*holo*rHCaBP	Ca^{2+}-loaded rHCaBP
ICP-MS	inductively coupled plasma mass spectrometry
IPTG	isopropyl β-D-thiogalactoside
MALDI	matrix-assisted laser desorption ionization
Mb	myoglobin
MCS	multi-cloning site
MES	2-(N-morpholino) ethanesulphonic acid
MS	mass spectrometry
NEM	N-ethylmaleimide
Neocuproine	2,9-dimethyl-1,10-phenanthroline
Ni-NTA	nickel-nitrilotriacetic acid
NO	nitric oxide
NOS	NO synthase
NTA	nitrilotriacetic acid

ODNB	5-(octyldithio)-2-nitrobenzoic acid
o-phen	1,10-phenanthroline
PAGE	polyacrylamide gel electrophoresis
PCR	polymerase chain reaction
QTOF	quadrupole time-of-flight
rHCaBP	recombinant human brain calbindin D_{28k}
RSNO	S-nitrosothiol
SDS	sodium dodecyl sulfate
TFA	trifluoroacetic acid
TNB^{2-}	5-thio-2-thiobenzoate anion

1.0 Introduction

1.1 Nitric oxide (NO)

NO is a reactive diatomic radical that is biosynthesized from L-arginine (Figure 1.1) by NO synthases (NOSs) (*1*). Three forms of NOS have been identified: endothelial NOS (eNOS) which generates NO in the endothelial lining of blood vessels, neuronal NOS (nNOS) which is present in neurons in the brain and generates NO to act as a neurotransmitter, and inducible NOS (iNOS) expressed in macrophages as a response to bacterial and viral infections. The activity of both nNOS and eNOS are Ca^{2+}/calmodulin-dependent, while iNOS activity is Ca^{2+}/calmodulin-independent (*2*).

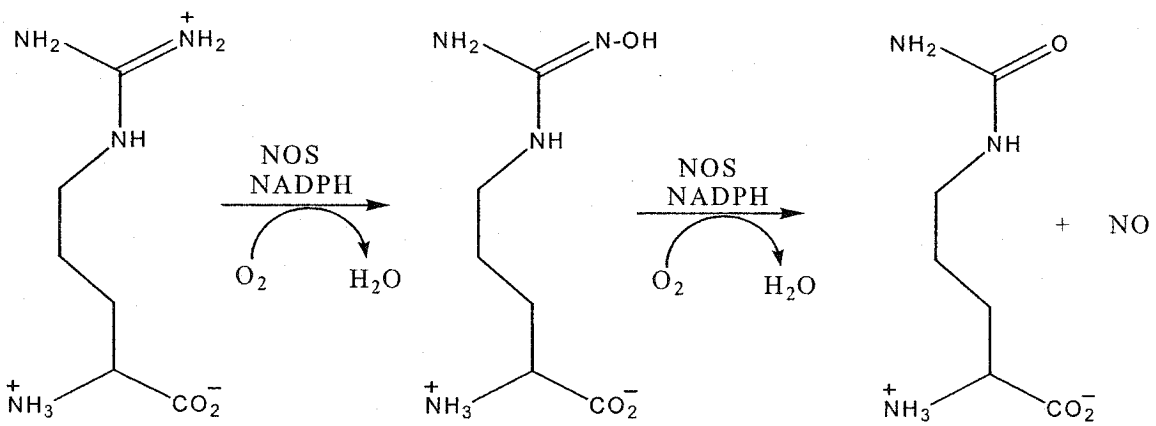

Figure 1.1. **The biosynthesis of NO**

NO has been definitively identified within endothelial cells as an endothelial-derived relaxing factor (EDRF), which is necessary for smooth muscle relaxation and the resulting vasodilation (*3*). A wide range of other functions of NO in bioregulation include roles in neurotransmission, inflammation, immunity, and programmed cell death (*4*). In

addition, NO has been implicated in neurodegenerative diseases such as AIDS dementia, and Huntington's and Parkinson's diseases (*5*).

NO is about 70 times more soluble in hydrophobic solvents than in aqueous solution (*6*). This feature allows NO to easily diffuse among cellular compartments and transmit information to its targets. However, NO has been proven to be very reactive; it reacts with other reactive oxygen species, metals, as well as with cysteine and tyrosine residues in proteins (*2*). It is now widely accepted that once NO is generated, it is short-lived with a half-life of only 0.05-1 s in blood (*7, 8*) and diffuses only a short distance. The hypothesis that NO is stabilized by a carrier molecule that prolongs its half-life and preserves its biological activity has been proposed (*9*) and demonstrated (*10*). The current belief (*11*) is that NO is transported in the body as S-nitrosothiols (RSNOs), from which NO can be released under certain conditions. RSNO species are generally much more stable than NO in solution (*12*).

1.2 RSNOs

RSNOs have been found to exhibit much the same physiological properties as NO itself (*2*), particularly in vasodilation (*13*) and in their antiplatelet properties (*14*). The RSNOs identified *in vivo* include S-nitrosoglutathione (GSNO) (*15*), S-nitrosocysteine (CysNO) (*11*) and S-nitrosoalbumin (*8*). Although RSNOs continue to receive much attention as intermediates in the transport, storage, and delivery of NO, as post-translational protein modifications in cell signalling and inflammatory processes, and as biochemical markers of reactive nitrogen oxides species (RNOS), the mechanism of RSNO formation *in vivo* is not clearly understood (*16*).

1.2.1 S-nitrosation (NO + RSH ⇌ RSNO)

It is generally accepted that the NO radical does not directly react with a thiol to yield RSNO (*17, 18*). The mechanism of RSNO formation from NO *in vivo* is a question of much debate (*16, 19, 20*). Proposed pathways include the reaction of thiols with NO in the presence of an electron acceptor such as NAD^+ (*20*), the autoxidation of NO to higher oxides of nitrogen (NO_x) which are effective S-nitrosating species, metal-catalyzed S-nitrosation (*21, 22*), and the reaction of dinitrosyl-iron complexes with thiols (*23*) (see Section 2.2). So far no enzyme has been conclusively identified as being involved in RSNOs formation *in vivo*.

1.2.2 *Trans*-S-nitrosation (RSNO + R'SH ⇌ R'SNO + RSH)

In a *trans*-S-nitrosation reaction the NO group is transferred from a RSNO to a different thiol (R'SH) thus generating another R'SNO (*2*). *Trans*-S-nitrosation has been suggested to be a mechanism of signal transduction in cells (*24*), but the mechanism of NO donation from RSNO to R'SH has received little attention. It was reported that in the presence of a chelator such as DTPA, *trans*-S-nitrosation follows reversible second-order kinetics with rate constants of 1–100 $M^{-1}s^{-1}$ and equilibrium constants close to unity (*25*). It is proposed that NO transfer occurs by nucleophillic attack of the thiolate anion on the nitrogen of the RSNO, and that no intermediate is involved (*2*). But recently Houk and coworkers (*26*) But recently Houk and coworkers explored computationally a novel anionic RSN(O)SR species (eq 1.1), the intermediate in transnitrosation reactions (*26*). Results from our lab are not consistent with such a mechanism. For example (*27*), we

have shown that S-nitrosation of thiols in hemoglobin by GSNO requires the presence of redox-active copper (see Section 5.2).

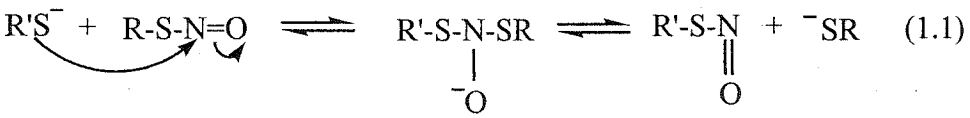

(1.1)

1.2.3 S-glutathiolation (GSX + R'SH ⇌ R'SSG + XH)

In many instances where *trans*-S-nitrosation has been described, the protein cysteines involved are also oxidized, and tend to form disulfides (*12, 28*) and nitroxyl (HNO) as primary products (*29*). Since the most abundant thiol in the cytoplasm is glutathione, it was assumed that S-nitrosation by GSNO is likely to promote S-glutathiolation, the incorporation of glutathione into proteins *via* mixed disulfide bond formation. S-glutathiolation is increasingly recognized as an important post-translational modification, and as an intracellular response to oxidative stress (*30, 31*). How GSNO, or some GSNO-derived species (GSX), triggers protein S-glutathiolation is far from understood, and explored here in Chapter 6.

1.3 Calbindin D_{28K} (CaBP)

Calbindin D_{28K} was first described in 1966 by Wasserman and Taylor. The protein was initially termed CaBP (used in this thesis) for calcium-binding protein. In 1985 it was renamed calbindin D_{28k} in reference to its calcium-binding properties, its vitamin D dependence, and its molecular size of 28 kDa (*32*).

CaBP has been found in diverse species including fish, amphibians, reptiles, birds, rats, and humans. It has been localized in a variety of tissues including the intestine, kidney and bone, and also in tissues which are not regulators of serum calcium such as

brain, placenta and pancreas (*32*). Since CaBP was found to be present in fish brain but not in fish kidney or intestine, it was suggested that CaBP evolved originally as a neuronal protein and that its presence in other tissues (kidney and intestine) occurred only with the development of higher species (*33*). CaBP is noted for its abundance and specific distribution in mammalian brain and sensory neurons (*34*). It constitutes as much as 0.1-1.5% of the total soluble protein in brain and in some cells it may be present at intracellular concentrations of up to 2 mM (*35*). Mammalian brain CaBP is no longer considered to be regulated by vitamin D in adults (*36*).

CaBP belongs to a family of intracellular proteins that have high affinities for calcium. Members of this family include calmodulin, parvalbumin, troponin C and the S 100 proteins (*33*). A common structural feature of all these proteins is the presence of an octahedral calcium binding structure formed by a helix-loop-helix conformation of the polypeptide chain termed an EF hand (*33*) (Figure 1.2). CaBP contains 6 EF hands and 4 of them bind Ca^{2+} with high affinity (*37*). The three-dimensional structure of CaBP is unknown.

CaBPs have ~261 residues and are highly conserved throughout their sequence. Mammalian CaBPs are about 98% homologous and 79% homologous to chicken CaBP (*33*) (Figure 1.3). It is widely accepted that a protein's evolutionary rate is inversely related to its functional significance. CaBP has an evolutionary rate which is similar to that of cytochrome c (0.3×10^{-9} amino acid^{-1} year^{-1}), a functionally important protein (*38*).

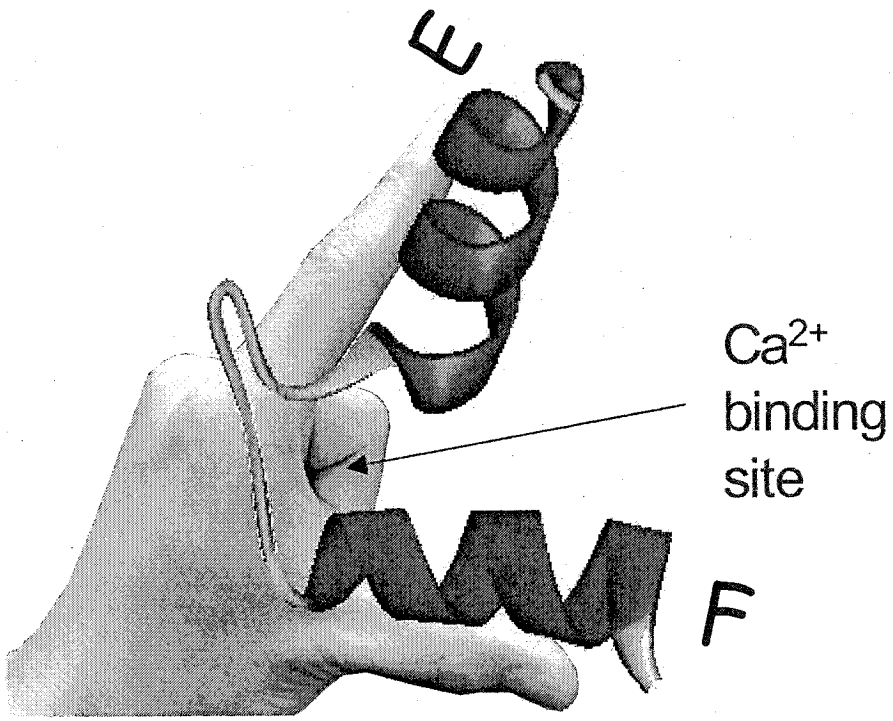

Figure 1.2. **EF-hand motif (helix-loop-helix).** Diagram provided by David Yong-Hoi Yeung, Concordia University.

Table 1.1. **Sequence comparison of human, bovine, rat, mouse and chick CaBPs.** The EF hand domains are the middle blocks of 28-29 residues. The GenBank accession numbers for human, bovine, rat mouse and chick CaBP are NP_004920, P04467, AAA40852, NP_033918 and KLCHI, respectively.

Domain				
1	Human	1 MAESHLQSSLITASQ	FFEIWLHFDADGSGYLEGKELQNLIQEL	QQARKKA 50
	Bovine	1 AESHLQSSLITASQ	FFEIWLHFDADGSGYLEGKELQNLIQEL	QQARKKA 49
	Rat	1 MAESHLQSSLITASQ	FFEIWLHFDADGSGYLEGKELQNLIQEL	LQARKKA 50
	Mouse	1 MAESHLQSSLITASQ	FFEIWLHFDADGSGYLEGKELQNLIQEL	LQARKKA 50
	Chick	1 MTAETHLQGVEISAAQ	FFEIWHHYDSDGNGYMDGKELQNFIQEL	QQARKKA 51
2	Human	51 GLELSP	EMKTFVDQYGQRDDGKIGIVELAHVLPTE	ENFLLLF 92
	Bovine	50 GLELSP	EMKTFVDQYGERDDGKIGIVELAHVLPTE	ENFLLLF 91
	Rat	51 GLELSP	EMKTFVDQYGQRDDGKIGIVELAHVLPTE	ENFLLLF 92
	Mouse	51 GLELSP	EMKSFVDQYGQRDDGKIGIVELAHVLPTE	ENFLLLF 92
	Chick	52 GLDLTP	EMKAFVDQYGKATDGKIGIVELAQVLPTE	ENFLLFF 93
3	Human	93 RCQQLKSCEE	FMKTWRKYDTDHSGFIETEELKNFLKDL	LEKANKT 137
	Bovine	92 RCQQLKSCEE	FMKTWRKYDTDHSGFIETEELKNFLKDL	LEKANKT 136
	Rat	93 RCQQLKSCEE	FMKTWRKYDTDHSGFIETEELKNFLKDL	LEKANKT 137
	Mouse	93 RCQQLKSCEE	FMKTWRKYDTDHSGFIETEELKNFLKDL	LEKANKT 137
	Chick	94 RCQQLKSSED	FMQTWRKYDSDHSGFIDSEELKSFLKDL	LQKANKQ 138
4	Human	138 VDDTKLAEY	TDLMLKLFDSNNDGKLELTEMARLLPVQ	ENFLLKF 181
	Bovine	137 VDDTKLAEY	TDLMLKLFDSNNDGKLELTEMARLLPVQ	ENFLLKF 180
	Rat	138 VHDTKLAEY	TDLMLKLFDSNNDGKLELTEMARLLPVQ	ENFLLKF 181
	Mouse	138 VDDTKLAEY	TDLMLKLFDSNNDGKLELTEMARLLPVQ	ENFLLKF 181
	Chick	139 IEDSKLTEY	TEIMLRMFDANNDGKLELTELARLLPVQ	ENFLIKF 182
5	Human	182 QGIKMCGKE	FNKAFELYDQDGNGYIDENELDALLKDL	CEKNKQD 225
	Bovine	181 QGVKMCGKE	FNKAFELYDQDGDGYIDENELDALLKDL	CEKNKQD 224
	Rat	182 QGIKMCGKE	FNKAFELYDQDGNGYIDENELDALLKDL	CEKNKQE 225
	Mouse	182 QGIKMCGKE	FNKAFELYDQDGNGYIDENELDALLKDL	CEKNKQE 225
	Chick	183 QGVKMCAKE	FNKAFEMYDQDGNGYIDENELDALLKDL	CEKNKKE 226
6	Human	226 LDINNI	TTYKKNIMALSDGGKLYRTDLALILCAG	DN 261
	Bovine	225 LDINNI	PTYKKSIMALSDGGKLYRTDLALILSAG	DN 260
	Rat	226 LDINNI	STYKKNIMALSDGGKLYRTDLALILSAG	DN 261
	Mouse	226 LDINNI	TTYKKNIMALSDGGKLYRTDLALILSAG	DN 261
	Chick	227 LDINNL	ATYKKSIMALSDGGKLYRAELALILCAE	EN 262

Its high abundance, conservation and low evolution rate indicate that CaBP plays an important physiological role or roles. It is reported that neurodegenerative diseases such as Alzheimer's and Parkinson's are linked to deficiencies in CaBP, which exhibits diminished expression with age (*39*). Human CaBP (HCaBP) seems to be also linked to epilepsy, amyotrophic lateral sclerosis and Huntington's disease (*40-42*).

The exact physiological function of CaBP is unknown. There is evidence that CaBP has a Ca^{2+}-buffering function in neurons thereby maintaining intracellular Ca^{2+} homeostasis and preventing cell death (*43, 44*). The structure of a Ca^{2+}-buffering protein is expected to be insensitive to Ca^{2+}-binding, but spectroscopic investigations and *in vitro* studies using antibodies have shown that CaBP undergoes a conformational shift upon Ca^{2+}-binding (*45, 46*). Thus, in this aspect CaBP behaves more like a Ca^{2+}-sensor protein such as calmodulin than a Ca^{2+}-buffer such as parvalbumin. Very recently, Linse and coworkers provided evidence that CaBP does have properties characteristic of a Ca^{2+}-sensor (*47*). These findings are important since they suggest that CaBP may have an as yet unidentified function in interacting with and regulating the activity of specific proteins in a calcium-dependent manner. Indeed it has been reported that chick intestinal CaBP interacts with chick intestinal alkaline phosphatase (*48*), rat renal CaBP activates Ca,Mg-ATPase *in vitro* (*49*), rat CaBP inhibits caspase-2 activity in osteoblastic cells (*50*), and interacts with Ran-binding protein M (*51*), and HCaBP activates *myo*-inositol monophosphatase (*35*).

1.4 Possible relationships between CaBP and NO biochemistry

Since HCaBP is especially abundant in the brain and it possesses five free cysteine residues, it contributes significantly to the intracellular thiol concentration. Very interestingly, using a novel proteomics approach, CaBP was identified to be one of the proteins S-nitrosated when rat brain tissue was treated with GSNO (*52*). Moreover, CaBP is found coexistent with NO synthase in the cerebellum (*53*) and hypothalamus (*54*). Also, intercellular Ca^{2+} waves in rat hippocampal slices and dissociated glial-neuron cultures are mediated by NO (*55*). Ca^{2+}-regulated protein S-nitrosation and denitrosation has been demonstrated for tissue transglutaminase (*56*). Therefore, a study of CaBP S-nitrosation would not only provide a good model system to probe mechanisms of protein S-nitrosation, but it also may shed light on the function of CaBP.

1.5 Cu,Zn-superoxide dismutase (CuZnSOD)

SOD is an essential component of the antioxidant defense of aerobic organisms. The primary function of CuZnSOD *in vivo* is proposed to be the efficient catalysis of superoxide ($O_2^{-\bullet}$) dismutation (*57*). The mechanism involves reactions 1.1 and 1.2.

$$Cu^{II}ZnSOD + O_2^{-\bullet} \rightarrow Cu^{I}ZnSOD + O_2 \qquad (1.1)$$

$$Cu^{I}ZnSOD + O_2^{-\bullet} + 2H^{+} \rightarrow Cu^{II}ZnSOD + H_2O_2 \qquad (1.2)$$

CuZnSOD is a homodimer with molecular weight of ~32 kDa. Each monomer hosts an active site where one Cu(II) ion and one Zn(II) ion are bound. The catalytic center is the copper ion, which is coordinated in the Cu(II) form by four histidine residues and by a weakly bound water molecule. The equilibrium constants for dissociation of copper from the copper site (6.0×10^{-18}) and of zinc from the zinc-binding site (4.2×10^{-14}) were determined at pH 7.4 by equilibrium dialysis for human CuZnSOD (*58*).

The intracellular concentration of CuZnSOD has been reported to be 10 μM in yeast cells, 10-30 μM in erythrocytes and hepatocytes, and exceptionally high in motor neurons (*59*). CuZnSOD is one of the major cuproenzymes found in mammals (*60*). CuZnSOD is becoming recognized as an important player in NO biochemistry not only because it scavenges $O_2^{-\bullet}$, which will react at the diffusion limit with NO to form peroxynitrite (*61*), but also because it has been reported that CuZnSOD mediates NO release from RSNOs (*59, 60*), and catalyzes the interconversion of NO and nitroxyl anion (*62*).

1.6 Hypotheses, scope and organization of this thesis

The objectives of the research conducted for this thesis were to study the mechanism of RSNO formation with emphasis on the role of copper in S-nitrosation. Cysteine and HCaBP were chosen as model reagents to carry out this work. Cysteine was chosen because it is the smallest free thiol in biological systems and CysNO has been identified *in vivo*. The effects of different metal chelators and added metals ions on NO and O_2 consumption, as well as CysNO formation in cysteine solutions were studied using amperometric (NO and O_2 electrodes) measurements and UV-vis absorption (Chapter 2). This study sheds light on the mechanisms of RSNO formation from reactions involving NO and RSH.

As discussed above, HCaBP was chosen because it possesses five free cysteine residues and because of its abundance in human brain. CaBP is considered to be a functionally important protein, but its exact function is unknown. Thus, exploring the mechanism of HCaBP S-nitrosation by low-molecular weight RSNOs will contribute to

our understanding of *trans*-S-nitrosation reactions (RSNO + R'SH ⇌ R'SNO + RSH) and perhaps provide more information on CaBP function. Previous results from our lab (*63*) have shown that S-nitrosation of hemoglobin by GSNO requires the presence of redox-active copper (eqs 5.1 and 5.2). Since essentially no free copper exists *in vivo*, the focus of the present work was to investigate if HCaBP S-nitrosation is catalyzed by protein-bound copper.

To carry out the HCaBP S-nitrosation study, a highly efficient HCaBP expression and purification system was set up (Chapter 3). Several techniques for the detection of S-nitrosated HCaBP were evaluated, including UV-vis and circular dichroism absorption, intrinsic fluorescence and mass spectrometry measurements, as well as the Saville assay for RSNO quantification. The number of cysteine residues S-nitrosated in Ca^{2+}-loaded and Ca^{2+}-free HCaBP was compared (Chapter 4). HCaBP S-nitrosation was carried out in the presence and absence of CuZnSOD, an abundant copper protein *in vivo*. Mass spectrometric measurements were used to probe S-NO formation in the protein. UV-vis absorption was used to detect scavenging by myoglobin of NO released from GSNO, and to detect the redox state of copper in the active site of CuZnSOD (Chapter 5). From the combined data, a mechanism for protein S-nitrosation is proposed.

HCaBP S-thiolation was observed while performing the experiments on S-nitrosation described in Chapters 4 and 5. Initially, we assumed that GSNO was directly involved as suggested in the literature (*64*). The mechanism of HCaBP S-glutathiolation in GSNO solutions under different reaction conditions was investigated. Since a GSNO decomposition product, GS(O)SG, was found to S-glutathiolate proteins, the pathway of

GSNO decomposition to GS(O)SG was investigated by mass spectrometry and UV-vis absorption (Chapter 6).

1.7 Contributions of colleagues

Chapters 4, 5 and 6 are published manuscripts. Chapters 2 and 3 are currently being prepared for publication. All abbreviations, citations, figures and table numbering systems in the published works were changed to the format of this thesis.

Chapter 4 was published in *Biochemistry* [Tao L., Murphy M. E. P. and English A. M. (2002), *Biochemistry* 41, 6185-6192] and is reproduced with the permission of the journal. I carried out all the work reported in this publication and prepared the manuscript. Both A. English and M. Murphy provided intellectual support and A. English edited the manuscript.

Chapter 5 was published in *Biochemistry* [Tao L. and English A. M. (2003), *Biochemistry* 42, 3326-3334] and is reproduced with the permission of the journal. I carried out all the work reported in this publication and prepared the manuscript. A. English provided intellectual support and edited the manuscript.

Chapter 6 was also published in *Biochemistry* [Tao L. and English A. M. (2004), *Biochemistry* 43, 4028-4038] and is reproduced with the permission of the journal. I carried out all the work reported in this publication and prepared the manuscript. A. English provided intellectual support and edited the manuscript.

Chapter 2 is currently being prepared for publication in *Journal of Biological Chemistry*. I carried out all the experimental work.

Chapter 3 is currently being prepared for publication in *Protein Expression and Purification.* A portion of the experimental work described in Chapter 3 was performed in collaboration with David Yong-Hoi Yeung and Adamo Petosa since both of these students are working on HCaBP in our lab.

2.0 Effects of metal ions on NO and O_2 consumption in cysteine solutions: Implications for mechanism of S-nitrosocysteine formation *in vivo*

2.1 Abstract

The effects of different metal chelators and added metals ions on NO and O_2 consumption, as well as S-nitrosocysteine (CysNO) formation in cysteine solutions were studied using amperometric (NO and O_2 electrodes) measurements and UV-vis absorption. Low concentrations of NO (0.4 – 60 μM), compatible with the detection limits of the techniques employed, were used since physiological concentrations of NO are low (0.1-1.0 μM). The results support a free-radical mechanism (*16*) for CysNO formation that involves $Cys^{\bullet}$ generation by reaction of cysteine with $^{\bullet}NO_2$ at higher NO concentrations (>15 μM) and with copper ions at lower NO concentrations (<1 μM). Since CysNO formation *via* $^{\bullet}NO_2$ consumes 3 molecules of NO, it is proposed that a copper-catalyzed pathway involving protein-bound copper occurs *in vivo*.

2.2 Introduction

In vivo, CysNO is found to be a critical neuroprotective molecule (*65*). However, *in vitro* CysNO is one of the most unstable S-nitrosothiols. In the dark and in the absence of metal ions, its half-life is 9 h at 37°C (*66, 67*). CysNO can be synthesized quantitatively by combining equimolar *L*-cysteine and sodium nitrite in 1 M HCl *in vitro*.

The mechanism of S-nitrosothiol formation *in vivo* is a question of much debate (*16, 19, 20*). It has been shown previously that the reaction of NO with sulfhydryl groups under anaerobic conditions at neutral pH does not produce *S*-nitrosothiols (*17, 18*). This has led to the conclusion that *S*-nitrosothiols are formed following the autoxidation of NO to higher oxides of nitrogen (NO_x) (a second-order reaction with respect to NO, eqs 2.1-2.3), by metal catalysis (*21, 22*), or by the action of dinitrosyl-iron complexes (eq 2.4)(*23*).

$$2\ NO^{\bullet} + O_2 \rightleftharpoons 2\ {}^{\bullet}NO_2 \qquad (2.1)$$

$${}^{\bullet}NO_2 + NO^{\bullet} \rightarrow N_2O_3 \qquad (2.2)$$

$$RSH + N_2O_3 \rightarrow RSNO + NO_2^- + H^+ \qquad (2.3)$$

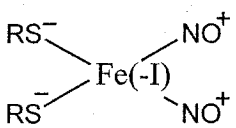

$$+\ R'SH \longrightarrow R'SNO + \text{decomposition products} \qquad (2.4)$$

However, the reaction of NO and oxygen is slow (eq 2.1), ~3-300 pM/s, at physiological concentrations of NO (0.1-1.0 μM), and the availability *in vivo* of free redox-active metals is unlikely (*68, 69*). Although reactions involving dinitrosyl-iron complexes represent a possible mechanism for the formation of *S*-nitrosothiols, the mechanism under physiological conditions remains unclear (*61*).

Gow and coworkers (*20*) proposed a novel mechanism for *S*-nitrosothiol formation that could operate at physiological concentrations of NO. In this mechanism NO reacts directly with a thiol (RSH) to produce a radical intermediate, RSNOH (eq 2.5). In the presence of an electron acceptor, such as oxygen, the intermediate is converted to a *S*-nitrosothiol and superoxide is formed (eq 2.6), which will react at the diffusion limit with NO to form peroxynitrite (*61*) (eq 2.7). The overall reaction of RSNO formation in

aerobic solutions at NO concentrations (< 50 μM) proposed by Gow *et al.* is given by eq 2.8 below.

$$RSH + NO^{\bullet} \rightleftharpoons RS{-}^{\bullet}N{-}O{-}H \qquad (2.5)$$

$$RS{-}^{\bullet}N{-}O{-}H + O_2 \rightarrow RS{-}N{=}O + O_2^{-\bullet} + H^+ \qquad (2.6)$$

$$O_2^{-\bullet} + NO^{\bullet} \rightarrow ONOO^- \rightarrow NO_3^- \qquad (2.7)$$

$$RSH + 2NO^{\bullet} + O_2 \rightarrow RS{-}N{=}O + ONOO^- + H^+ \qquad (2.8)$$

More recently Feelisch and coworkers proposed that RSNOs may be formed *via* intermediate one-electron oxidation of thiols mediated by the nitrogen dioxide radical ($^{\bullet}NO_2$), and the subsequent reaction of thiyl radicals with $NO^{\bullet}$ (eqs 2.1, 2.9 and 2.10) (*16*).

$$2\,NO^{\bullet} + O_2 \rightleftharpoons 2\,{}^{\bullet}NO_2 \qquad (2.1)$$

$$RSH + {}^{\bullet}NO_2 \rightarrow RS^{\bullet} + NO_2^- + H^+ \qquad (2.9)$$

$$RS^{\bullet} + NO^{\bullet} \rightarrow RSNO \qquad (2.10)$$

In the published work (*16, 20, 21*), the possibility of metal catalysis in RSNO formation was not fully explored. A metal chelator, DTPA or EDTA, was present in all reaction solutions, but the effects of omitting the chelators were not investigated. It is not clear if EDTA and/or DTPA can fully inhibit metal-catalyzed RSNO formation. For example, $Fe(EDTA)^-$ is reportedly a better Fenton reagent than iron salts (*70*). Also, Cu^{II} bound to an amino acid, a tripeptide or serum albumin can catalyze the generation of NO from S-nitrosothiols (*61*). In this chapter, the effects of different chelators and added metals ions on NO and O_2 consumption, as well as CysNO formation in cysteine solutions, are studied and the mechanism of CysNO formation discussed.

2.3 Experimental procedures

Materials: NO gas was purchased from Praxair. *L*-Cysteine and deferoxamine mesylate (desferal) were purchased from Sigma; diethylenetriaminepentaacetic acid (DTPA) and ethylenediamine tetraacetic acid (EDTA) from ICN Pharmaceuticals; $CuSO_4 \cdot 5H_2O$ from Anachemia; 2,9-dimethyl-1,10-phenanthroline hydrochloride (neocuproine) from Fluka; Cu,Zn-superoxide dismutase (CuZnSOD) from Roche Molecular Biochemicals; 1,10-phenanthroline (*o*-phen) from G. Frederick Smith; and $FeCl_3 \cdot 6H_2O$ from BDH Chemicals.

Preparation of NO solutions: The NO gas purge system shown in Figure 2.2 was constructed to prepare saturated NO solutions. MilliQ water in the rubber-stoppered collection vial was purged for 30 min with N_2 and 30 min with NO gas. Higher oxides of nitrogen were removed by passage of the gas through a 10% KOH trap before the collection vial (*71*). This resulted in a saturated solution of NO (~1.5 mM) as measured

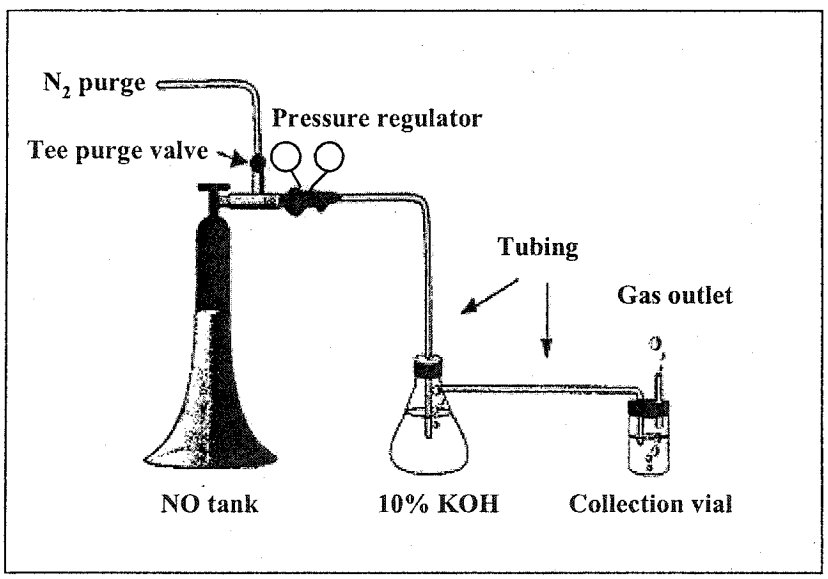

Figure 2.1. **Preparing a saturated NO aqueous solution in a fume hood.** Adapted from the ISO-NO Mark II Instruction Manual, World Precision Instruments, Inc.

by an NO meter (Model ISO-NO, World Precision Instruments, Sarasota, FL). The meter was calibrated by the chemical generation of NO from $NaNO_2$ according to the instruction manual provided with the meter.

Preparation of cysteine solutions: Cysteine (10-1000 mM) was dissolved in 100 mM phosphate buffer (pH 7.4) with or without chelators and immediately degassed for 30 min with N_2. Fresh cysteine solutions were prepared each day.

Amperometric analysis of NO consumption: NO concentrations were continuously monitored using a NO-selective electrode in 10 mL of 100 mM phosphate buffer (pH 7.4) with or without added chelators (100 μM DTPA, 20 μM neocuproine, 500 μM desferal, or 250 μM *o*-phen), CuZnSOD (15 μM) or metals salts (10 μM $CuSO_4$ or 10 μM $FeCl_3$). An aliquot (3~10 μL) of saturated NO solution was added to a 20-mL reaction vial with constant stirring at room temperature. Cysteine from a freshly prepared stock solution or the same amount of buffer (blank) was added to the vial once the electrode reading reached the maximum (at the arrow shown in Figure 2.2).

Amperometric analysis of O_2 consumption: The O_2 concentration was continuously monitored by electrochemical reduction to H_2O_2 using a computer-interfaced O_2 electrode (Hansatech DW1). The electrode was calibrated before each experiment by a 2-point calibration. Briefly, two crystals of sodium dithionite were added with stirring to 1 mL of water in the 1-mL electrochemical chamber. After 2~3 min the output was stable and provided the signal for 0 mM O_2 at 25 °C. The O_2 concentration of air-saturated water at 25 °C (0.253 mM) was used as the second calibration point.

UV-vis studies: Cysteine (4.5 mM) was incubated with 40-60 μM authentic NO for 1.5 min at room temperature in 100 mM phosphate buffer (pH 7.4) ± chelators, ±

added metals. The reaction solutions were shielded from light and their absorbance between 300-400 nm was measured at 25°C on Cary Varian 1 UV-vis spectrophotometer with the following settings: 0.1 nm interval, 0.1 nm/s scan rate (6 nm/min), 1.0 nm band width, 1.0 s signal averaging time. Appropriate blanks, run under the same conditions without NO, were subtracted from the sample spectra.

2.4 Results

2.4.1 Amperometric analysis of NO consumption

Effects of metal chelators: It was reported by Gow and coworkers (*20*) that cysteine accelerates the consumption of NO in air-saturated buffer in the presence of DTPA. Consistent with this report, we found that cysteine does accelerate the decomposition of NO (Figure 2.2 solid line *vs* dashed line).

In order to investigate the possible role of copper ions in NO consumption, we examined the loss of NO from an open aerobic solution with and without copper chelators (DTPA or neocuproine) in the presence and absence of cysteine. Figure 2.3 shows that in the absence of copper chelators, cysteine accelerates by a factor of 3 the NO consumption. The copper chelators, DTPA (specific for Cu^{II}) and neocuproine (specific for Cu^{I}), inhibit NO decay by a factor of 2 in the presence but not in the absence of cysteine (Figure 2.3). The rates of NO decay were calculated from the decrease in NO concentration in the 100-s interval following the maximum NO-meter reading (see Figure 2.2).

It has been reported that iron catalyzes both the decomposition and synthesis of S-nitrosothiols (*72*). Hence, the possible role of iron in NO consumption was also

investigated. The iron chelators, desferal (specific for Fe^{III}) and *o*-phen (specific for Fe^{II}), also inhibit NO decay in the presence but not in the absence of cysteine (Figure 2.4).

Effects of added metal ions on NO decay rates: Interestingly, the addition of $FeCl_3$ and $CuSO_4$ increases the NO decay rate 2- and 4-fold in the presence but not in the absence of cysteine (Figure 2.5).

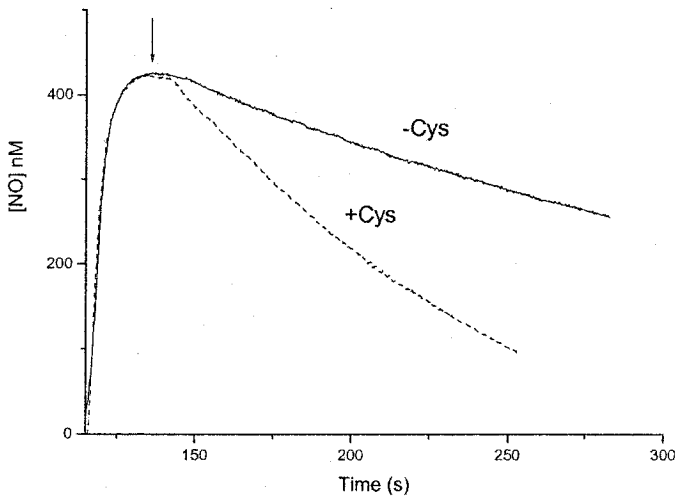

Figure 2.2. **Cysteine increases the rate of NO consumption in air-saturated buffer.** Continuous monitoring of the NO concentration with a NO-specific electrode was carried out following addition of a saturated NO solution (1.5 mM) to 10 mL of air-saturated 100 mM phosphate buffer (pH 7.4) at time 0 s. The stirring velocity and temperature (25°C) were kept constant, and 70 µL of 100 mM cysteine (700 µM final concentration) was added at the arrow. The dashed and solid lines represent the NO-meter readings in the presence and absence of cysteine, respectively. Note that no chelators were added to the buffer in this experiment. This was a single-point determination under the conditions specified here.

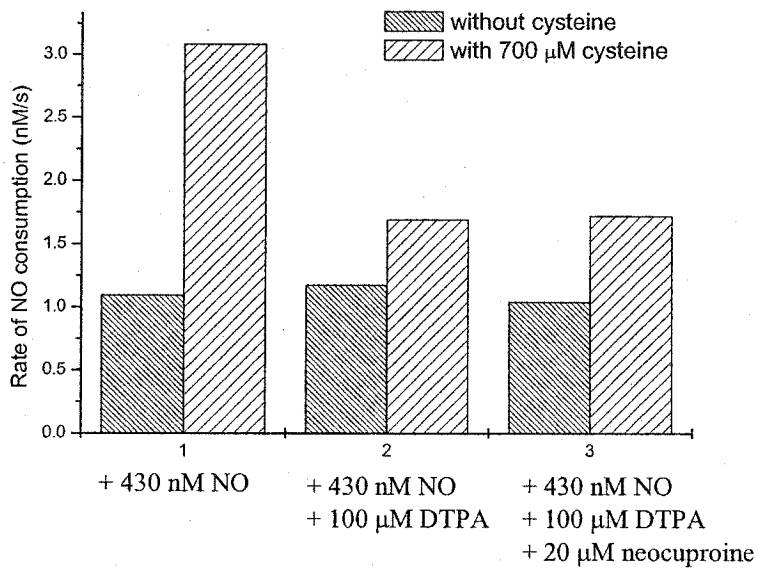

Figure 2.3. **Amperometric measurements of the effects of copper chelators on NO decay rates (nM/s) in air-saturated buffer with and without cysteine.** Nitric oxide from a saturated solution (1.5 mM) was added to 10 mL of air-saturated 100 mM phosphate buffer (pH 7.4) containing chelators where indicated. The stirring velocity and temperature (25°C) were kept constant, and 70 μL of 100 mM cysteine (700 μM final concentration) or 70 μL buffer was added when the peak electrode output had been reached as shown in Figure 2.2. The rates of NO decay were measured during the 100-s interval following cysteine or buffer addition. This was a single-point determination under the conditions specified here.

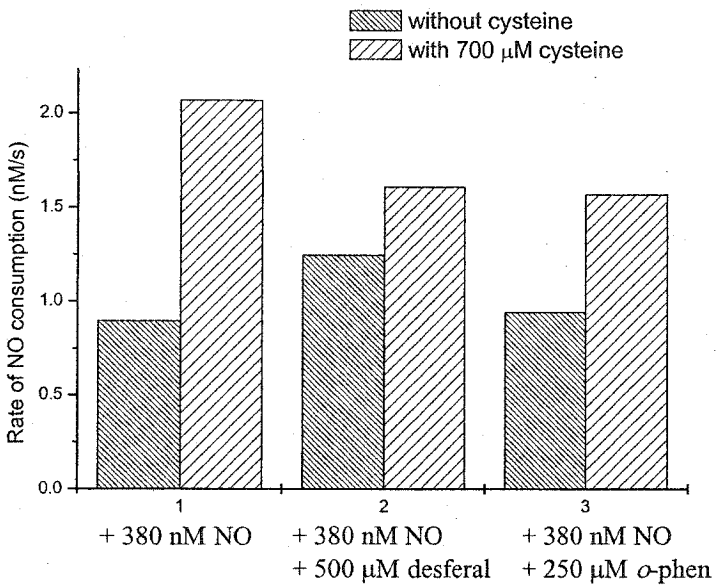

Figure 2.4. **Amperometric measurements of the effects of iron chelators on NO decay rates (nM/s) in air-saturated buffer with and without cysteine.** Experimental conditions are given in the legend of Figure 2.3. This was a single-point determination under the conditions specified here.

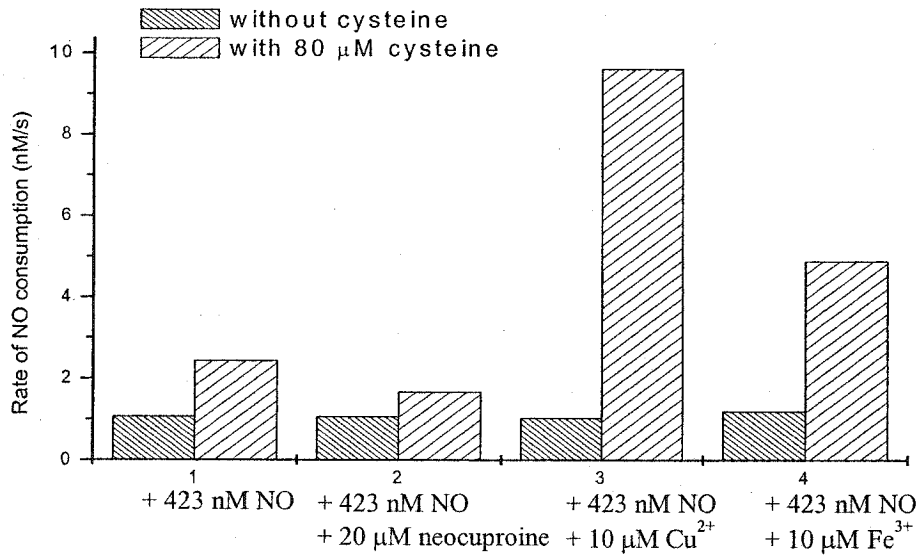

Figure 2.5. **Amperometric measurements of the effects of added metal ions on NO decay rates (nM/s) in air-saturated buffer with and without cysteine.** The experimental conditions are given in the legend of Figure 2.3. This was a single-point determination under the conditions specified here.

Effects of CuZnSOD: Superoxide, which may be produced by reaction 2.6, reacts with NO at the diffusion limit ($k = 5 \times 10^9\ M^{-1}s^{-1}$) (*73*). Hence, CuZnSOD was added to the reaction solution to compete with $NO^{\bullet}$ for any $O_2^{-\bullet}$ formed (reaction 2.7). Cysteine accelerates the consumption of NO under aerobic conditions to a similar extent in the presence or absence of 15 μM CuZnSOD (Figure 2.6), but the acceleration is less due to the larger concentration of NO in these samples than in the previous samples (Figures 2.3-2.5) as discussed in Section 2.5. Importantly, Figure 2.7 shows that when NO was added to buffer containing CuZnSOD alone, the detectable concentration of free NO was less than that in the absence of enzyme.

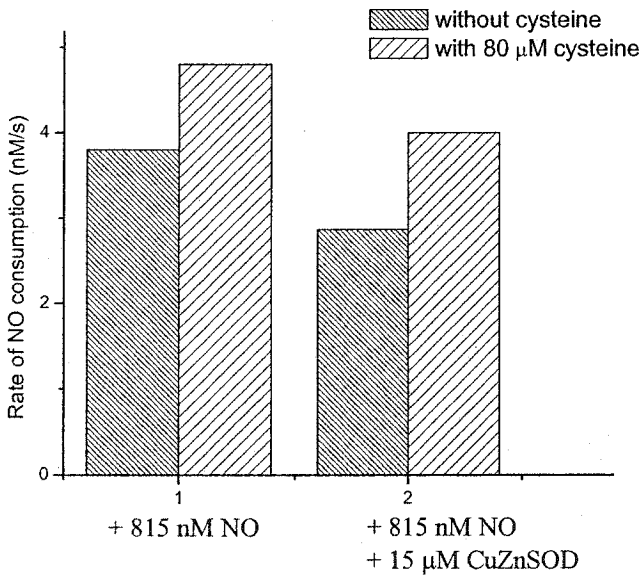

Figure 2.6 **Amperometric measurements of the effects of added CuZnSOD on NO decay rates (nM/s) in air-saturated buffer with and without cysteine.** The experimental conditions are given in the legend of Figure 2.3. This was a single-point determination under the conditions specified here.

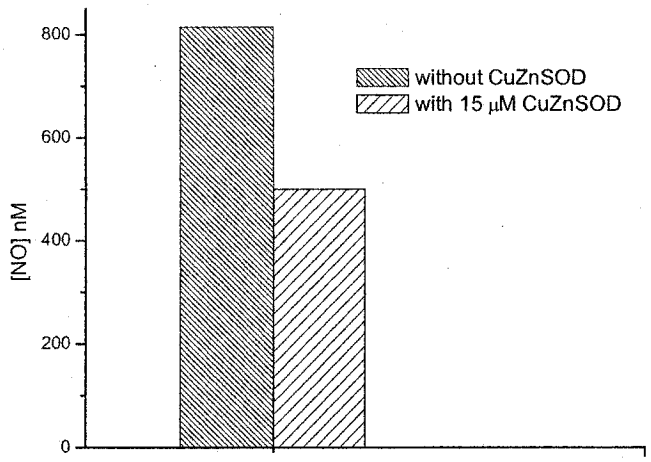

Figure 2.7. **Amperometric measurements of the effects of CuZnSOD on the free NO concentration in air-saturated buffer.** Nitric oxide from a saturated solution was added to 2 mL of 100 mM phosphate buffer (pH 7.4) containing 15 μM CuZnSOD where indicated, and the NO concentrations given are those at the peak electrode output with constant stirring at 25°C. This was a single-point determination under the conditions specified here.

2.4.2 UV-vis studies

The absorption of reaction mixtures containing cysteine and NO was examined between 300-400 nm where S-nitrosothiols absorb (*8*). The molar absorptivity of CysNO is low, ε_{336} = 725 $M^{-1}cm^{-1}$ (*74*), so to detect a 336-nm band the concentration of NO added had to be increased. However, thiols were reported to accelerate NO consumption rates only at [NO] <50 μM (*20*). At higher NO concentrations the addition of thiols does not alter the consumption of NO (*17*) since the reaction of NO with O_2, which is second-order with respect to NO (eq 2.1), becomes dominant (*69*). Moreover, the thiol concentration reportedly has to exceed the NO concentration by approximately 100-fold to influence the NO consumption rates (*20*). To work within these limitations, the spectrum of a solution containing ~ 40 μM of NO and 4.5 mM of cysteine was examined and a difference peak centered at 340 nm was observed (Figure 2.8). This indicates the

formation of CysNO, and the amount formed decreased in the presence of chelators, including 100 μM DTPA, 20 μM neocuproine or 1 mM EDTA (Figure 2.8). However, the iron chelators (desferal and *o*-phen) did not inhibit CysNO formation (Figure 2.9), which may be due to the higher concentration of NO (58 μM) or the less effect of iron chelators on CysNO formation (see Section 2.5.1).

When $CuSO_4$ (10 μM) or $FeCl_3$ (10 μM) was added to cysteine alone, metal complex formation gave rise to an absorbance that would interfere with CysNO absorbance (Figure 2.10). Also in the difference spectra [(cysteine + NO) – (cysteine)] it is difficult to identify any SNO absorption (Figures 2.10A, B; spectrum 3).

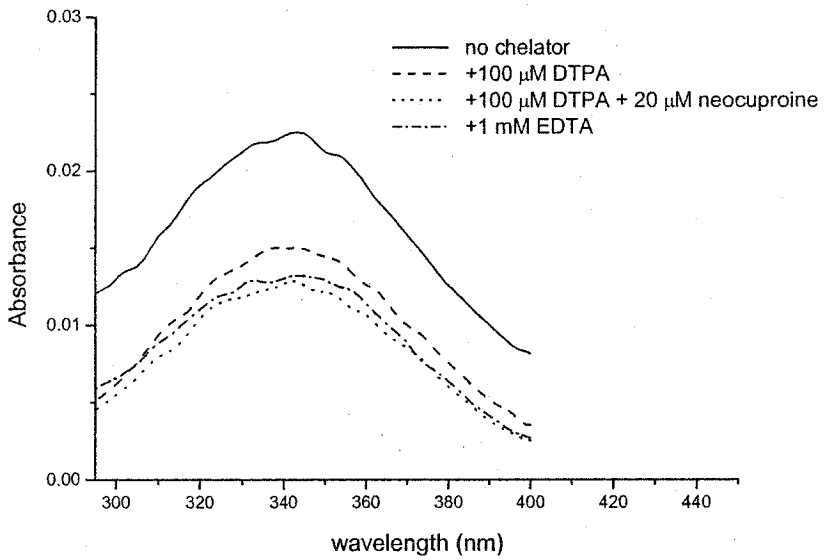

Figure 2.8. **Effects of metal chelators on (cysteine + NO) – (cysteine) difference spectra in air-saturated buffer.** Cysteine (4.5 mM) was incubated with 40 μM NO in the absence (solid line) and in the presence of 100 μM DTPA (dashed line), 100 μM DTPA + 20 μM neocuproine (dotted line), or 1 mM EDTA (dashed–dotted line). All samples were prepared in 100 mM phosphate buffer (pH 7.4) at room temperature in the dark. Blanks were prepared with the same reagents except NO was omitted. The spectra were recorded in a 1-cm cuvette 1.5 min after the reagents were mixed and the appropriate blanks were subtracted from the sample spectra. This was a single-point determination under the conditions specified here.

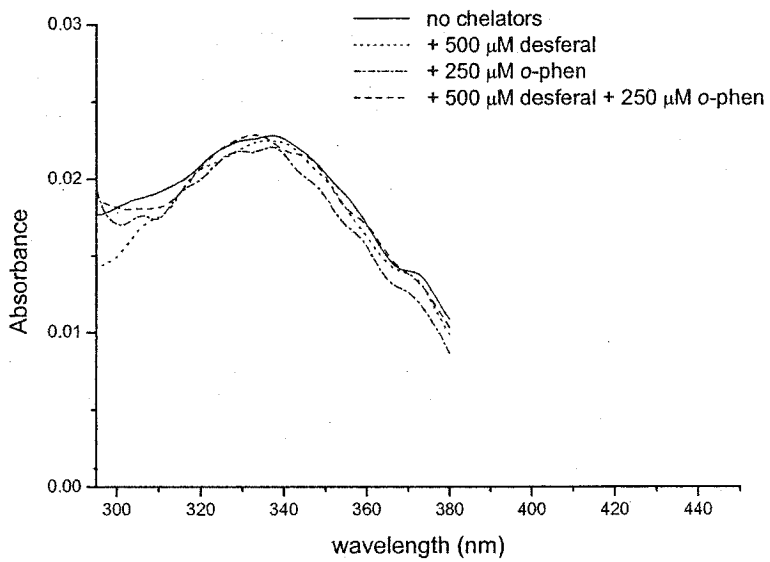

Figure 2.9. **Effects of iron chelators on (cysteine + NO) – (cysteine) difference spectra in air-saturated buffer.** Cysteine (4.5 mM) was incubated with 58 μM NO in the absence (solid line) or in the presence of 500 μM desferal (dotted line), 250 μM *o*-phen (dashed–dotted line), or 500 μM desferal + 250 μM *o*-phen (dashed line). The experimental conditions are given in the legend of Figure 2.8. This was a single-point determination under the conditions specified here.

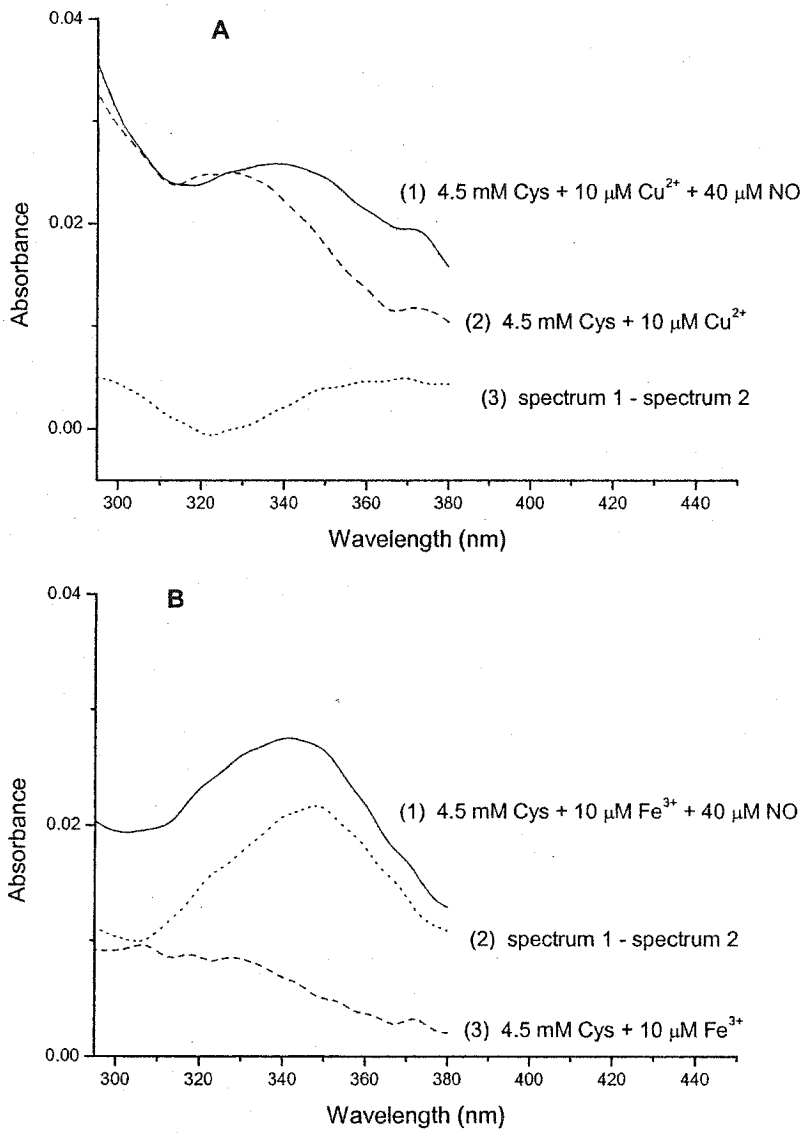

Figure 2.10. **Effects of added $CuSO_4$ or $FeCl_3$ on CysNO formation in air-saturated buffer. (A)** Cysteine (4.5 mM) was incubated with 10 μM Cu^{2+} in the presence (spectrum 1) or absence of 40 μM NO (spectrum 2). **(B)** Cysteine (4.5 mM) was incubated with 10 μM Fe^{3+} in the presence (spectrum 1) or absence of 40 μM NO (spectrum 2). All samples were prepared in 100 mM phosphate buffer (pH 7.4) at room temperature in the dark. The spectra were recorded in a 1-cm cuvette 1.5 min after the reagents were mixed and a buffer-only blank was subtracted from the sample spectra. This was a single-point determination under the conditions specified here.

2.4.3 Amperometric analysis of O_2 consumption

An oxygen-electrode was used to monitor O_2 consumption under various conditions. Figure 2.11 shows that the change in O_2 concentration $\Delta[O_2]$ was 8.5 μM when 15 μM NO was added to air-saturated buffer in an electrode chamber in the presence or absence of metal chelators. The $\Delta[O_2]$ increased by ~ 4 μM when 2 mM cysteine was present but the chelators had no detectable effects (Figure 2.11).

Figure 2.12 shows the time course over 1 min of O_2 consumption on NO addition to 2 mM cysteine solutions. Within 30 s after NO addition, the O_2 concentration has leveled off in the presence of chelators (Figure 2.12A). Added Fe^{3+} has little effect on the O_2 consumption (Figure 2.12B). However, added Cu^{2+} promotes O_2 consumption in the cysteine solution both in the absence and presence of NO (Figure 2.12 C and D). The rate of O_2 consumption is strongly dependent on the concentration of added Cu^{2+} with $\Delta[O_2]$ ~ 6 μM and 11 μM in the 30 s prior to NO addition in the presence of 0.5 μM and 1 μM Cu^{2+}, respectively. Following 15 μM NO addition, $\Delta[O_2]$ values of ~20 and 30 μM were observed in the 0.5 μM and 1 μM Cu^{2+} solutions, respectively, before the consumption of O_2 stopped (Figure 2.12 C and D).

The effect of added copper ions (1 μM final concentration) on the rate of O_2 consumption by cysteine was confirmed in a separate experiment (Figure 2.13). The time course of O_2 consumption by cysteine alone was examined over longer times in the absence of NO (Figure 2.14). Over the time period studied the rates appear to be largely independent of the O_2 concentration, hence the kinetics are zero order. Also the rates are highly dependent on the presence of chelators, indicating that the observed O_2 consumption is metal catalyzed. Furthermore, in the absence of NO, the consumption of

O_2 does not stop after ~100 s as seen in Figure 2.12, but is continuous at the same rate over the 1000-s (~17 min) period monitored here (Figure 2.14). Thus, it appears that NO or an NO-derived species inhibit the metal-catalyzed consumption of O_2.

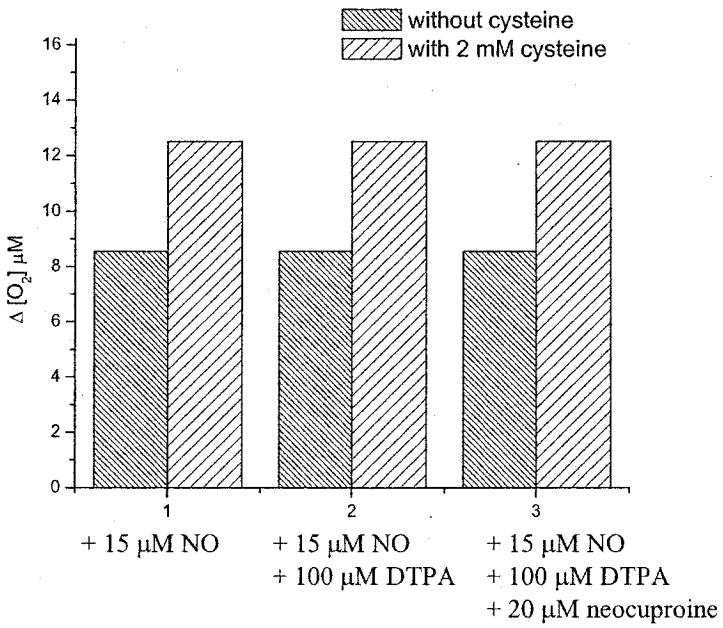

Figure 2.11. **Oxygen consumption as a result of NO addition to air-saturated buffer with and without cysteine.** Oxygen consumption was monitored by an O_2 electrode in 1 mL of 100 mM phosphate buffer (pH 7.4) at room temperature with constant stirring in an electrode chamber in the absence (1) and presence (2 and 3) of chelators and 2 mM cysteine. $\Delta[O_2]$ is the difference in the O_2 concentration before NO addition and within 1 min post NO addition. A 10 μL aliquot of saturated NO solution (1.5 mM) was added to give a final NO concentration of 15 μM. The $\Delta[O_2]$ (2.5 μM) due to dilution on addition of the NO solution was subtracted from the $\Delta[O_2]$ values plotted. This was a single-point determination under the conditions specified here.

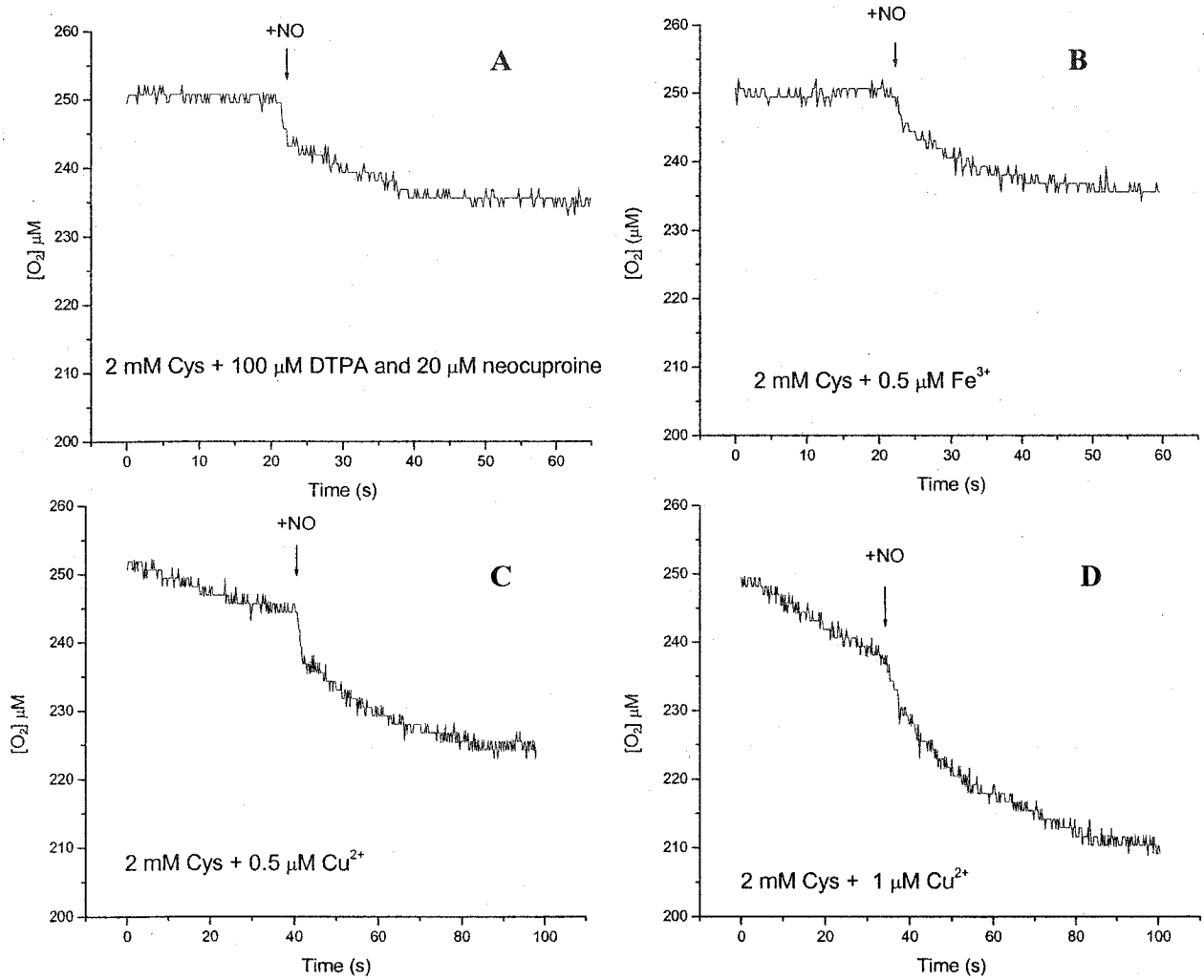

Figure 2.12. **Time course of O_2 consumption on adding 15 μM NO to air-saturated cysteine under different conditions.** Oxygen consumption was monitored by an O_2 electrode in 1 mL of 100 mM phosphate buffer (pH 7.4) at room temperature with constant stirring in an electrode chamber. This was a single-point determination under the conditions specified here.

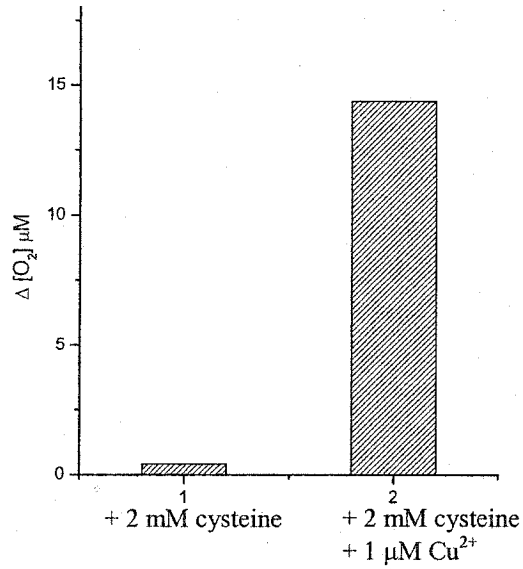

Figure 2.13. **Oxygen consumption within 1 min in an air-saturated solution of cysteine in the absence and presence of 1 μM $CuSO_4$ without NO.** Oxygen concentrations were monitored by an O_2 electrode in 1 mL of 100 mM phosphate buffer (pH 7.4) containing 2 mM cysteine at room temperature with constant stirring in an electrode chamber. $\Delta[O_2]$ is the difference in oxygen concentration in the solutions 1 min after addition of 1 μM Cu^{2+} or buffer. This was a single-point determination under the conditions specified here.

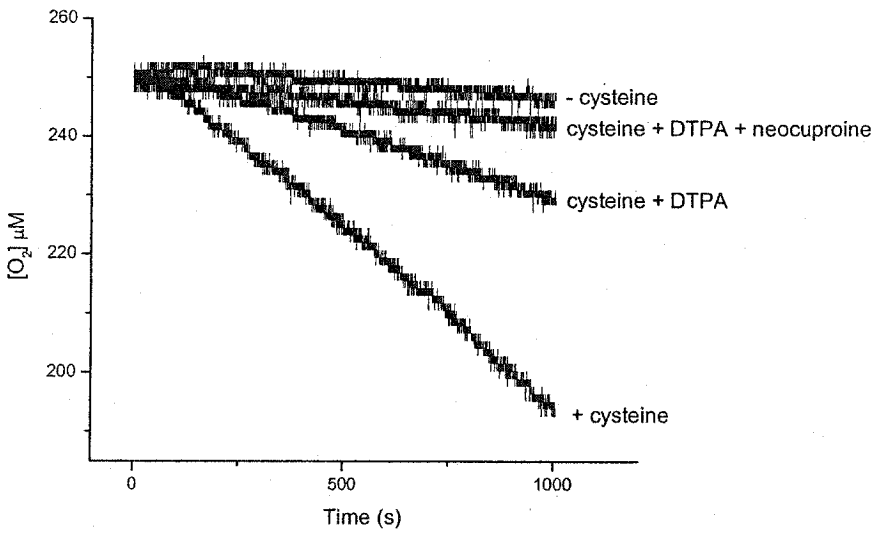

Figure 2.14. **Time course of O_2 consumption in air-saturated solutions in the absence of NO.** Oxygen concentrations were monitored by an O_2 electrode in 1 mL of 100 mM phosphate buffer (pH 7.4) at room temperature with constant stirring in an electrode chamber. Cysteine (800 μM), 100 μM DTPA and 20 μM neocuproine were present where indicated. This was a single-point determination under the conditions specified here.

2.5 Discussion

2.5.1 NO consumption

NO will be oxidized in oxygenated aqueous solution:

$$2\ NO^{\bullet} + O_2 \rightleftharpoons 2\ {}^{\bullet}NO_2 \qquad (2.1)$$

This reaction was shown, even at micromolar concentrations of NO, to follow a third-order rate equation: $d[NO]/dt = k[NO]^2[O_2]$ (*75*), $k = 7\times 10^6\ M^{-2}s^{-1}$(*76, 77*). The second-order dependence on [NO] makes the half-life of this molecule in aqueous solution highly dependent on its concentration (*76*). For example, if it is assumed that the physiological concentration of NO is ≤ 0.1 μM and the average intracellular O_2 concentration is 20-50 μM, the rate of reaction between NO and O_2 would be 1-3.5 pM/s (*69*), and the first half-life of NO would be 8-19 h. Therefore, at low concentrations of NO, autoxidation may not be competitive with other reactions of NO, which could be the case *in vivo*.

In this study, the NO concentrations used were dictated by the detection limits of the techniques employed. For example, 40-60 μM NO was added to cysteine in order to detect SNO absorbance, and 15 μM NO was required in the O_2 consumption measurements to obtain reasonable signal-to-noise ratios. The direct amperometric detection of NO is the most sensitive method used in this study, so lower concentrations of NO (~ 400 nM) could be used in these experiments.

Figure 2.15 summarizes the known reactions between GSH and NO in aerobic solutions (*76, 78-85*). The reaction of ${}^{\bullet}NO_2$ with GSH dominates when [GSH]»NO, and produces GSNO, GSSG and NO_3^- as stable products. Also, the rate-limiting step (${}^{\bullet}NO_2$ production) is second-order in NO and first-order in GSH. Assuming that cysteine and

NO undergo similar reactions with comparable rates, we will attempt to interpret the results obtained here.

In the experiment shown in Figure 2.2, ~ 400 nM of NO and 700 μM of cysteine were present. Therefore, based on rate constants given in Figure 2.15 for the reactions of $^{\bullet}NO_2$, the pseudo-first-order rate constants under the present experimental conditions are $k'_{NO} = 400\ s^{-1}$ and $k'_{Cys} = 1.4 \times 10^4\ s^{-1}$. Hence, in the presence of $>10^3$-fold excess cysteine, NO should be consumed more rapidly *via* reactions 2.12 and 2.7 than *via* N_2O_3 formation, the route of $^{\bullet}NO_2$ consumption in the absence of cysteine.

$$Cys + {}^{\bullet}NO_2 \rightleftharpoons Cys^{\bullet} + NO_2^- + H^+ \qquad (2.11)$$

$$Cys^{\bullet} + NO^{\bullet} \rightarrow CysNO \qquad (2.12)$$

$$O_2^{-\bullet} + NO^{\bullet} \rightarrow ONOO^- \rightarrow NO_3^- \qquad (2.7)$$

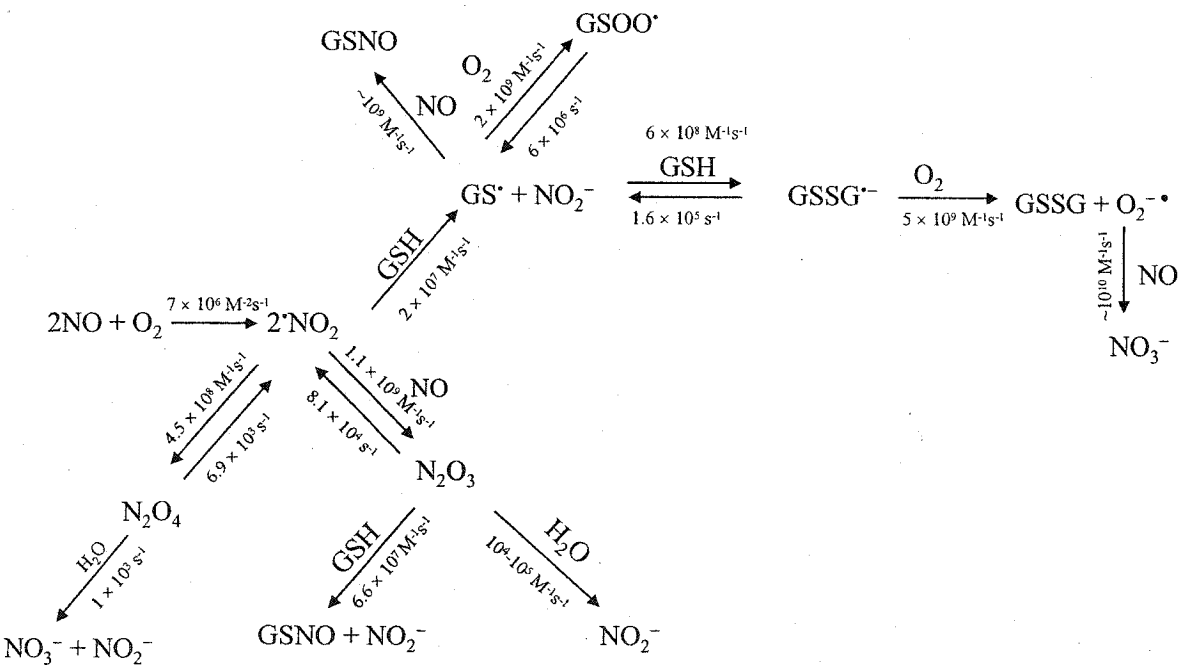

Figure 2.15. **Reactions of NO and GSH in aerobic solutions without metal ions.** The literature rate constants were obtained from (*76, 78-85*).

The metal chelators decrease NO decay rates in the presence of cysteine but not in its absence (Figures 2.3 and 2.4). Thus, metal-ion impurities increase NO consumption by cysteine-dependent routes but do not alter the reaction between NO and O_2. Consistent with this, addition of Fe^{3+} or Cu^{2+} increased the NO decay rates only in the presence of cysteine (Figure 2.5). Also, copper chelators decrease the intensity of 340-nm absorption peak in difference spectra due to CysNO formation (Figure 2.8). These results indicate that copper increases NO consumption by promoting CysNO formation. However, the iron chelators have no effect on the observed intensity of the 340-nm difference peak (Figure 2.9), suggesting that trace iron does not give rise to detectable amounts of CysNO.

The proposed reactions initiated by Cu^{2+} or Fe^{3+} in aerobic solutions containing NO and cysteine are given in Figure 2.16. The metal is reduced by cysteine and the $Cys^{\bullet}$ radical either reacts with $NO^{\bullet}$ to yield CysNO or with another cysteine and O_2 to give cystine (Cys_2) and $O_2^{-\bullet}$. If the reduced metal $M^{(n-1)+}$ is reoxidized by O_2 the cycle can start over.

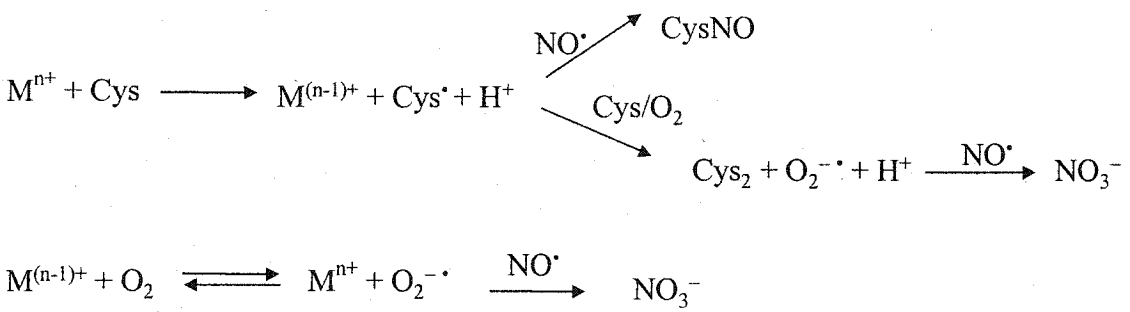

Figure 2.16. **Reactions initiated by metal ions M^{n+} in aerobic solutions containing cysteine and NO.**

Redox cycling is more likely for $M^{n+} = Cu^{2+}$ given the relative ease with which Cu^{+} is oxidized. For example, the reduction potentials of the Cu^{2+}/Cu^{+} and Fe^{3+}/Fe^{2+} couples in aqueous solution are (*86*):

$$Cu^{2+} + 1e^{-} \rightarrow Cu^{+} \qquad E^{0} = 0.159\ V \qquad (2.13)$$

$$Fe^{3+} + 1e^{-} \rightarrow Fe^{2+} \qquad E^{0} = 0.771\ V \qquad (2.14)$$

Thus, trace copper has a larger impact on CysNO formation (Figure 2.8 *vs* 2.9), and on NO (Figure 2.5) and O_2 consumption (Figure 2.12) because Cu^{2+} will be reformed more readily than Fe^{3+} by autoxidation. The impact of added Fe^{3+} on NO consumption seen in Figure 2.5 does not require redox cycling of the metal because of the large concentration of Fe^{3+} added (10 μM) compared to NO (423 nM). Thus, in this case sufficient $Cys^{\bullet}$ would be formed to compete with O_2 for NO and significantly increase the measured NO consumption rate. However, the impact of trace Fe^{3+} impurity (< 1 μM) in a solution containing 58 μM NO is expected to be negligible in the absence of redox cycling of the metal, consistent with the negligible effects of the iron chelators on the spectra in Figure 2.9.

Both Cu^{2+} and Fe^{3+} form complexes with cysteine (*87, 88*). When 10 μM $CuSO_4$ or $FeCl_3$ was added to an aerobic solution of cysteine alone, formation of a $M(Cys)_x$ complex was indicated by the absorption spectra (Figure 2.10). When NO was added the spectra changed suggesting that $M(Cys)_y\ (L)_z$ may form, where L is NO or an NO-derived ligand.

CuZnSOD catalyzes the dismutation of superoxide, $O_2^{-\bullet}$, to dioxygen and hydrogen peroxide with high efficiency (*57*). Therefore, CuZnSOD should decrease superoxide-dependent NO consumption in the presence of added thiol. However,

CuZnSOD addition has little overall effect on the acceleration of NO consumption by cysteine (Figure 2.6) probably because the reduction of $Cu^{II}ZnSOD$ by cysteine (Figure 5.6; Chapter 5) generates $Cys^{\bullet}$ radicals, which can react with NO as proposed in Figure 2.17. Thus, increased NO consumption by $Cys^{\bullet}$ radicals counterbalances decreased NO consumption by $O_2^{-\bullet}$ radicals when CuZnSOD is present. Gow and coworkers (*20*) demonstrated that H_2O_2 was produced on addition of CuZnSOD and claimed that this supports $O_2^{-\bullet}$ production *via* reaction 2.6. However, Figure 2.17 predicts greater H_2O_2 production in aerobic solutions of cysteine and CuZnSOD in the absence of added NO since NO competes with cysteine for the $Cys^{\bullet}$ radicals formed.

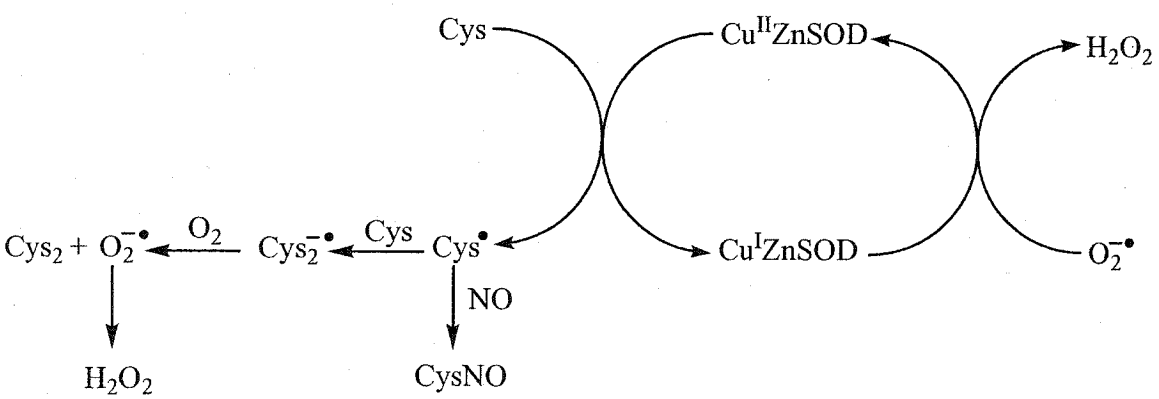

Figure 2.17. **Proposed reactions in cysteine/NO solution containing CuZnSOD.**

The reversible reduction of NO to nitroxyl (HNO) by $Cu^{I}ZnSOD$ has been reported (*89, 90*). This may also contribute to NO consumption in the presence of CuZnSOD depending on the rates of NO and HNO reaction with the reduced and oxidized enzyme. In this context it is of interest that the NO concentration measurements in the absence of cysteine showed that NO binds to $Cu^{II}ZnSOD$ (Figure 2.7).

2.5.2 O_2 consumption

Free cysteine is not stable in air-saturated aqueous solutions since it undergoes oxidation to cystine (*91*). Cysteine oxidation is proposed to be a copper-catalyzed reaction (*87*), and we observed here that added copper promotes oxygen consumption in cysteine solutions (Figures 2.13 and 2.14). Moreover, the copper chelators DTPA and neocuproine decrease oxygen consumption in cysteine solutions (Figure 2.14). The proposed mechanism of copper-catalyzed cysteine oxidation is as follows (*87*):

$$Cu^{2+} + 2Cys \rightleftharpoons [Cu^{II}(Cys)_2] \rightleftharpoons [Cu^{I}(Cys^{\bullet})Cys] + 2H^{+} \qquad (2.15)$$

$$[Cu^{I}(Cys^{\bullet})Cys] + O_2 \rightleftharpoons [Cu^{II}(Cys^{\bullet})Cys]^{+} + O_2^{-\bullet} \qquad (2.16)$$

$$[Cu^{II}(Cys^{\bullet})Cys]^{+} \rightleftharpoons [Cu^{I}(Cys^{\bullet})Cys^{\bullet}]^{+} \rightleftharpoons Cys_2 + Cu^{+} \qquad (2.17)$$

$$Cu^{+} + O_2 \rightleftharpoons Cu^{2+} + O_2^{-\bullet} \qquad (2.18)$$

The products of reactions 2.15-2.18 ($O_2^{-\bullet}$ + Cys_2) are the same as those predicted from the reaction scheme in Figure 2.16 in the absence of NO ([NO] = 0 M). Redox cycling of copper explains the catalysis of O_2 consumption by added Cu^{2+} in Figures 2.12-2.14 in the absence of NO. Moreover, Figure 2.14 reveals that the chelators decrease the rate of O_2 consumption but do not completely inhibit the redox turnover of trace copper present as an impurity. This is particularly evident for the cysteine + DTPA sample, and reveals that reactions 2.15-2.18 can occur even in the presence of added DTPA.

When NO is added, Figure 2.16 predicts that it can either react with $Cys^{\bullet}$ (eq 2.12) (*19*) and/or $O_2^{-\bullet}$ (eq 2.7) at the diffusion limit (*92*).

$$Cys^{\bullet} + NO^{\bullet} \rightarrow CysNO \qquad (2.12)$$

$$O_2^{-\bullet} + NO^{\bullet} \rightarrow ONOO^{-} \rightarrow NO_3^{-} \qquad (2.7)$$

However, the time course of O_2 consumption in Figure 2.12 indicates that NO is largely consumed *via* direct reaction with O_2 (eq 2.1). Addition of ~15 μM NO should consume ~7.5 μM O_2 to generate 15 μM $^{\bullet}NO_2$. The immediate $\Delta[O_2]$ of ~8 μM observed in Figures 2.12 A, B on NO addition is consistent with reaction 2.1 being the main NO consumption path. The reaction with cysteine of $^{\bullet}NO_2$ generated by reaction 2.1 will give rise to the $Cys^{\bullet}$ radical and NO_2^- (eq 2.9). The $Cys^{\bullet}$ radical can react with any remaining NO to give CysNO (eq 2.12). However, from the O_2 consumption time courses in Figure 2.12 it appears that most of the added NO reacted with O_2 and was subsequently converted to NO_2^-. This is consistent with the results published for GSH nitrosation under similar conditions (*16*). In the latter study, addition of 12.5 μM NO to 1 mM GSH in air-saturated buffer gave 1.2 μM GSNO, 8.4 μM NO_2^- and 2.2 μM NO_3^-.

The slow O_2 consumption 10-20 s after NO addition in Figure 2.12 A, B can be attributed to the reaction of $Cys^{\bullet}$-derived species with O_2 (Figure 2.15). Importantly, 0.5 μM Fe^{3+} has little effect on O_2 consumption, which is likely due to the absence of Fe^{2+}/Fe^{3+} redox cycling as discussed in Section 2.5.1. The spike in O_2 consumption on NO addition to the solutions containing added copper (Figure 2.12 C, D) reveals that NO is largely consumed *via* reaction 2.1 also in these solutions. This likely occurs because the O_2 concentration exceeds the $Cys^{\bullet}$ or $O_2^{-\bullet}$ concentrations. Consistent with this, there is no detectable difference in O_2 consumption in cysteine/NO in the presence or absence of chelators (Figure 2.11). However, oxidation of added Cu^+ species by O_2 to give $O_2^{-\bullet}$ is a detectable pathway for O_2 consumption before NO addition (Figure 2.12 C, D). O_2 consumption appears to stop at ~ 40 s after NO addition, but continues for over 1000 s in the absence of NO (Figure 2.14). Figure 2.10 reveals that there are different metal

complexes in solution before and after NO addition. The natures of the copper species formed following NO consumption are of interest. These species do not appear to undergo sustainable reactions of the type given by eqs 2.15 – 2.18 since the O_2 consumption levels off at ~ 100 s in Figure 2.12 C, D.

2.6 Conclusions

The variation in NO and O_2 consumption observed here is consistent with the reaction schemes given in Figures 2.15 and 2.16. The well-documented reaction between NO and O_2 generates $^{\bullet}NO_2$ which oxidizes cysteine to $Cys^{\bullet}$. The subsequent reaction of the thiyl radical with the remaining NO gives rise to CysNO. However, at the NO concentration (15 μM) used in the O_2-monitoring experiments most of the NO is converted to NO_2^-, as reported for GSH S-nitrosation under similar condition (*16*). Copper ions can increase the $Cys^{\bullet}$ concentration under aerobic conditions by consuming O_2. Thus, increased $Cys^{\bullet}$ is generated to react with NO to form CysNO. At the lower NO concentration (~ 400 nM) used in the NO-electrode experiments the addition of copper has a dramatic effect on the NO consumption rate (Figure 2.5) presumably by increasing the $Cys^{\bullet}$ concentration (Figure 2.16). The effects of copper can also be seen in the spectra in Figure 2.8, where the CysNO concentration increased in the absence of copper chelators due, presumably, to increased $Cys^{\bullet}$ production. Copper ions also catalyze the reductive cleavage of CysNO (*93*) but this must occur on a slower time scale here to allow CysNO build up.

The mechanism proposed by Gow *et al.* (*20*) for CysNO formation (eqs 2.5-2.8) is consistent with some of the results observed here. Assuming that NO reacts directly with

cysteine (eq 2.8) then increasing the cysteine concentration should increase the thiol-induced acceleration of NO consumption (Figure 2.3 *vs* 2.6). However, Gow *et al.* report a 2.4-fold increase in NO consumption in the presence of cysteine whereas we observed typically a 1.5-fold increase or less in the presence of a chelator (Figures 2.3-2.6). For example, at 815 nM NO (Figure 2.6), the acceleration of NO consumption by cysteine even in the absence of a chelator is only 1.3-fold although Gow *et al.* state that the effects of thiol on NO decay were relevant at NO concentrations up to 50 μM. Clearly, this is unlikely the case since the O_2-electrode measurements reveal a rapid spike in O_2-consumption consistent with reaction 2.15 occurring on addition of 15 μM NO to air-saturated cysteine (Figure 2.12). The discrepancy between the present results and those of Gow *et al.* may be due in part to differences in experimental set up. NO measurements were performed in our studies using 10 mL of solution in a 20-mL glass reaction vial. Gow *et al.* carried out their NO measurements in 46-well plastic plates using 1 mL of solution per well (*20*). Loss of NO by diffusion from the plastic wells was probably greater than from the glass reaction vials employed here. Gow *et al.* also state that the generation of H_2O_2 in the presence of CuZnSOD provides evidence for the direct reaction of cysteine with NO. However, generation of H_2O_2 on CuZnSOD addition will occur in the absence of NO (Figure 2.17). Thus, H_2O_2 production does not provide definitive evidence for RSNOH oxidation by O_2 (eq 2.6).

In summary, Figure 2.15 predicts that addition of NO to thiols/O_2 will give rise largely to NO_2^- *via* $^{\bullet}NO_2$ reduction or hydrolysis of N_2O_3 or N_2O_4. However, a copper-catalyzed scheme such as that shown in Figure 2.16 can form $Cys^{\bullet}$ radicals by O_2 consumption, and these radicals should compete favourably with $O_2^{-\bullet}$ for low

concentrations of NO to form CysNO. The mechanism given in Chapter 5 for S-nitrosation of protein-based (HCaBP) thiols by GSNO follows a similar copper-catalyzed thiyl-radical pathway (eqs 5.5–5.7), except that GSNO is both the copper oxidant and source of NO, and the copper catalyst (CuZnSOD) and cysteine are protein-bound. CysNO formation *via* a similar copper-catalyzed pathway requires just one molecule of NO (Figure 2.16). In contrast, CysNO formation *via* the $^{\bullet}NO_2$ pathway consumes 3 molecules of NO (Figure 2.15). Thus, Cu^{2+} should be the preferred reagent over $^{\bullet}NO_2$ at low NO concentrations. Furthermore, protein-bound copper could lead to a selective S-nitrosation catalyst unlike freely diffusing $^{\bullet}NO_2$.

3.0 Construction, expression and purification of recombinant human brain calbindin D_{28k} (rHCaBP) as a His-tagged protein

3.1 Introduction

3.1.1 Fusion proteins

A fusion protein consists of a protein of interest linked to an affinity tag. The tag may either be a small peptide (e.g., His-tag, hexa-histidine or FLAG-tag, the octapeptide, N-Asp-Tyr-Lys-Asp-Asp-Asp-Asp-Lys-C), or a full-length protein (e.g., maltose-binding protein, glutahione S-transferase or thioredoxin). Fusion proteins are chosen because of their high level of expression and their ease of purification. A fusion protein usually can be purified to >90% in a single affinity chromatography step, and recovered from the matrix under mild elution conditions that preserve its antigenicity and functionality.

In this study the His-tag system was chosen because it is small and normally does not interfere with the structure or function of the purified protein (*94-96*). The presence of a His-tag can even increase the activity of expressed proteins (*97*), probably because the purification is faster (*98*). Using commercially available vectors, the His-tag can be placed at the C- or N-terminal of the target protein along with a protease recognition site to facilitate removal of the affinity tag from the purified protein upon addition of the protease. In addition, the Ni-NTA affinity matrix for His-tagged proteins is cheaper than the anti-FLAG or the glutathione Sepharose 4B matrixes used for FLAG- and GST-fusion proteins, respectively.

Nitrilotriacetic acid (NTA) is a tetradentate chelating agent that occupies four of the six ligand binding sites in the coordination sphere of a metal ion such as Ni^{2+} (Figure

3.1). This leaves two sites available on Ni^{2+} to interact with a hex-His-tag, and the high affinity that the His-tag possesses for the immobilized metal gives rise to rapid and effective purification of the target protein. Hence, this approach is named immobilized metal affinity chromatography (IMAC). Ni-NTA is coupled in high density to a stable, solid resin such as Sepharose CL-6B resulting in high binding capacity for hexa-His-tagged proteins. These proteins can be eluted from the resin by the inclusion of imidazole in the buffer (Figure 3.1). This technology reported by Janknecht allows the purification of proteins present at less than 1% of total cell extract to greater than 95% homogeneity in one step (*97*). The construction and expression of recombinant His-tagged human brain calbindin D_{28k} (rHCaBP) and its purification using Ni-NTA are described in this chapter.

3.1.2 Recombinant forms of CaBP

In 1994 Kumar *et al.* set up a system to express and purify recombinant rat brain CaBP (*99*). The cDNA for rat CaBP was cloned into the pET3a vector and the protein was expressed in BL21(DE3)pLysS *E. coli* cells. Although this system expresses gram amounts of rat CaBP, the purification method was somewhat cumbersome and the final purified protein contained 5% of a degradation product plus higher molecular weight aggregates. In 2003, this system was improved by (*100*) expressing rat CaBP as a GST fusion protein based on the same vector and expression-cell line mentioned above. The purification procedure relied primarily on a GST column with glutathione elution followed by thrombin cleavage, but the yield and purity were not reported (*100*).

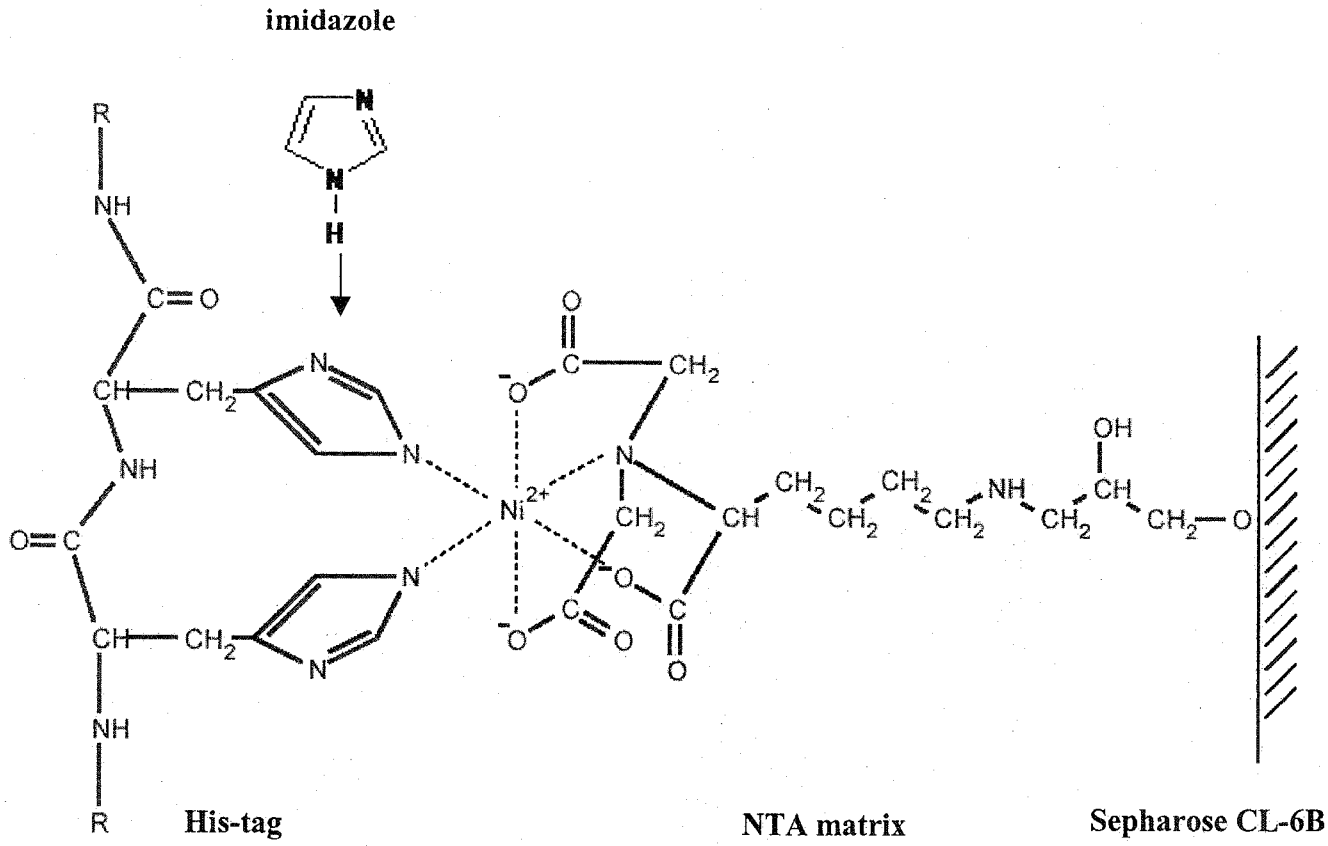

Figure 3.1. **Mode of complexation of a His-tagged protein with the Ni-NTA Sepharose CL-6B affinity resin.** Addition of free imidazole ligand results in elution of the His-tagged protein. Adapted from Reference [93].

In 1999, Thulin and Linse reported the first purification of rHCaBP (*101*). HCaBP was cloned into a pET3a vector and expressed in *E. coli* BL21 cells. The purification procedure consisted of heating the cell lysate to 75°C to precipitate bacterial proteins, ion-exchange chromatography on a DEAE-cellulose column in the presence of calcium, and ion-exchange chromatography on a DEAE-Sephacel column in the presence of EDTA to remove the contaminants that coeluted with HCaBP from the cellulose column. The final yield was 20-50 mg pure protein per liter of culture. As mentioned above this method includes a 75°C heating step and the isolation buffer is 10 mM MES at pH 5.6 to reduce deamidation. Given that the conformational stability of HCaBP is not known (*100*), exposure of the protein to high temperature and low pH is not desirable.

pGYMX-HCaBP was constructed by professor Michael Murphy's group at the University of British Columbia. This plasmid contained a cDNA clone of HCaBP (*102*) inserted into the *Nhe*I and *Xba*I sites of the expression vector pGYMX (*103*) to produce a fusion protein with an N-terminal His-tag followed by a factor Xa cleavage site. Expression from pGYMX-HCaBP is not genetically stable so the HCaBP gene along with a DNA fragment encoding the His-tag was subcloned into pTrc99A using the *Nco*I and *Xba*I restriction sites. Purification procedures relied primarily on a Ni-NTA affinity chromatography, and expression from both pGYMX-HCaBP and pTrc99A-HCaBP yield up to 15 mg pure protein per liter of culture (M. Murphy, personal communication). Details on the expression of these recombinant forms of HCaBP have not been published by the UBC group.

Because many HCaBP mutants are to be prepared in our lab in the future, a high yield and economical expression and purification system was desirable. We initially

chose the pTrc99A-HCaBP system because this system was tested at UBC and it gives a reasonable yield of protein. Unfortunately, the pTrc99A-HCaBP plasmid was no longer available from UBC, but we were able to obtain pGYMX-HCaBP. Both pGYMX and pTrc99A have the same restriction sites, *Nco*I and *Xba*I, which facilitated transfer of the insert. JM105 is a recommended host for pTrc99A (*104*).

Both reported recombinant forms of HCaBP (*99, 101*) were cloned into the pET3a vector and expressed in BL21 or BL21(DE3)pLysS cell lines. These systems can yield up to 20-50 mg of protein per liter of culture, which is about double that expected from the pTrc99A-HCaBP-JM105 system. Since pET3a does not carry a tag sequence such as hexa-His or GST, affinity purification can not be used in protein isolation and the purification procedure is cumbersome. Thus, another pET vector, pET15b, which carries an N-terminal His-tag followed by a thrombin cut site was selected as an alternative to the pTrc99A vector. The HCaBP insert was subcloned into pET15b, and pET15b-HCaBP was expressed in *E. coli* BL21 cell lines as outlined in the following sections.

Two goals were met in this study. First the yield of protein expression in the BL21-pET15b-HCaBP system was increased over pTrc99A-HCaBP system. Second, by changing the factor Xa recognition site to a thrombin site the cost was decreased as factor Xa is more expensive than thrombin. However, more importantly, factor Xa does not work efficiently in the presence of reductant (*105*) and imidazole (*106*). HCaBP has 5 free thiols and reportedly has a propensity to form disulfide crosslinks (*107*). In order to protect the free thiols during protein purification a reducing environment is necessary. Thrombin is a better choice since it can function in 500 mM imidazole and in 5 mM β-mercaptoethanol (J. Bonvin, Concordia University, personal communication).

3.2 Experimental procedures

3.2.1 Materials

Oligonucleotides of standard purity were obtained from Biocorp Inc. Restriction enzymes were from MBI Fermentas, and the Rapid DNA Ligation Kit was from Roche. DNA ladders were from Roche or Fermentas. Isopropyl β-D-thiogalactoside (IPTG) and ampicillin (sodium salt) were obtained from BioShop Canada Inc. BugBuster protein extraction reagent, benzonase nuclease, and factor Xa kits were from Novagen. Complete EDTA-free protease inhibitor cocktail tablets were from Roche. Ni-NTA Agarose was from Qiagen. Thrombin was generously provided by Dr. Joanne Turnbull, Concordia University. β-mercaptoethanol was from ICN. Dialysis membrane (MW cut-off 12-14 kDa) from Spectrapor was washed according to the manufacturer's instructions. NAP-5 and NAP-10 were from Amersham Pharmacia Biotech. Ultrafree-0.5 centrifugal filters were from Millipore. The Gelcode Blue Stain Reagent was from Pierce. All other chemical reagents were obtained commercially and were of the highest quality available.

3.2.2 Strains and plasmids

E. coli strains BL21 and BL21(DE3)pLysS were purchased from Novagen. JM105 cell line was a generous gift from Dr. Paul Joyce, Concordia University. These strains were used for both plasmid production and for protein expression. The HCaBP gene from human brain in plasmid pGYMX was generously provided by Dr. Michael Murphy, University of British Columbia. The plasmids pTrc99A and pET15b, generous

gifts from Dr. Susan Aitken (Carleton University) and Dr. Joanne Turnbull (Concordia University), respectively, were used as vectors for the HCaBP gene.

3.2.3 Cloning of the HCaBP gene into the expression vectors

3.2.3.1 Cloning into the pTrc99A plasmid

DNA digestion and purification: Expression from pGYMX-HCaBP was not genetically stable, so the HCaBP gene along with a DNA fragment encoding the His-tag and factor Xa cutting site were subcloned into pTrc99A (Figure 3.2). The pGYMX-HCaBP vector was digested with both *Xha*I and *Nco*I in Y^+/TANGO buffer (supplied with the digestion enzymes; MBI Fermentas) for 16 h at 37°C, and the HCaBP insert (782 bp) was gel isolated from a 1% agarose gel using the QIAquick Gel Extraction kit from QIAGEN. The pTrc99A vector was also doubly digested with *Xha*I and *Nco*I, purified on a QIAquick spin column (QIAGEN), and eluted with 45 μL MilliQ water. *Xha*I/*Nco*I-digested pTrc99A (~ 30 μg in 45 μL) was dephosphorylated by incubating with 5 μL of 10X dephosphate buffer (supplied with the phosphatase; MBI Fermentas) and 2 μL of alkaline phosphatase at 37 °C for 1 h. The dephosphorylated vector was purified using a QIAGEN PCR purification kit and eluted in 30 μL H_2O.

DNA Ligation: The HCaBP insert (~50 ng in 1 μL) was mixed with dephosphorylated pTrc99A vector (~50 ng in 2 μL), 2 μL of 5X sample buffer, and 5 μL of sterile H_2O. Then 10 μL of 2X ligase buffer and 1 μL of T4 DNA ligase (Roche) were added, and the ligation solution was incubated for 10 min at 22°C. Ligase inactivation is not recommended for the Rapid DNA Ligation Kit from Roche.

Transformation: Competent JM105 cells were prepared according to the Inoue method (*108*) as follows: A single JM105 colony was picked from a plate that had been incubated for 16-20 h at 37°C, transferred into 25 mL of LB media (prepared according to (*109*)) in a 250-mL flask, and incubated for 6-8 h at 37°C with vigorous shaking (250-300 rpm). To three 500-mL flasks containing 100 mL of SOB media (prepared according to (*109*)), 0.2 mL, 0.8 mL, and 1.6 mL of starter culture were added, and all three flasks were incubated at 18°C with shaking at 200 rpm. After ~15 h, the OD_{600} of the cultures was recorded and growth was continued until one of the cultures reached an OD_{600} of 0.55. This culture flask was transferred to an ice-water bath for 10 min and the two other cultures were discarded. The cells were harvested by centrifugation at 2500g for 10 min at 4°C. The supernatant was discarded and Kimwipes were used to remove any drops trapped in the necks of the centrifuge tubes to ensure that no liquid remained. The cells were gently resuspended in 30 mL of ice-cold Inoue transformation buffer (10 mM PIPES (pH 6.7), 55 mM $MnCl_2$, 15 mM $CaCl_2$, and 250 mM KCl) that was sterilized prior to use by filtration on a 0.22 μM filter (Millipore). The cells were harvested by centrifugation at 1500g for 10 min at 4°C. The supernatant was discarded carefully, and the cells resuspended gently in 8 mL of ice-cold Inoue transformation buffer. DMSO (0.6 mL) was added, the bacterial suspension was mixed by swirling, and stored on ice for 10 min. Working quickly, aliquots of the cell suspension were dispensed into sterile microfuge tubes that had been pre-chilled in an ethanol dry ice bath. The competent JM105 cells were stored at –80°C until use.

Between 1 and 10 μL of ligation mixture was added to transform 100 μL of competent JM105 cells. After addition of the foreign DNA, the cells were incubated on

ice for 30 min. The vial was then placed at 42°C for 30 s and immediately on ice for 2 min. This heat-shock treatment ensures that the DNA is transformed into the bacterial cells. SOC media (900 μL) prepared according to (*109*) was added and the cells were incubated for 45 min at 37°C with shaking at 200 rpm. To screen for ampicillin resistant colonies, the transformed *E. coli* were pelleted (2500g, 5 min), the supertnant (~800 μL) was decanted and the cells (~200 μL) were plated onto an agar plate containing ampicillin. The cells were grown overnight (~16 h) at 37°C.

Plasmid analysis: Twelve colonies were picked from a plate containing JM105 cells transformed with pTrc99A-HCaBP. The cells were transferred into twelve sterile culture tubes (Fisher) containing 3 mL of LB-ampicillin media. Cultures were grown overnight in an incubator-shaker at 37°C and 200 rpm, and 500 μL of culture from each tube was mixed with 500 μL of 50% sterilized glycerol, rapidly frozen in liquid N_2, and stored at –80°C. Plasmid DNA was extracted from 2.5 mL of each culture using the QIAGEN Plasmid Miniprep kit and eluted with 50 μL water from the spin columns. An aliquot of DNA from each colony was digested with both *Xha*I and *Nco*I. The digestion reaction was carried out using 5 μL of DNA, 1 μL of 10X buffer, 3 μL of H_2O, 0.5 μL of *Xha*I, and 0.5 μL of *Nco*I. Samples were incubated at 37 °C for 1 h and analyzed on a 0.8% agarose gel.

3.2.3.2 Cloning into the pET15b plasmid

PCR to engineer DNA insert: The nucleotide sequence of the open reading frame denoted as the HCaBP gene was retrieved from GenBank using accession number NM_004929. Primers P1 (5'-CAA CTC GAG ATG GCA GAA TCC CAC CTG-3') and P2 (5'-CAT TGG ATC CGT TAT CCC CAG CAC AG-3'), complementary to the 5'- and

3'- ends of the HCaBP gene, respectively, were constructed to allow the incorporation of flanking *Xho*I (underlined in P1) and *BamH*I (underlined in P2) restriction sites. The HCaBP gene was amplified by PCR from plasmid pGYMX-HCaBP using high fidelity Taq polymerase (Roche). This DNA fragment was cloned behind the *lac1* promoter (for expression in *E. coli*) in plasmid pET15b to create HCaBP with an N-terminal hexa-His-tag followed by a thrombin recognition site (Figure 3.3). A typical PCR reaction consisted of the following reagents in a reaction volume of 50 μL: 5 μL of 10X reaction buffer (Roche), 1 μL of each primer at 50 pmol/μL, 1 μL of 10 mM dNTP mix, 1 μL of DNA template (50 fmol/μL, 0.1~0.2 μg), 1 μL Taq DNA polymerase (2.5 μ/μL; Roche), and 40 μL of milliQ water. The conditions used for PCR were: cycle 1 (denaturation) 5 min at 94°C, then Taq DNA polymerase was added; cycles 2~31 (amplification) 1 min at 94°C, 1 min at 55-60 °C, 1 min at 72°C; cycle 32 (extension) 10 min at 72°C.

DNA digestion and purification: The PCR product was cleaned on a QIAquick spin column (QIAGEN), eluted with 30 μL H_2O, doubly digested with *Xho*I and *BamH*I restriction enzymes, and purified using a QIAGEN PCR purification kit again. The pET15b plasmid stored in DH5α was extracted using a QIAGEN Plasmid Maxiprep kit, doubly digested with *Xho*I and *BamH*I, purified using a QIAGEN PCR purification kit, and dephosphorylated as described in Section 3.2.3.1.

DNA ligation: The procedure was the same as that given in Section 3.2.3.1.

Transformation: Approximately 1~10 μL ligation mixture was used to transform 100 μL of competent BL21 or BL21(DE3)pLysS *E. coli* cells. The procedure was the same as that given in Section 3.2.3.1.

Plasmids analysis: The procedure was the same as that given in Section 3.2.3.1.

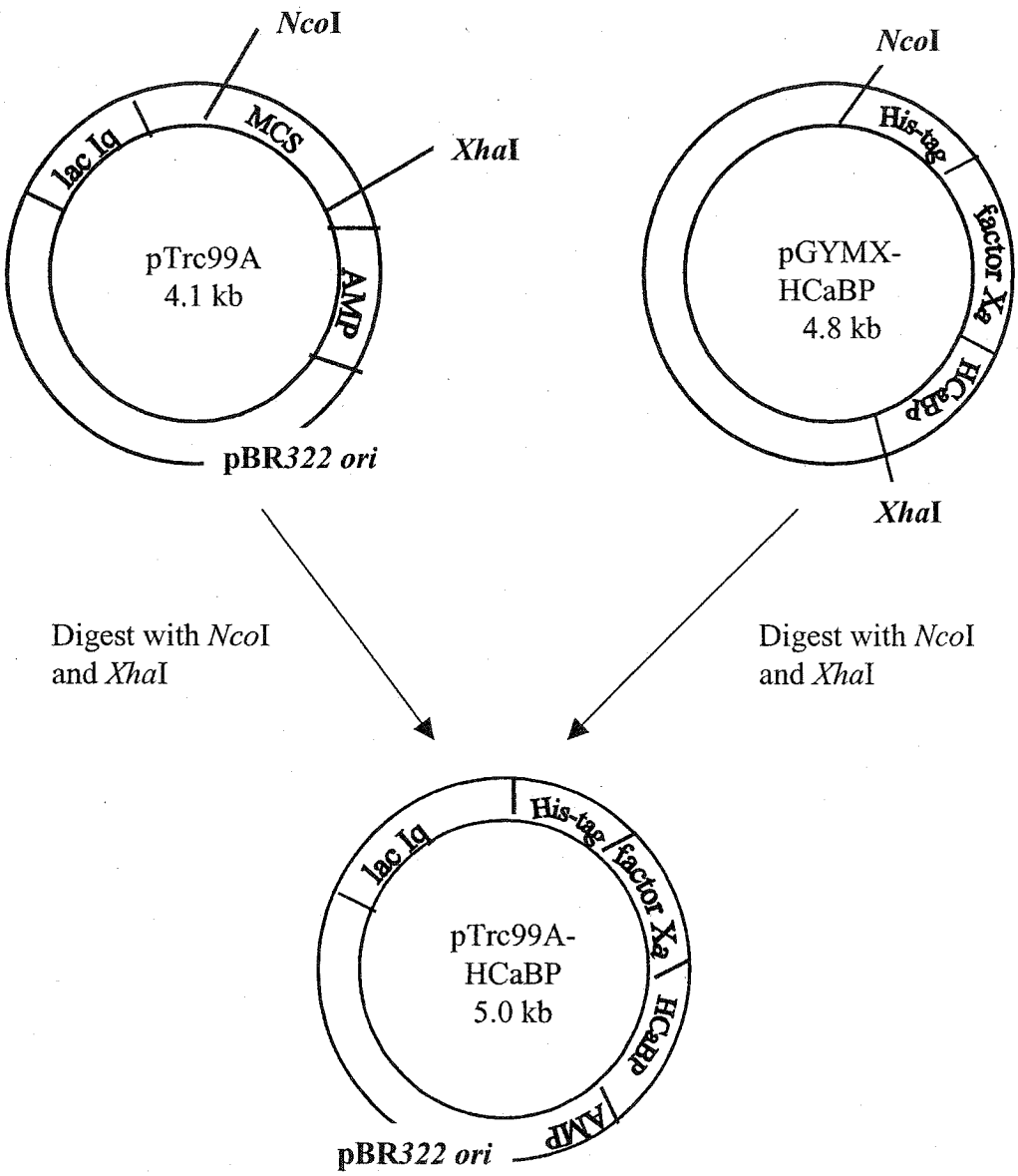

Figure 3.2. **Construction of pTrc99A-HCaBP.** MCS = multi-cloning site

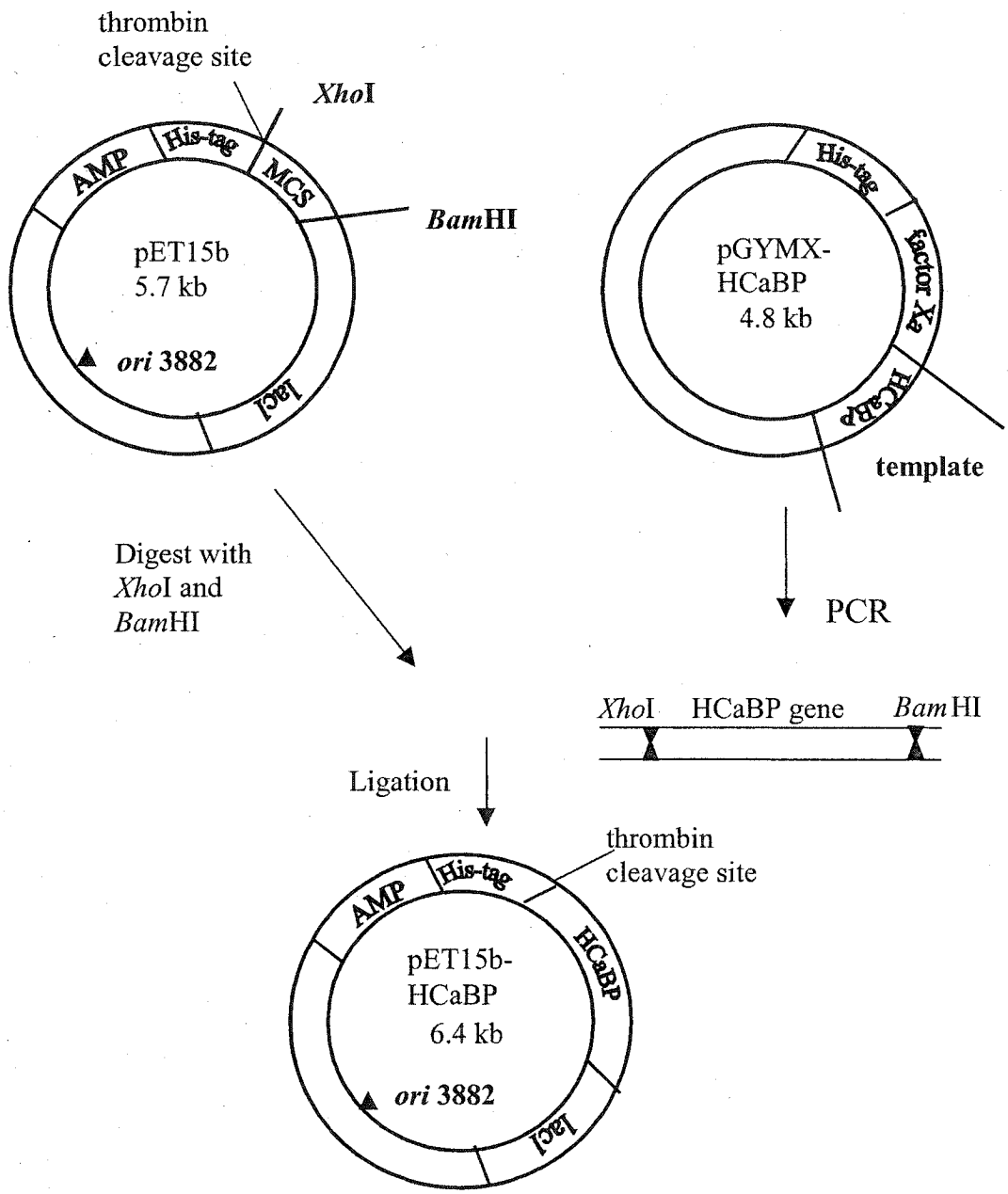

Figure 3.3. **Construction of pET15b-HCaBP.** MCS = multi-cloning site

3.2.3.3 Construction of pET15b-HCaBP(GSH)

P1 (Section 3.2.3.2) added 6 residues (GSHMLE) to the N-terminus of HCaBP following the thrombin cut site. Also, a stop codon (TAG) was erroneously omitted from P2. To add a stop codon at the end of the HCaBP gene and to decrease the number of amino acid residues added to the HCaBP N-terminus to 3 residues (GSH), two new primers were designed as follows: P3 (sense): 5'-ATA TGC TCC ATA TGG CAG AAT CCC ACC TG-3'; P4 (antisense): 5'-TAG GAT CCG GAT CAG TTA TCC CCA GC-3'. P3 and P4 are complementary to the 5'- and 3'- ends of the HCaBP gene, respectively, and allow the incorporation of the flanking restriction sites *Nde*I (underlined in P3) and *BamH*I (underlined in P4). The HCaBP gene was amplified by PCR from plasmid pET15b-HCaBP (Figure 3.3) using Taq DNA polymerase (Fermentas). pET15b-HCaBP(GSH) (Figure 3.4) was constructed using the steps described in Section 3.2.3.2.

3.2.3.4 DNA sequencing

The pET15b-HCaBP construct from Section 3.2.3.2 was sequenced in the Center for Structural and Functional Genomics (Concordia University). This was carried on a CEQ 2000XL DNA sequencer and the DNA was prepared from cells using a Promega Wizard™ plasmid preparation kit. The set of primers used for sequencing were: P5 (sense): 5'-GCA GCA GCC ATC ATC ATC ATC A-3' and P6 (antisense): 5'-CAA AAA ACC CCT CAA GAC CCG-3'. Since the first 10-50 bases in the sequence may be of poor quality due to the "salt front" the designed primers are ~50 bases away from the sequence frame. The CEQ 2000XL DNA sequencer can sequence on average 600 bases for each primer. Since the HCaBP gene is 786 bp, two primers are needed to cover the

coding sequence. Use of sense and antisence primers allows for maximum overlap of the regions sequenced (~400 bases) on each strand.

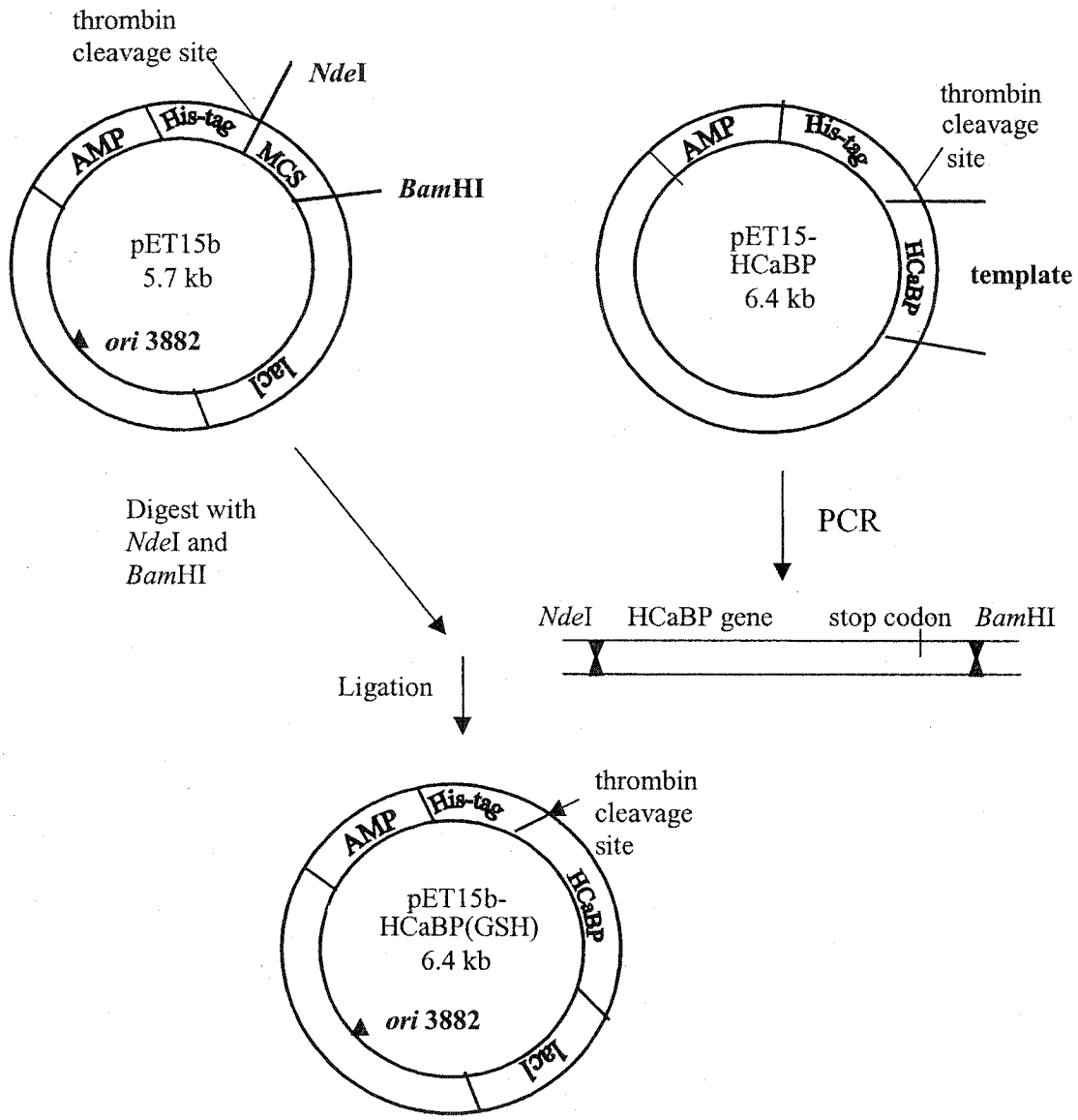

Figure 3.4. **Construction of pET15b-HCaBP(GSH).** MCS = multi-cloning site

3.2.4 Overexpression of rHCaBP

Frozen JM105 cells containing the pTrc99A-HCaBP plasmid were used to inoculate 50 mL of LB/ampicillin medium. The culture was grown at 37°C for ~14 h, and 10 mL were transferred to 1 L of LB/ampicillin and grown at 37°C until the OD_{600} reached 0.55~0.6. Then 1 mL of 1 M IPTG was added to 1 L of culture, and the cells were grown overnight (16~20 h). The cells were harvested at 6000g for 15 min at 4°C and frozen at –20°C until needed. Overexpression of HCaBP from BL21 or BL21(DE3)pLysS cells containing pET15b-HCaBP was carried out using the same procedure except that after adding IPTG, the culture was grown for only 3 h before the cells were harvested by centrifugation.

To check for protein expression, 3 mL of LB/ampicillin was added to 15-mL sterile culture tubes. Using a sterile pipet tip, a single bacterial colony was transferred from a freshly streaked plate into each tube containing 3 mL LB/ampicillin. The tubes were capped and placed in an incubator-shaker for 4 h at 37°C and 220 rpm. A 1-mL aliquot was removed for the uninduced control for each sample and 2 μL of 1 M IPTG was added to the remaining 2-mL samples, and the cells were grown for an additional 2 h before harvesting by centrifugation for 4 min at 13000g. The cells were washed with ice-cold phosphate buffer (pH 7.4) and resuspended in 300 μL of lysis solution (20 mM TrisHCl, pH 7.4). An equal volume of 0.5-mm glass beads was added and the samples were vortexed vigorously for 4X 30-s intervals with a 30-s break for cooling on ice between each vortexing. Cell debris was removed by centrifugation at 5000g for 10 s and the supernatants were transferred to pre-chilled (0°C) phosphate buffer containing DNAase. The tubes were incubated on ice for 6 min and then 10 μL of each supernatant

was mixed with 10 μL of 2X SDS sample loading buffer (see Section 3.2.6). The samples were heated at 95°C for 5 min, spun at 13000g for 1 min, and 18 μL of each supernatant was loaded on a 10% SDS gel for SDS-PAGE analysis.

3.2.5 Purification of His-tagged rHCaBP

Purification under native conditions: BugBuster Extraction Reagent (5 mL) was added per gram culture pellet to resuspend the cells. One μL (25 units) of Benzonase Nuclease was added per mL of BugBuster reagent, and one protease tablet per 50 mL solution. The cell suspension was incubated on a shaking platform at 10 rpm for 10-20 min at room temperature. Since Benzonase was added, the extract was not viscous at the end of the incubation. The insoluble cell debris was removed by centrifugation at 16,000g for 20 min at 4°C, and the supernatant was transferred to a fresh tube. Ni-NTA matrix (1 mL of matrix per 5-10 mg of His-tagged protein) in phosphate buffer was mixed with the supernatant. Imidazole was added to a final concentration of 5 mM, and the mixture rotated on a rotator for 1 h at 4°C. The sample was poured into an empty 20×2-cm column and the flow-through collected for SDS-PAGE analysis. The 1-mL Ni-NTA matrix bed was washed with 100 mL of wash buffer (20 mM sodium phosphate, 0.5 M NaCl, 5% glycerol, 10 mM β-mercaptoethanol, 5 mM imidazole, pH 7.4), followed by 15 mL of wash buffer with 10 mM imidazole, and then 15 mL of wash buffer with 50 mM imidazole. HCaBP was eluted with 3 mL of elution buffer (20 mM sodium phosphate, 0.5 M NaCl, 5% glycerol, 10 mM β-mercaptoethanol, 300 mM imidazole, pH 6.0) and aliquots of 1 mL were collected. Finally, the matrix bed was washed with 2 mL of elution

buffer with 200 mM imidazole (i.e., 500 mM imidazole total). SDS-PAGE was used to monitor each step of the purification.

Purification under denaturing conditions: His-tagged HCaBP was also purified under denaturing conditions according to the procedure in the QIAexpressionist (*94*). Briefly, cells were lysed in buffer A (100 mM sodium phosphate, 10 mM TrisHCl, 8 M urea, pH 8.0). Following centrifugation the supernatant was mixed with the Ni-NTA matrix and the sample was poured on the 20×2-cm column as described above. The matrix bed was washed successively with 4 bed volumes of each of buffers B, C and D (buffers B, C and D were prepared by adjusting buffer A to pH 6.3, 5.9 and 4.5, respectively, with HCl). Fractions from each step were collected for SDS-PAGE analysis.

Removal of the His-tag: The His-tag was cleaved by factor Xa in HCaBP expressed in JM105 cells since there is a factor Xa recognition site [IE(or D)GR↑] between the N-terminal hexa-His-tag and the protein. The Ni-NTA purified protein was dialyzed against 20 mM TrisHCl (pH 8.0) containing 100 mM NaCl and 2 mM $CaCl_2$, and digested with 100:1 (w/w) protein to factor Xa (Promega) for 18 h at room temperature to remove the His-tag. Any remaining His-tagged HCaBP was removed by rebinding the sample to the Ni-NTA beads.

The His-tag was cleaved by thrombin in HCaBP expressed in the BL21 cell types since there is a thrombin recognition site [LVPR↑GS] following the N-terminal hexa-His-tag. The Ni-NTA purified protein was incubated with thrombin at a protein to thrombin ratio of 1000:1 (w/w) in a dialysis tube (MW cut off 12-14 kDa) and dialyzed overnight at 4°C against 3 changes of 20 mM TrisHCl (pH 7.4) containing 100 mM NaCl, 0.1 mM $CaCl_2$, and 5 mM β-mercaptoethanol. The thrombin-treated sample was

reapplied onto the Ni-NTA column (pre-equilibrated with dialysis buffer) to remove any tagged protein remaining.

3.2.6 SDS-polyacrylamide gel electrophoresis

Denaturing SDS-PAGE was performed on 10% acrylamide gels (3.3 mL of 30% acrylamide/bis-acrylamide, 2.5 mL of 1.5 M TrisHCl pH 8.8, 100 μL of 10% SDS, 4.05 mL of H_2O, 5 μL of N,N,N',N'-tetramethylethylene diamine, and 50 μL of 10% ammonium persulfate) and 4% stacking gels (0.66 mL of 30% acrylamide/bis-acrylamide, 1.26 mL of 0.5 M TrisHCl pH 6.8, 50 μL of 10% SDS, 3 mL of H_2O, 5 μL of N,N,N',N'-tetramethylethylene diamine, 25 μL of 10% ammonium persulfate). Protein samples were diluted with 2X SDS-sample loading buffer (2.4 mL of 0.5 M TrisHCl pH 6.8, 2.0 mL of glycerol, 4.0 mL of 10% SDS, 0.5 mL of 0.2% bromophenol blue, and just before use 50 μL/mL of β-mercatoethanol was added when reducing conditions were required) and incubated in a heat block for 5 min at 95°C prior to loading on the gel. The gel (10×7 cm) was run in running buffer (192 mM glycine, 25 mM Tris-base, 0.1% SDS, pH 8.3) in a BIO-RAD Mini-PROTEAN® II Cell under constant current at 30-60 V. Protein MW markers (MBI Fermentas) were used to estimate the molecular weight of proteins in the samples. Proteins were visualized by staining the gels with Gel Code Blue stain reagent.

3.6.7 Mass spectrometry

Electrospray ionization mass spectrometry (ESI-MS) was carried out on a Waters Micromass QTOF2 mass spectrometer. Protein samples were exchanged into water on NAP-5 gel-filtration columns, concentrated by ultrafiltration using Ultrafree-0.5 centrifugal filters, and added to 60 μL of 50% acetonitrile/0.2% formic acid to give a final protein concentration of 1-2 μM. Samples were directly infused into the Z-spray

source of the QTOF2 at a flow rate of 1 μL/min. Mass calibration was carried out using human [Glu^1]-fibrinopeptide B. Protein mass spectra were deconvoluted using MaxEnt 1 software (Waters Micromass).

3.3 Results

3.3.1 Construction of pTrc99A-HCaBP, pET15b-HCaBP and pET15b-HCaBP(GSH) vectors.

pTrc99A-HCaBP vector: After digestion and ligation, HCaBP with a N-terminal His-tag and factor Xa recognition site was cloned into *Xha*I and *Nco*I sites of pTrc99A from pGYMX (Figure 3.2). As shown in Figure 3.5, after digestion the expected open pTrc99A vector and HCaBP gene were observed on the gel. The gel-isolated HCaBP DNA and the open phosphorylated pTrc99A vector were ligated and transformated into *E. coli* JM105 competent cells. Plasmid DNA from twelve colonies was analyzed by digestion with *Xha*I and *Nco*I as shown in Figure 3.6. The desired construct was present in all colonies since the expected 4.1-kb (pTrc99A) and 847-bp (HCaBP) fragments are seen in lanes 1-12 in Figure 3.6.

pET15b-HCaBP vector: PCR was used to introduce *Xho*I and *BamH*I sites at the 5'- and 3'-ends of the HCaBP sequence for cloning into pET15b. Digestion of pET15b and the HCaBP PCR fragment with *Xho*I and *BamH*I yielded the expected 5.7-kb open vector and 789-bp fragment (Figure 3.7). Following transformation and growth of the BL21 *E. coli* transformants overnight, 12 colonies were picked and *Xho*I and *BamH*I double digestions were performed. Figure 3.8 shows that most of the colonies contained the expected 789-bp HCaBP insert and 5.7-kb pET15b vector.

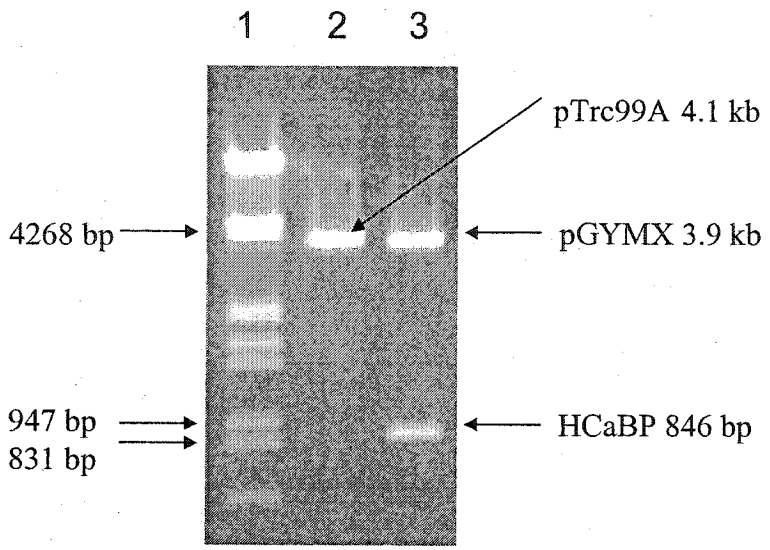

Figure 3.5. **Analysis of the DNA fragments from the restriction digestions of pTrc99A-HCaBP and pGYMX-HCaBP.** Lane 1, MW markers (564–21226 bp); lane 2, pTrc99A cut with *Nco*I and *Xba*I; lane 3, pGYMX-HCaBP cut with *Nco*I and *Xba*I. Analysis was carried out on a 1% agarose gel.

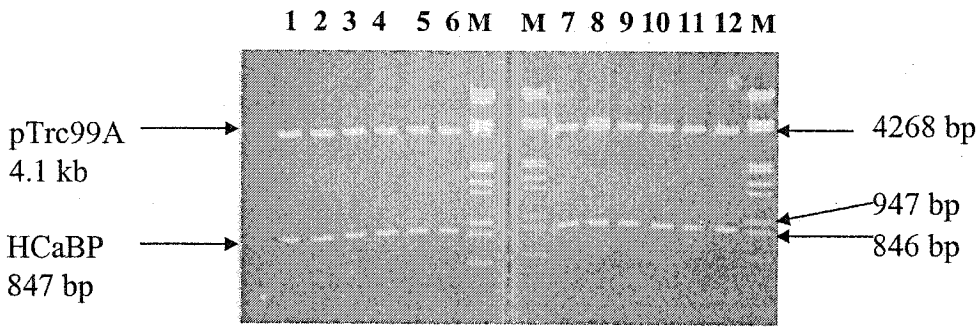

Figure 3.6. **Restriction analysis of the plasmids isolated from JM105 *E. coli* cells transformed with pTrc99A-HCaBP.** The plasmids were digested by *Nco*I and *Xba*I. Lanes 1-12, DNA fragments from 12 colonies; lane M, MW markers (564–21226 bp). Analysis was carried out on a 1% agarose gel.

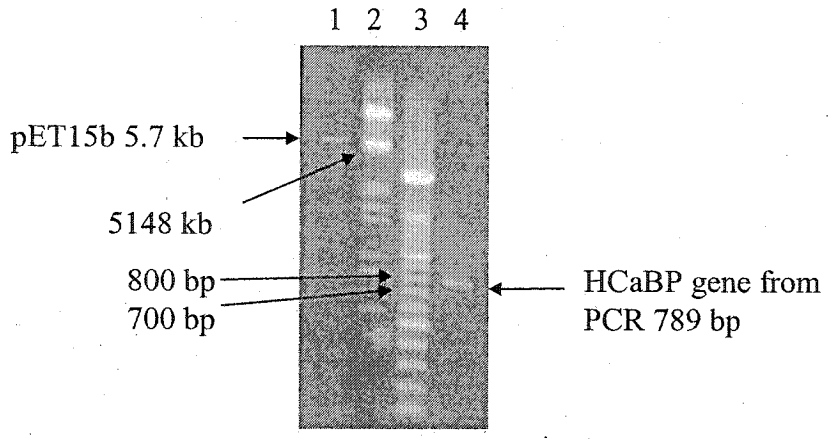

Figure 3.7. **Analysis of the DNA fragments from PCR and pET15b following restriction digestion by *Xho*I and *BamH*I.** Lane 1, pET15b cut with *Xho*I and *BamH*I; lane 2, MW markers (564–21226 bp); lane 3, MW markers (100-2072 bp); lane 4, PCR fragment cut with *Xho*I and *BamH*I. Analysis was carried out on a 1% agarose gel.

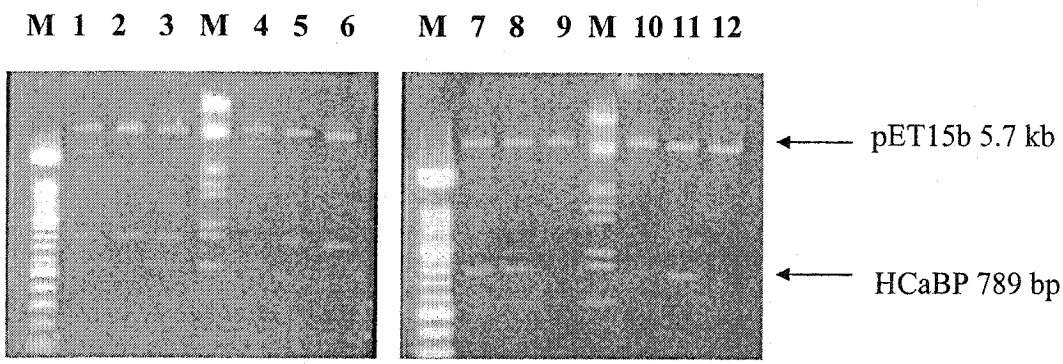

Figure 3.8. **Restriction analysis of the plasmids isolated from BL21 *E. coli* cells transformed with pET15b-HCaBP.** The plasmids were digested by *Xho*I and *BamH*I prior to analysis on 1% agarose gel. Lanes 1-12, DNA fragments from 12 colonies, lane M, MW markers (100-2072 bp).

Construction of pET15b-HCaBP(GSH): This construct was prepared to add a stop codon at the end of the HCaBP gene, and to eliminate some of the extra amino acid residues at the N-terminus of the protein in pET15b-HCaBP. *Nde*I and *BamH*I restriction sites, and a stop condon were introduced by PCR at the 5'- and 3'-ends of the HCaBP gene. The PCR step yielded the expected 808-bp fragment (Figure 3.9). The doubly digested (*Nde*I and *BamH*I) PCR fragment and pET15b vector were ligated (Figure 3.4), and plasmids were isolated from 14 colonies. Restriction analysis (Figure 3.10) shows that most of the colonies selected contained the expected 795-bp HCaBP insert and the 5.7-kb pET15b vector.

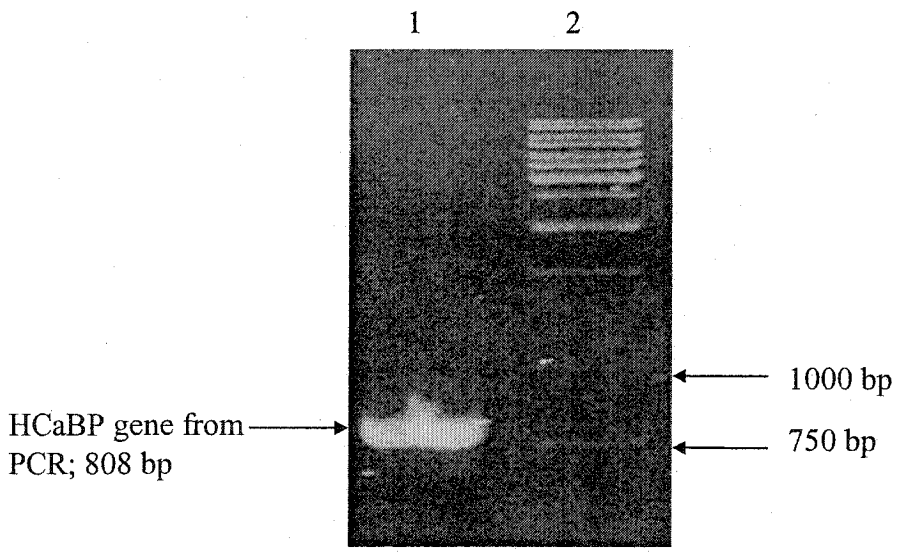

Figure 3.9. **Analysis of the DNA fragments from PCR of HCaBP(GSH).** Lane 1, PCR fragment; lane 2, MW markers (250-10000 bp). Analysis was carried out on a 1% agarose gel.

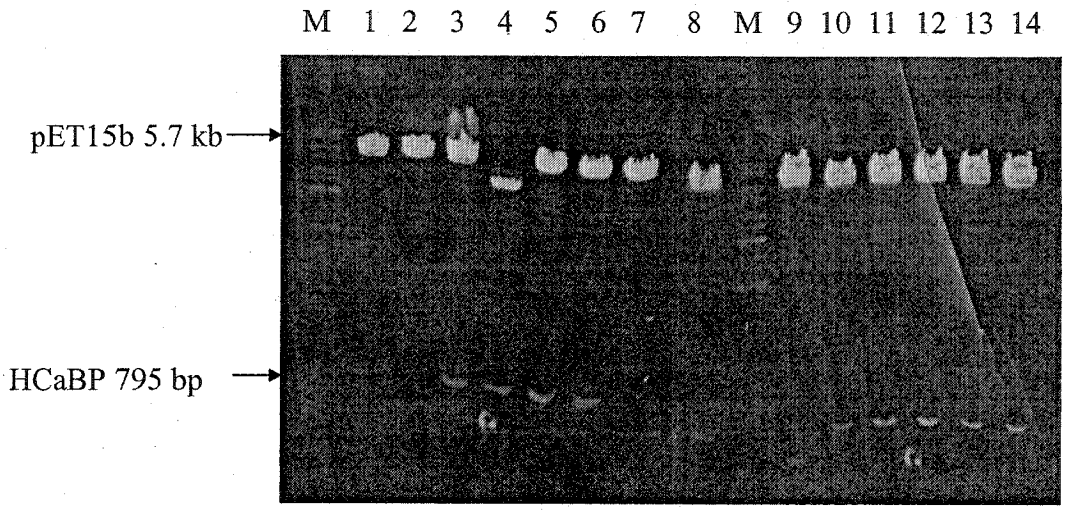

Figure 3.10. **Restriction analysis of the plasmids isolated from BL21(DE3)pLysS *E. coli* cells transformed with pET15b-HCaBP(GSH).** The plasmids were digested by *Nde*I and *BamH*I prior to analysis on a 1% agarose gel. Lanes 1-14, DNA fragments from 14 colonies; lane M, MW markers (250-10000 bp).

3.3.2 Overexpression and purification of rHCaBP

Expression from pTrc99A-HCaBP: JM105 cells transformed with pTrc99A-HCaBP were used to inoculate 1 L of LB/ampicillin media. At an OD_{600} of 0.55-0.8 the culture was induced with IPTG to express the fusion protein as outlined in Section 3.2.4. Approximately 4-5 g of cell pellet was obtained per litre of culture. The proteins in the lysate, pellet and supernatant from the incubate with BugBuster, Benzonase Nuclease, and protease tablet were analyzed by SDS-PAGE. Most of the fusion protein was present in the supernatant as expected for a soluble protein such as HCaBP. The His-tag was cleaved by factor Xa and any remaining His-tagged rHCaBP was removed by rebinding the sample to the Ni-NTA beads (Section 3.2.5).

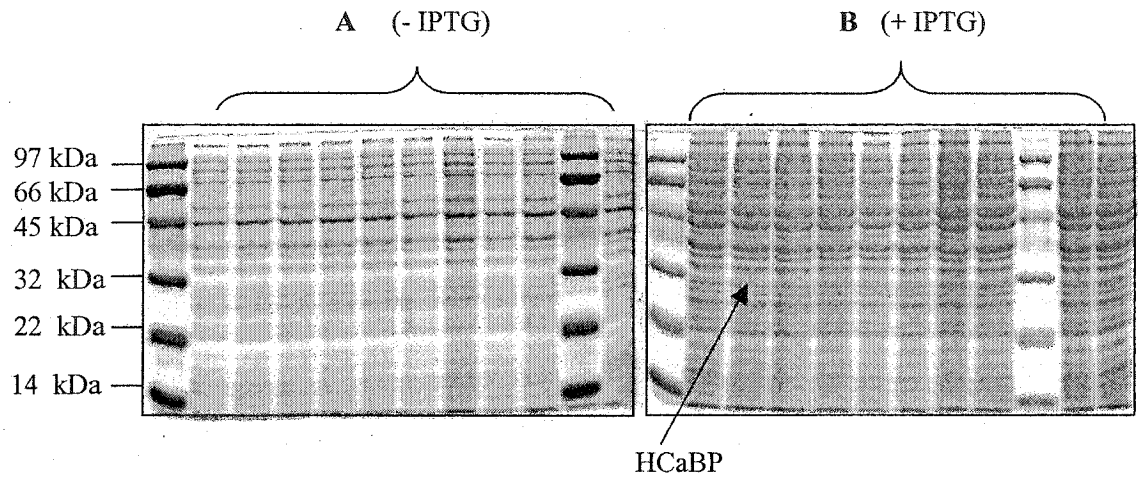

Figure 3.11 **SDS-PAGE (10%) analysis of HCaBP expression in JM105 *E. coli* cells.** Ten colonies of JM105 cells transformed with pTrc99A-HCaBP were used to inoculate 3 mL of LB/ampicillin media (Section 3.2.4). Cells were grown for 2 h, ITPG was added to each tube and the cells grown for an additional 2 h. Proteins in the whole-cell lysates were analyzed by 10% SDS-PAGE under reducing conditions. **(A)** Proteins in whole-cell lysates after 2 h growth. **(B)** Proteins in whole-cell lysates after 2 h induction with ITPG. A band containing HCaBP (MW = 31721 Da) is seen in (B) but not in (A).

From Figure 3.11B we can see that after 2 h induction with IPTG, HCaBP is over expressed. After overnight induction (16 h) and Ni-NTA purification, ~15 mg HCaBP per liter of culture was obtained with 84% purity (Figure 3.12). After the His-tag was cleaved and the protein was passed through the Ni-NTA column again, the purity increased (Figure 3.13, lane 2 *vs* lane 5) to 93% and the yield was 9-12 mg/L of culture. The impurities, which have a high affinity for Ni-NTA were bound to the column (lanes 8 and 9) but the His-tag-free HCaBP was in the flow-through (lanes 5-7).

Since HCaBP is a calcium-binding protein, different concentrations of $CaCl_2$ were added to the LB media to determine the effects on protein expression. Figure 3.14 shows that adding 1-50 mM $CaCl_2$ to the media did not change the level of HCaBP expression.

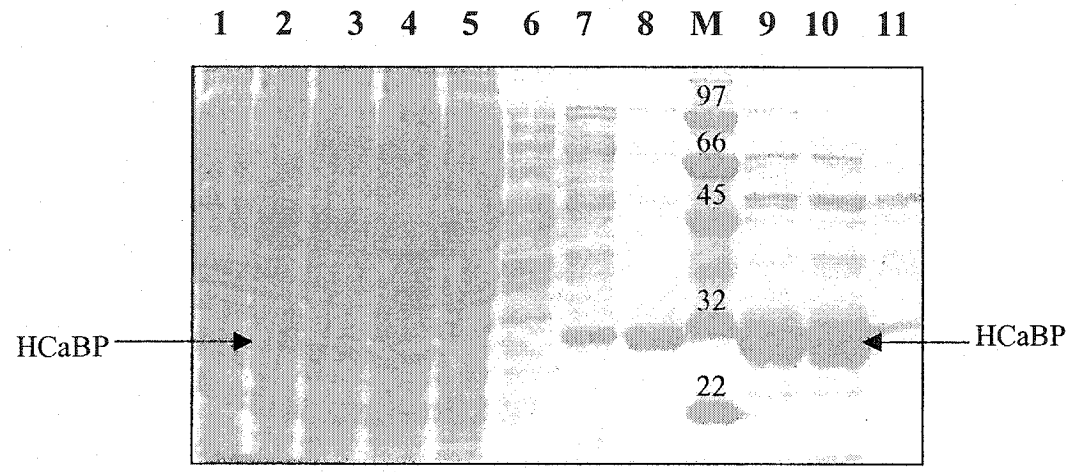

Figure 3.12. **SDS-PAGE (10%) analysis of HCaBP purification from JM105 *E. coli* cells.** Analysis was performed under reducing conditions on a 10% polyacrylamide gel. Lane 1, uninduced whole-cell lysate; lanes 2 and 3, lysates of cells induced by IPTG; lane 4, supernatant of sample in lane 2; lane 5, Ni-NTA column flow-through; lane 6, 5 mM imidazole wash; lane 7, 25 mM imidazole wash; lane 8, 50 mM imidazole wash; lane M, MW standards (in kDa); lanes 9 and 10, 300 mM imidazole eluate; lane 11, 500 mM imidazole eluate.

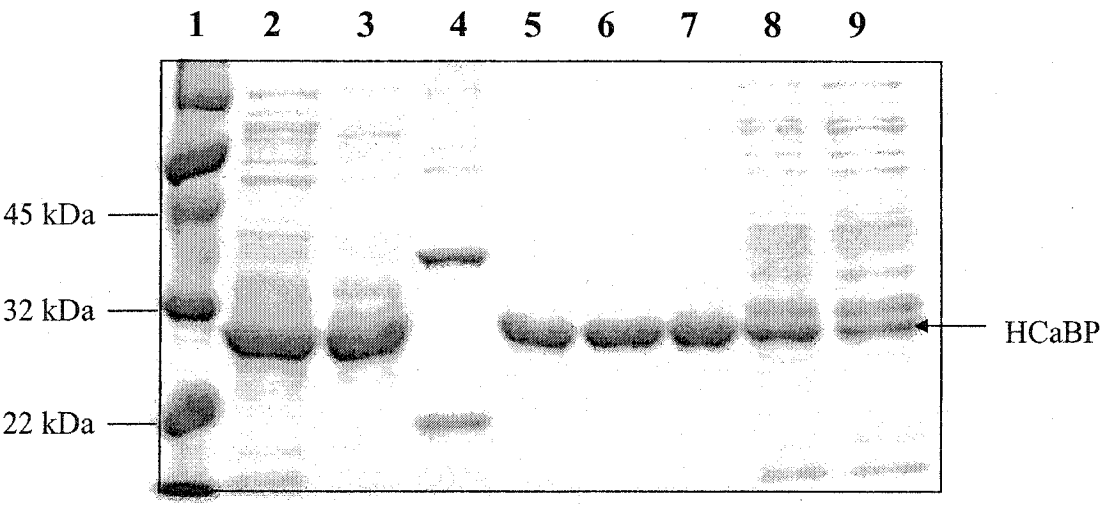

Figure 3.13. **SDS-PAGE (10%) analysis of tag cleavage from His-tagged HCaBP.** Analysis was performed under reducing conditions for all the samples except that in lane 7. Lane 1, MW standards; lanes 2 and 3, 300 mM imidazole eluate from Ni-NTA column; lane 4, factor Xa cleavage control containing a protein, which is cleaved by factor Xa into 32-kDa and 17 kDa; lanes 5 and 6, Ni-NTA column flow-through after His-tagged HCaBP was cleaved by factor Xa; lane 7, sample in lanes 5 and 6 under non-reducing conditions (i.e., no β-mecaptoethanol); lanes 8 and 9, 500 mM imidazole eluate.

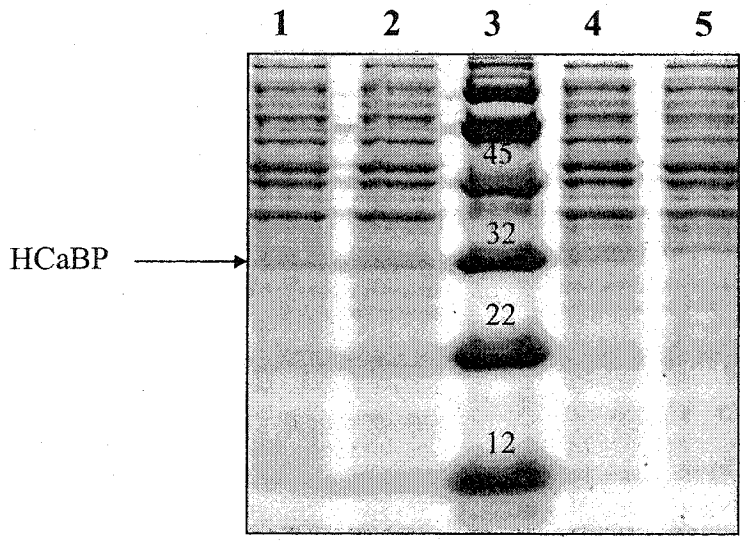

Figure 3.14. **SDS PAGE (10%) analysis of HCaBP expression in JM105 *E. coli* cells in the presence of added $CaCl_2$.** JM105 cells transformed with pTrc99A-HCaBP were grown in LB media with 50 mM $CaCl_2$ (lane 1); 5 mM $CaCl_2$ (lane 2); 1 mM $CaCl_2$ (lane 4). MW standards (in kDa) and control (JM105 cells without pTrc99A-HCaBP and without added $CaCl_2$) are in lanes 3 and 5, respectively.

Expression from pET15b-HCaBP in BL21 cells: HCaBP expression was not detected in the BL21 cell line (Figure 3.15A, lane 8). Changing the IPTG-induction time (1 h, 2 h, 4 h, 5 h and 16 h; data not shown) or purifying the protein under denaturing conditions (Figure 3.15B), did not lead to the detection of HCaBP in the BL21 lysates.

Expression from pET15b-HCaBP(GSH) in BL21(DE3)pLysS cells: BL21(DE3)pLysS cells highly overexpress HCaBP(GSH) (Figure 3.16, lane 2) unlike the BL21 cells (Figure 3.15, lane 1). A purity of >95% with a HCaBP yield of ~34 mg /L of culture was obtained (Figure 16, lane 10).

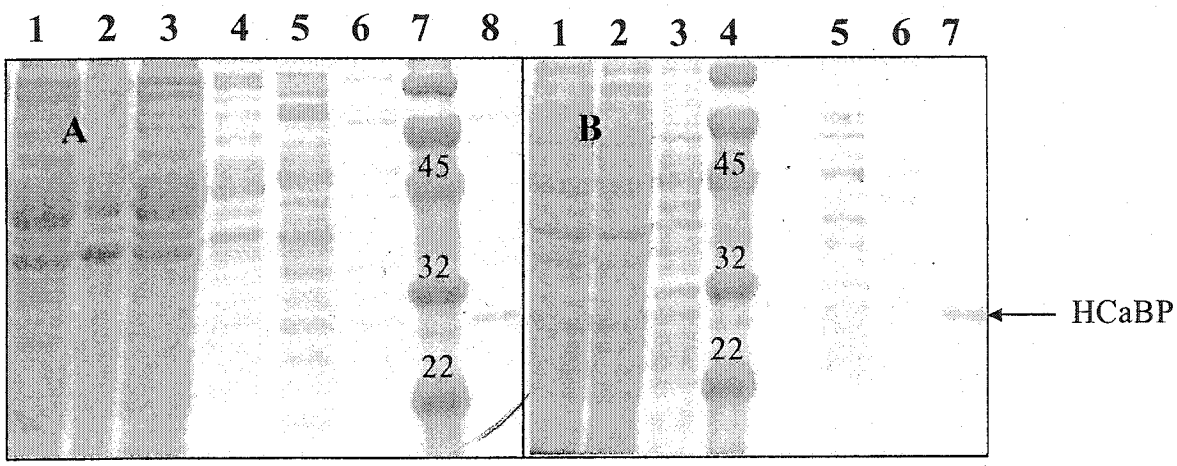

Figure 3.15. **SDS-PAGE (10%) analysis of HCaBP expression in BL21 *E. coli* cells.** Analysis was performed under reducing conditions on a 10% polyacrylamide gel. **(A)** Ni-NTA purification under native conditions (see Section 3.2.5). Lane 1, supernatant from BL21 cell lysate; lane 2, pellet from BL21 cell lysate; lane 3, column flow-through; lane 4, 5 mM imidazole wash; lane 5, 25 mM imidazole wash; lane 6, 50 mM imidazole wash; lane 7, MW standards; lane 8, 300 mM imidazole elute. **(B)** Ni-NTA purification under denaturing conditions (see Section 3.2.5). Lane 1, supernatant from BL21 cell lysate; lane 2, column flow-through; lane 3, first pH 6.3 wash; lane 4, MW standards; lane 5, second pH 6.3 wash; lane 6, pH 5.9 wash; lane 7, pH 4.5 eluate.

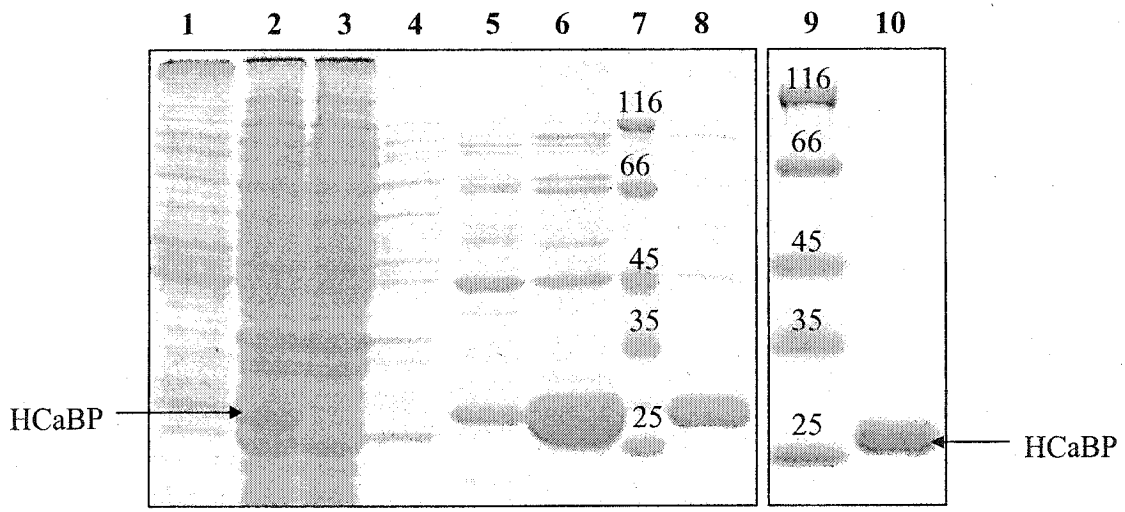

Figure 3.16. **SDS-PAGE (10%) analysis of HCaBP(GSH) expression in BL21(DE3)pLysS *E. coli* cells.** Analysis was performed under reducing conditions on a 10% polyacrylamide gel. Lane 1, pellet from cell lysate; lane 2, supernatant from cell lysate; lane 3, Ni-NTA column flow-through; lane 4, 5 mM imidazole wash; lane 5, 20 mM imidazole wash; lane 6, 50 mM imidazole elute; lane 7, MW standards (in kDa); lane 8, 300 mM imidazole eluate; lane 9, MW standards (in kDa); lane 10, Ni-NTA column flow-through after His-tagged HCaBP was cleaved by factor Xa.

3.3.3 Analysis of constructs

Molecular weight of HCaBP expressed from pTrc99A-HCaBP in JM105 cells: Since the HCaBP gene was directly transferred from pGYMX-HCaBP to pTrc99A-HCaBP (Figure 3.2), the integrity of the construct was established by measuring the mass of the purified protein. The deconvoluted ESI mass spectrum of His-tagged HCaBP exhibits a single peak with M_r 31722 ± 2 Da. This corresponds to the average mass predicted from the native HCaBP sequence (*38*) plus the His-tag ($MATSH_6IEGRAS$) minus the initial methionine (M). After removing the His-tag the deconvoluted ESI mass spectrum of HCaBP exhibits a single peak with M_r 30183 ± 3 Da. This corresponds to the average mass predicted for the native HCaBP sequence (*38*) plus two amino acids (AS).

Sequence of the HCaBP gene from pET15b-HCaBP-BL21: The sequence of the HCaBP gene in the pET15-HCaBP vector was found to be identical to that published for HCaBP (GenBank accession number NM_004929).

Molecular weight of HCaBP from pET15b-HCaBP(GSH)-BL21(DE3)pLysS: The construction correctness was confirmed by detecting the mass of the purified protein. The deconvoluted ESI mass spectrum of His-tagged HCaBP exhibits a major peak with M_r 32057 ± 5 Da. This corresponds to the average mass predicted from the native HCaBP sequence (*38*) plus the His-tag ($MGSSH_6SSGLVPRGSH$) minus the initial methionine (M). The deconvoluted ESI mass spectrum of HCaBP after His-tag removal exhibits a single peak with M_r 30306 ± 4 Da. This corresponds to the average mass predicted from the native HCaBP sequence (*38*) plus three amino acids (GSH). Hence, this recombinant form of HCaBP is denoted as HCaBP(GSH).

3.3.4 Free thiols in HCaBP and analysis of disulfide formation

HCaBP expressed from pTrc99A-HCaBP-JM105 contained a different number of free thiols with and without the His-tag. His-tagged rHCaBP possesses 5 free thiols as determined by 5,5'-dithiolbis(2-nitrobenzoic acid) (DTNB) titration (Table 4.1) and modification by the thiol specific reagent, N-ethylmaleimide (NEM). However, after removal of His-tag only 1-3 free thiols were detected. The reason for this discrepancy is not clear, but it is assumed that it arises because the free thiols were not protected from oxidation during His-tag cleavage by factor Xa. HCaBP expressed from pET15b-HCaBP(GSH)-BL21(DE3)pLysS was protected from oxidation by the addition of β-mercaptoethanol (see Section 3.2.5) during the whole protein purification process. The number of free thiols was determined following incubation with NEM. The ESI mass spectra in Figure 3.17 show that both His-tagged HCaBP(GSH) and HCaBP(GSH) without the His-tag are modified by 5 NEM groups, indicating that both forms of the protein possess 5 free thiols.

HCaBP is reported to have a propensity to form disulfide crosslinks (*107*). To detect how readily HCaBP(GSH) dimerizes, ~20 μM protein was incubated in 20 mM TrisHCl/1 mM $CaCl_2$ in the absence of any reductants at room temperature for up to 24 h. Figure 3.18 shows that over 24 h neither His-tagged HCaBP(GSH) nor HCaBP(GSH) formed detectable dimers.

3.4 Discussion

The three HCaBP expression systems examined here are summarized in Table 3.1. From this work, we can see that HCaBP is toxic to *E. coli*. BL21 cells only express a

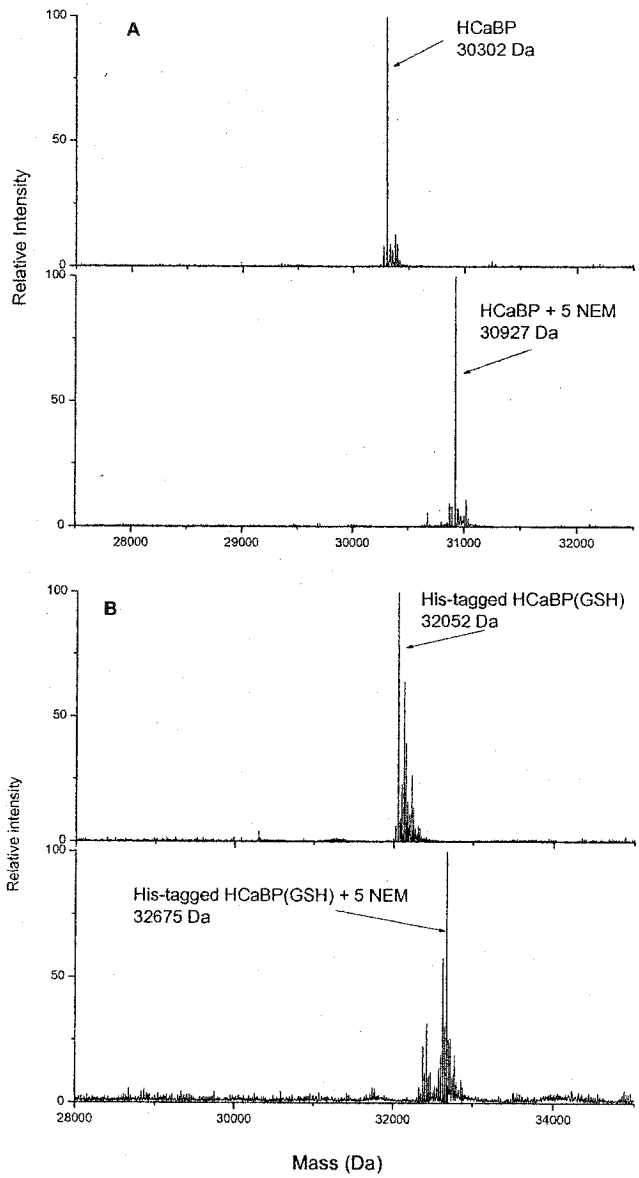

Figure 3.17 **ESI-MS analysis of HCaBP(GSH) before and after incubation with NEM.** Protein samples were incubated with 50-fold molar excess NEM in 20 mM TrisHCl with 1 mM $CaCl_2$ for 30 min at room temperature, exchanged into water on a NAP-5 column, concentrated by ultrafiltration, added to 50% acetonitrile/0.2% formic acid to give a final protein concentration of 1-2 μM, and directly infused into the Z-spray source of the QTOF2 mass spectrometer at a flow rate of 1 μL/min. **(A)** 18.6 μM HCaBP(GSH) before (upper spectrum) and after (lower spectrum) incubation with NEM. **(B)** 19.9 μM His-tagged HCaBP(GSH) before (upper spectrum) and after (lower spectrum) incubation with NEM. The instrumental parameters were: capillary voltage 3.8 kV, cone voltage 45 V, multiplier 550 V, MCP 2100 V and TOF – 9.1 kV.

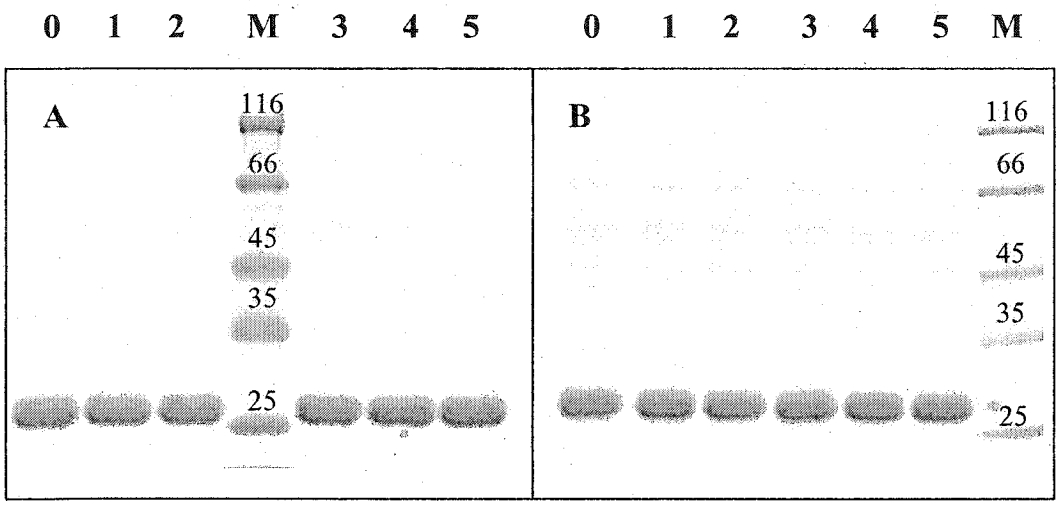

Figure 3.18. **SDS-PAGE (10%) analysis of HCaBP(GSH) dimerization. (A)** 18.6 μM HCaBP(GSH) and **(B)** 19.9 μM His-tagged HCaBP(GSH) were incubated in 20 mM TrisHCl with 1 mM $CaCl_2$ at room temperature for 0 h (lane 0), 1 h (lane 1), 2 h (lane 2), 4 h (lane 3), 7 h (lane 4), and 24 h (lane 5). MW markers were run in lanes M. Analysis was performed under non-reducing conditions on a 10% polyacrylamide gel.

Table 3.1 **HCaBP expression systems examined here**

Vector	cell line	tag cut site	purity	yield (mg/L culture)
pTrc99A-HCaBP	JM105	factor Xa	93%	9
pET15b-HCaBP	BL21	thrombin	–	<1
pET15b-HCaBP(GSH)	BL21(DE3)pLysS	thrombin	>93%	34

very small amount of HCaBP (Figure 3.15) when transformed with pET15b-HCaBP. JM105 cells transformed with pTrc99A-HCaBP express ~9 mg purified protein per liter of culture, but HCaBP is not the most highly expressed protein in the cells (Figure 3.12).

The BL21(DE3)pLysS cell line provides tigher control of protein expression for the production of toxic proteins (*110*). HCaBP(GSH) is the most abundance protein expressed in pET15b-HCaBP(GSH)-transformed BL21(DE3)pLysS cells (Figure 3.16), yielding 34 mg/L of culture of purified HCaBP(GSH).

HCaBP has 5 free thiols and forms disulfide crosslinks (*107*). Thiol modification is the focus of this thesis, so it is important to keep all the thiols in their reduced state during protein purification. The pTrc99A-HCaBP expression vector possesses a factor Xa cut site, but factor Xa is inactivated by thiols such as DTT (*105*) and high concentrations of imidazole (*106*). The pET15b-HCaBP expression vector has a thrombin cut site, and as confirmed here thrombin is active in 5 mM β-mercaptoethanol and high concentration of imidazole.

The advantages mentioned in the previous paragraph make BL21(DE3)pLysS-pET15b-HCaBP an excellent HCaBP expression system. The published purification procedures for the recombinant forms of rat (*99*) and HCaBP (*101*) include several steps and harsh conditions such as heating to 75°C and exposure to low pH buffer. Purified recombinant rat CaBP (*99*) contained 5% of a degradation product plus higher molecular-weight aggregates. The HCaBP purification procedure used by Thulin and Linse sometimes causes protein precipitation and dimerization (E. Thulin, personal communication). The BL21(DE3)pLysS-pET15b-HCaBP(GSH) system described here produces purified His-tagged HCaBP in a single affinity chromatography step. Cleavage

of the His-tag with thrombin yields HCaBP(GSH) with >95 % purity and >30 mg of protein per liter of culture. This method is fast and economical, and what is most important is that all the free thiols in HCaBP(GSH) are protected from oxidation during the isolation procedure. Both His-tagged HCaBP(GSH) and HCaBP(GSH) possess 5 free thiols and no dimerization was observed in solution containing ~20 μM protein over 24 h at room temperature in the absence of reductant (Figure 3.18).

3.5 Forms of rHCaBP used in this thesis

Since the expression, isolation, purification and characterization of rHCaBP(GSH) was only recently completed, this form of HCaBP was not available for the studies described in Chapters 4-6 of this thesis.

His-tagged rHCaBP expressed in JM105 *E. coli* cells and purified at UBC was used to carry out the research described in Chapters 4 and 5. rHCaBP expressed in JM105 *E. coli* cells in our lab was used for the rHCaBP experiments described in Chapter 6.

4.0 S-nitrosation of Ca^{2+}-loaded and Ca^{2+}-free recombinant calbindin D_{28K} from human brain (rHCaBP)

4.1 Abstract

HCaBP is noted for its abundance and specific distribution in mammalian brain and sensory neurons. It can bind 3 to 5 Ca^{2+} ions and may act as a Ca^{2+} buffer to maintain intracellular Ca^{2+} homeostasis, but its exact role is still unknown. In the present study, mass spectrometric analysis reveals that the 5 cysteine residues in recombinant rHCaBP are derivatized with N-ethylmaleimide, consistent with the determination of 5.3 ± 0.4 and 4.7 ± 0.4 free thiols in the protein using the thiol specific reagents, 5,5'-dithio-bis(2-nitrobenzoic acid) and 5-(octyldithio)-2-nitrobenzoic acid, respectively. The results of UV-Vis and circular dichroism absorption, intrinsic fluorescence and mass spectrometry measurements indicate that both Ca^{2+}-loaded (*holo*) and Ca^{2+}-free (*apo*) rHCaBP are S-nitrosated by S-nitrosocysteine (CysNO). The number of cysteine residues S-nitrosated in *holo*rHCaBP and *apo*rHCaBP are 2.6 ± 0.05 and 4.4 ± 0.09, respectively, as determined by the Saville assay. HolorHCaBP also undergoes S-nitrosation at 1-3 cysteine residues when exposed to S-nitrosoglutathione (GSNO), and Cys100 was found to be an S-nitrosation site by peptide mass mapping. Treatment of *holo*rHCaBP with free NO resulted in a mass increase of 59 ± 2 Da, corresponding to two NO adducts. Since up to four cysteine residues can be S-nitrosated in rHCaBP, it is proposed that the protein may act as a NO buffer or reservoir in the brain in a manner similar to serum albumin in blood. It is significant in this context that rHCaBP is found coexistent with nitric oxide synthase

in the cerebellum, and that S-nitrosation varies with Ca^{2+}-binding, with S-nitrosation occurring to a greater extent in *apo*rHCaBP than in the *holo*protein. Furthermore, exposure of rHCaBP to either CysNO or GSNO also leads to rapid S-thiolation of Cys187. We demonstrate here for the first time that intrinsic protein fluorescence is a sensitive probe of protein S-nitrosation. This is due to efficient Förster energy transfer ($R_0 \sim 17$ Å) between tryptophan donors and S-nitrosothiol acceptors.

4.2 Introduction

Calbindin D_{28k}, also known as Ca^{2+}-binding protein (CaBP), is a member of a large family of intracellular Ca^{2+}-binding proteins (*1*). The sequence of CaBP, which possesses 6 EF hands and binds three to five Ca^{2+} ions (*11*), is highly conserved in the human, bovine, rat and chick protein. Sequence conservation is not just in the Ca^{2+}-binding domains, indicating that CaBP may be involved in other biologically important functions in addition to the proposed role of Ca^{2+} buffer (*3, 4*). CaBP is also noted for its abundance and specific distribution in mammalian brain and sensory neurons (*5*). It is reported that neurodegenerative diseases such as Alzheimer's and Parkinson's are linked to deficiencies in CaBP, which exhibits diminished expression with age (*6*). Human CaBP (HCaBP) seems to be also linked to epilepsy, amyotrophic lateral sclerosis and Huntington's disease (*7-9*).

NO is a molecule that has, in recent years, been shown to play many roles in bioregulation. It is known to be involved in vasodilation, platelet aggregation, inflammation, and neuronal communication (*10*). In addition, NO has been implicated in many neurodegenerative diseases such as AIDS dementia, and Huntington's and

Parkinson's diseases (*11*). Since NO is a labile free radical, how it exerts its biological effects has become the focus of intense research. Recently it has been discovered that NO can react with the thiol groups of small molecules such as glutathione or cysteine to form S-nitroso compounds, which in turn can donate NO to proteins in a process called *trans*-S-nitrosation (*12*). These S-nitroso compounds are believed to be prevalent in the body (*13*) and are thought to facilitate NO transport, to prolong the life of NO in blood and tissues, to target its delivery, and to mitigate its cytotoxic potential (*8*). Stamler and coworkers have proposed that proteins with the consensus sequence C (D, E) are likely candidates for S-nitrosation on their cysteine residues (*112*). The crystal structure of human CaBP is not yet known, but the primary sequence reveals that the protein possesses five cysteine residues, two of which (Cys100 and Cys219) have the putative *trans*-S-nitrosation consensus sequence C (E).

In the brain, NO influences synaptic plasticity, apoptosis, neuronal development, and even complex behavioral responses (*16*). CaBP is especially abundant in the brain, making up 0.1~1.5% of the total soluble protein (*111*). It is known that Ca^{2+}-loaded calmodulin, another well-known Ca^{2+}-binding protein, is required to activate NO synthase (*16*), and association of calmodulin with the constitutive NO synthase isozymes is essential for NO production (*113*). Hence it is reasonable to propose that CaBP may also play a role in NO biochemistry in the brain. Moreover, there is evidence showing that CaBP may interact with as-yet-unknown target molecules (*114*); could perhaps one of these be NO synthase? Interestingly, CaBP is found coexistent with NO synthase in the cerebellum (*53*). Also, intercellular Ca^{2+} waves in rat hippocampal slices and

dissociated glial neuron cultures are mediated by NO (*55*), and Ca^{2+} regulates S-nitrosation and denitrosation of tissue transglutaminase (*56*).

Given the possible crosstalk between Ca^{2+} and NO signalling (*55, 56*), it is of interest to determine whether Ca^{2+}-binding proteins also react with free NO or NO donors. In this work, a number of spectroscopic methods and mass spectrometry are used to directly probe S-nitrosation of the cysteine residues in recombinant human CaBP (rHCaBP).

4.3 Materials and methods

Materials: NO was purchased from Praxair. Isopropyl β-D-thiogalactoside (IPTG), DL-dithiothreitol (DTT), L-cysteine, 5,5'-dithio-bis(2-nitrobenzoic acid) (DTNB), ethylene glycol-bis(aminoethylether)-N,N',N',N'-tetraacetic acid (EGTA), mercuric chloride, sulphanilamide, N-(1-naphthyl)ethylenediamine dihydrochloride, ammonium sulfamate and N-ethylmaleimide (NEM) were purchased from Sigma. 5-(Octyldithio)-2-nitrobenzoic acid (ODNB) was purchased from Fluka, sodium nitrite from Anachemia Chemicals, S-nitroso-L-glutathione (GSNO) from Cayman, calcium acetate [$Ca(OAc)_2$] and acetonitrile (HPLC grade) were from Fisher, and trifluoroacetic acid (TFA, HPLC grade) was from Aldrich. Nanopure water from a Barnstead or Millipore system was used to prepare all solutions.

Preparation of rHCaBP: A cDNA clone of rHCaBP (*102*) was inserted into the *Nhe*I and *Xba*I sites of the expression vector pGYMX (*103*) to produce an amino-terminal His-tagged fusion protein. Expression from the pGYMX-HCaBP vector was not genetically stable, and the rHCaBP gene along with a DNA fragment encoding the His

tag was subcloned into pTrc99A (Amersham Pharmacia Biotech) using the *Nco*I and *Xba*I restriction sites. *E. coli* cells transformed by pTrc99A-HCaBP were grown in LB media and induced with 1 mM IPTG overnight. Harvested cells were passed through a French press, and the centrifuged cell lysate was applied to a nickel chelate affinity column (Invitrogen) and eluted using increasing concentrations of imidazole. Fractions found to contain rHCaBP at > 95% purity, as judged by Coomassie-stained SDS-PAGE, were pooled and dialysed against 20 mM TrisHCl (pH 7.4) and 1 mM DTT. The concentration of the protein was determined spectrophotometrically ($\varepsilon_{280} = 28037\ M^{-1}cm^{-1}$ for *holo*rHCaBP and 26000 $M^{-1}cm^{-1}$ for *apo*rHCaBP) (*114*). The protein was stored as a stock solution (6 mg/ml) in 20 mM TrisHCl (pH 7.4), 0.1 mM $Ca(Oac)_2$ and 1 mM DTT at –80°C. DTT was removed immediately prior to use by gel filtration on a G25 NAP-10 1.3 × 2.6 cm column (Amersham Pharmacia Biotech) equilibrated with 5 mM TrisHCl (pH 7.4) and concentrated by ultrafiltration (Amicon Centricon unit with a YM-10 filter; Millipore). Given the nature of the experiments carried out here, it was not possible to use working solutions containing DTT as recommended for HCaBP due to its propensity to form disulfide cross-links (*107*). Care was taken to minimize handling of the protein at room temperature and to work with dilute solutions to avoid cross-linking. No evidence of covalent dimer formation was obtained by mass spectrometry. Between 10–20-fold excess of EGTA was added to generate the Ca^{2+}-free protein (*apo*rHCaBP), which was purified on the NAP-10 column and concentrated as before.

Preparation of S-nitrosocysteine: CysNO was synthesized by combining equimolar amounts of cysteine in 250 mM HCl containing 0.1 mM Na_2EDTA with sodium nitrite in water (*115*), and the pH adjusted to 7.4 by adding 1 M NaOH dropwise.

This stock solution of CysNO was diluted to the required concentration using 5 mM TrisHCl buffer (pH 7.4). CysNO was always prepared freshly before use, shielded from light, and kept on ice.

Preparation of NO solutions: MilliQ water in a rubber-stoppered vial was sparged for 30 min with N_2 and 30 min with NO gas. Higher nitrogen oxides were removed by passage of the gas through a 10% KOH trap before the collection vial. This resulted in a saturated solution of NO (~1.5 mM) as measured by a NO meter (ISO-NO, World Precision Instruments, Sarasota, FL).

S-nitrosation of rHCaBP: The protein was treated with a 10-fold molar excess CysNO or GSNO in 5 mM TrisHCl (pH 7.4) at room temperature for 30 min and gel-filtered on a NAP-10 column to remove excess CysNO. The protein was also exposed to an ~20-fold molar excess of free NO in 10 mM ammonium acetate buffer at pH 4.0 for 30–40 min at room temperature.

Determination of free cysteines in rHCaBP with DTNB and ODNB: The number of free cysteine residues in rHCaBP was determined by monitoring the absorbance at 412 nm (ε=14.15 $mM^{-1}cm^{-1}$) on a Cary Varian spectrophotometer of the 2-nitro-5-thiobenzoate anion (TNB^{2-}) generated by 2–4 μM rHCaBP in 100 mM potassium phosphate buffer (pH 7.27) containing 1 mM EDTA. The TNB^{2-} anion was produced by the reaction of DTNB or ODNB with the free SH groups of rHCaBP (*116*). To further determine the status of the five cysteine residues in rHCaBP, the protein was incubated with a 33-fold molar excess NEM at room temperature in 5 mM TrisHCl (pH 7.4) for 5 min and frozen at –80°C to quench the reaction. The NEM-modified protein was analyzed by mass spectrometry as outlined below.

Spectrophotometric analyses: UV–vis and CD absorption and fluorescence measurements were used to investigate the S-nitrosation of rHCaBP. Spectra were recorded at 25°C on a Beckman DU Series 650 spectrophotometer, a Jasco J-710 spectropolarimeter purged with N_2 at a flow rate of 5 L/min, and an AMINCO-Bowman Series 2 luminescence spectrometer. All samples were in 5 mM TrisHCl buffer (pH 7.4) in 1 cm cuvettes. Appropriate blanks, run under the same conditions, were subtracted from the sample spectra.

S-Nitrosothiols in rHCaBP: The Saville assay was used to determine the number of S-nitrosothiols (*117*). Briefly, 1 mL of ammonium sulfamate (0.5% w/v in water) was added to 200 μL of ~60 μM CysNO-exposed rHCaBP in 5.8 mL of 0.25 M sulfuric acid. Then 10 mL of $HgCl_2$/sulfanilamide solution (prepared from 1 volume of 1% w/v $HgCl_2$ in water and 4 volumes of 3.4% w/v sulfanilamide in 0.4 M HCl) was added, 0.1% w/v of N-(1-naphthyl)ethylenediamine in 0.4 M HCl was added to the mark in a 25-mL volumetric flask, and the absorbance at 540 nm was read after 10 min. A standard curve was prepared by the same procedure but substituting rHCaBP with CysNO.

Calculation of R_0: The Förster distance, R_0, is the donor–acceptor separation at which the donor fluorescence is quenched by 50% and is defined by (*118*):

$$R_0 = (9.79 \times 10^3)(k^2 n^{-4} Q_a J)^{1/6} \qquad (4.1)$$

k^2 was assumed to be 0.67 for random orientation between the donor and acceptor transition dipoles (*119*); n, the refractive index of the protein matrix between the donor and acceptor, was given a value of 1.4 (*120*); and Q_a, the quantum yield for tryptophan fluorescence in the absence of acceptors, was taken as 0.2 (*121*). The spectral overlap J (cm^3M^{-1}) between the donor emission (tryptophan residues in rHCaBP) and acceptor

absorption [free GSNO, which is more stable than free CysNO at pH 7.4 (*32*), was used to estimate CysNO absorption in rHCaBP because of interfering protein absorption at ~300 nm] was calculated from (*118*):

$$J = \frac{\int F_\lambda \varepsilon_\lambda \lambda^4 \, d\lambda}{\int F_\lambda \, d\lambda} \qquad (4.2)$$

where F_λ is the emission intensity of the donor at wavelength λ (nm) and ε_λ is the extinction coefficient of the acceptor at λ (nm). The integrals in eq 4.2 were calculated numerically between 300 and 400 nm using a step of 1 nm.

Mass Spectrometry: Electrospray ionization mass spectrometry (ESI-MS) was carried out on a ThermoFinnigan SSQ7000. Samples in 5 mM TrisHCl buffer (pH 7.4) were mixed (1:20 v/v) with 75% acetonitrile/0.05% TFA and injected into the ESI source at a flow rate of 5 μL/min. The ESI source temperature was maintained at 70°C. Spectra were scanned from m/z 500–2200 at a rate of 3s/scan. Mass-scale calibration was carried out using myoglobin and L-methionyl-arginyl-phenylalanyl-alanine acetate (MRFA) as reference compounds. Protein mass spectra were deconvoluted using BioWorks software (ThermoFinnigan).

Peptide mass mapping: Endoproteinase Glu-C digestion was carried out in 0.4% ammonium acetate (pH 4.0) at 40 °C for 2h at a rHCaBP/Glu-C ratio of 15/1 (w/w). The reaction was stopped by addition of methanol to a final concentration of 5%. The peptides were desalted using C18 tips ($ZipTip_{C18}$; Millpore) and eluted from the tips with 60% acetonitrile/0.1% TFA. The eluate (1.5 μL) was mixed with 1.5 μL of matrix solution [100 μL of α–cyano-4-hydroxycinnamic acid (40 mg/mL in acetone), 10 μL of

nitrocellulose (20 mg/mL in acetone), 40 μL of acetone, and 50 μL of 2-propanol], and 1.5 μL of the peptide–matrix mixture was spotted onto a 100-well, gold-plated MALDI plate and air-dried. Samples were analyzed using an Applied Biosystems Voyager-DE MALDI-TOF mass spectrometer, equipped with a 337 nm N_2 laser. Parent ion masses were measured by the time-of-flight (TOF) analyzer with an accelerating voltage of 20 kV. The mass spectrometer was calibrated externally using calibration mixture no. 1 from Applied Biosystems.

4.4 Results

4.4.1 Determination of free cysteines in rHCaBP with DTNB and ODNB

As the crystal structure for rHCaBP has not yet been determined, reactions with excess DTNB and ODNB were performed in 100 mM phosphate buffer (pH 7.27) to determine how many free cysteines are present in the protein and thus the number of potential S-nitrosation sites. The determination of free thiols with DTNB and ODNB is quite sensitive due to the strong absorption (ε_{412}=14.15 $mM^{-1}cm^{-1}$) of the product, TNB (eq 4.3) (*116*). ODNB reacts faster with free thiols in proteins than DTNB because of the absence of one negative charge and the presence of a lipophilic hydrocarbon chain in the former (eq 4.4) (*122, 123*). Sequence information shows that HCaBP has five cysteine residues (*3*), and the DTNB and ODNB assays determined 5 free thiols (Table 4.1), indicating that rHCaBP has no disulfide bonds.

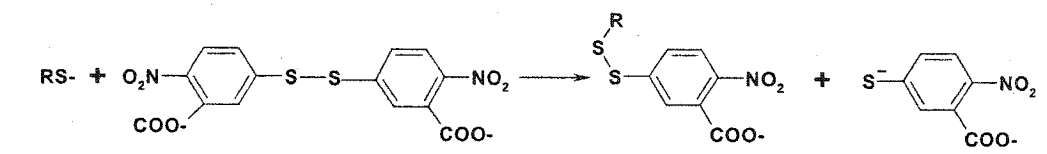

Free thiol DTNB^{2-} TNB^{2-}

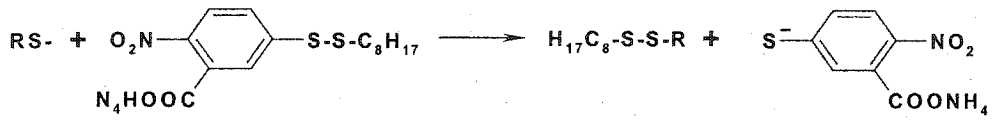

Free thiol ODNB TNB^{2-}

Table 4.1. **Determination of free thiols in rHCaBP**

reagent	free thiols/protein (mol/mol) [a]
DTNB	5.3 ± 0.4
ODNB	4.7 ± 0.4

[a] The molar ratios given represent the mean ± RMSD (root mean square deviation) of three to four determinations.

4.4.2 Spectroscopic characterization of S-nitrosated rHCaBP

UV-Vis absorption: This is a commonly used method to determine the presen ce of a S-nitrosated product because the N-π^* electronic transition between nitrogen and sulfur in S-nitroso compounds gives rise to absorption at ~335 and 550 nm (*74*). The 550 nm band is nearly electric dipole forbidden, so its extinction coefficient is much less than that at 335 nm. After the reaction of CysNO with rHCaBP, the solution was passed through a NAP-10 column to remove excess CysNO, and the UV-Vis spectrum was

recorded. Figure 4.1 shows that the rHCaBP product exhibits an absorption maximum at 333 nm, consistent with S-nitrosation of cysteine residues in the protein. Furthermore, the S-nitrosated *apo*protein exhibits stronger absorption than the *holo*protein.

Circular dichroism (CD): Although ~335 nm absorption is a convenient method to detect S-nitrosation, other nitrosated derivatives such as nitrosated-tryptophan (*36*) as well as NO_2^-, a by-product of CysNO decomposition, absorb at 330–350 nm. To confirm the S-nitrosation of rHCaBP and to investigate the microenvironment of the S–NO bonds in the protein, CD spectra were recorded. S-nitroso compounds give characteristic CDbands at 335 and 550 nm. In contrast to the absorption of unpolarized light, CD absorption is stronger at 550 than at 335 nm, and the visible absorption is well separated from protein CD signals, including other NO-modified species (*74*). The visible–CD spectra of rHCaBP taken before and after incubation with CysNO are shown in Figure 4.2. S-nitrosated *apo*rHCaBP exhibits a stronger CD signal than the S-nitrosated *holo*protein. Red shifting of the CD band reveals that the SNO moiety is more exposed in the absence of Ca^{2+} (549 nm) than in the Ca^{2+}-loaded protein (545 nm) given that the CD maximum for free CysNO is at 551 nm (data not shown). Finally, the relative intensities of the CD (Figure 4.2) and unpolarized absorption (Figure 4.1) indicate greater S-nitrosation of Ca^{2+}–free vs Ca^{2+}–loaded rHCaBP.

Intrinsic fluorescence: Because of the weak intensity of SNO bands, UV–vis and CD absorption methods consume a significant amount of sample. Since NO donors also absorb at the same wavelengths as the S-nitrosated protein products, excess CysNO must be removed before the protein spectra are recorded. To find a more sensitive method,

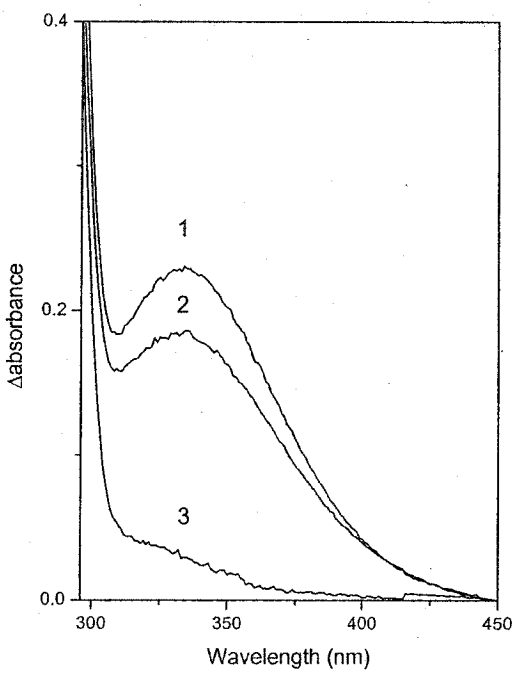

Figure 4.1. **UV–vis absorption of S-nitrosated rHCaBP.** UV-vis spectra of (1) 66 μM S-nitrosated *apo*rHCaBP, (2) 67 μM S-nitrosated *holo*rHCaBP, and (3) 69 μM untreated *holo*rHCaBP. Spectra were recorded in a 1-cm cuvette at 25°C in 5 mM TrisHCl buffer (pH 7.4). Excess CysNO was removed from the S-nitrosated samples by gel filtration on a NAP-10 column (see text).

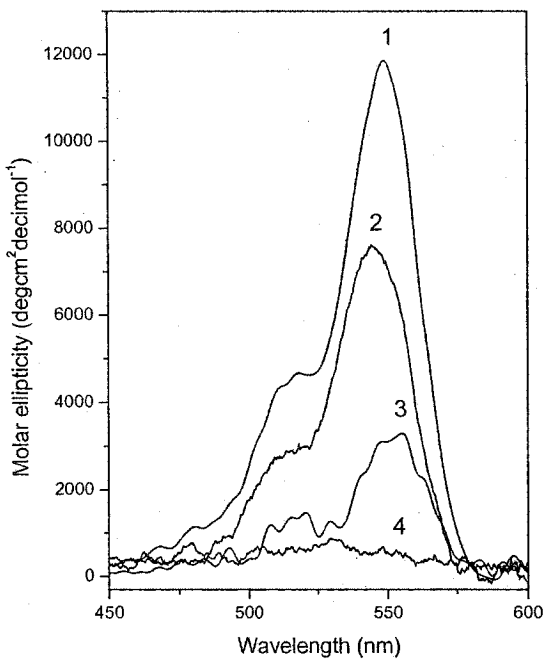

Figure 4.2. **Visible CD spectra of S-nitrosated rHCaBP.** (1) 66 μM S-nitrosated *apo*rHCaBP and (2) 58 μM S-nitrosated *holo*rHCaBP at pH 7.4, (3) 69 μM S-nitrosated *holo*rHCaBP at pH 3, and (4) 59 μM *holo*rHCaBP at pH 7.4. See Figure 4.1 for experimental conditions. The pH was adjusted to 3 in sample 3 by the addition of 1 M HCl.

which would also be useful in kinetic analyses of the CysNO/rHCaBP reaction, intrinsic fluorescence of the rHCaBP reactants and products was examined. rHCaBP has 14 Phe, 8 Tyr, and 2 Trp residues. When excited at 295 nm, *holo*rHCaBP emits at 328 ± 1 nm (Figure 4.3A). Thus, compared to free tryptophan (350 nm), the environment around the tryptophan residues in *holo*rHCaBP is quite hydrophobic. When Ca^{2+} is removed from the protein, the tryptophan environment does not appear to be perturbed, as the intrinsic fluorescence of the *apo*- and *holo*protein is very similar (Figure 4.3A). In contrast,

Berggard and coworkers reported significantly higher intrinsic fluorescence for their Ca^{2+}-loaded rHCaBP compared to the *apo* form, but surprisingly the wavelength maximum and shape of the emission bands were exactly the same. Since fluorescence intensities are error prone due to the many factors that can lead to quenching, we also recorded the emission of our rHCaBP at high concentration (77 μM), similar to that used by Berggard *et al.* (68 μM) [Figure 5, in (*114*)]. We obtained the same results (data not shown) as those shown in Figure 4.3 using 8 μM protein. Second, their rHCaBP displayed an emission maximum at 335 nm whereas ours fluoresced maximally at 328 nm. Third, they reported that ANS bound to *apo*rHCaBP gave a higher intensity and blue-shifted emission compared to ANS bound to the Ca^{2+}-loaded form. We obtained opposite results with our rHCaBP (data not shown); the fluorescence of ANS bound to *apo*rHCaBP increased and blue-shifted when Ca^{2+} was added to the protein solution, just as observed for chicken calbindin D_{28K} and calmodulin (*114*). (Please see note on page 99.)

Spectral overlap between tryptophan emission at 320-340 nm and S–NO absorption at 330-340 nm should give rise to efficient energy transfer between tryptophan and CysNO residues. As expected, the fluorescence intensity of both *holo-* and *apo*rHCaBP decreases dramatically following S-nitrosation, with greater quenching in the *apo*protein (Figure 4.3A). To confirm that the quenching is due only to tryptophan → CysNO energy transfer, additional experiments were carried out. Figure 4.3C shows that incubation of free tryptophan with CysNO at room temperature for 30 min has a negligible effect on its fluorescence, establishing that the quenching in Figure 4.3A is not due to freely diffusing CysNO or its dissociation products.

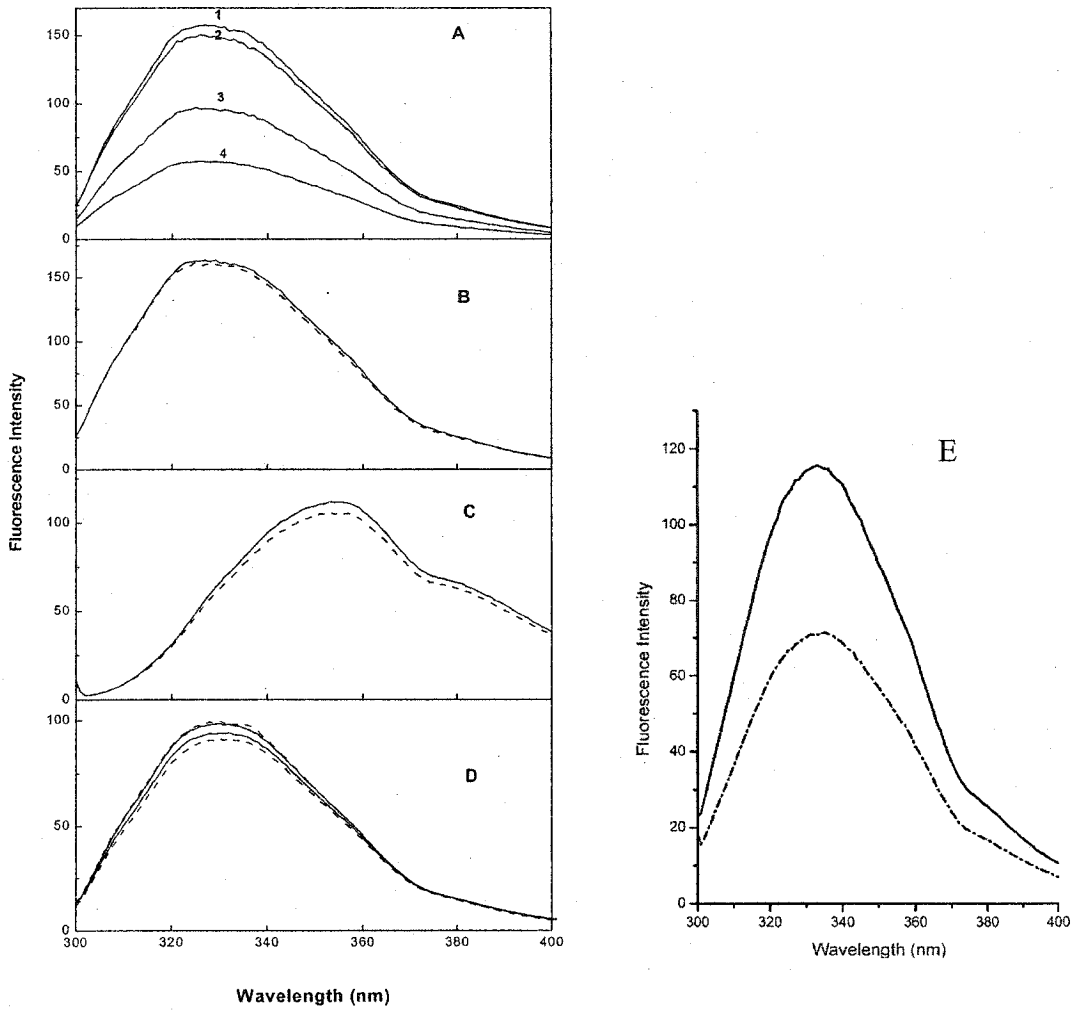

Figure 4.3. **Effects of S-nitrosation on the intrinsic fluorescence of rHCaBP**. (A) spectrum 1, 8 μM *holo*rHCaBP; spectrum 2, 8 μM *apo*rHCaBP; spectrum 3, 8 μM S-nitrosated *holo*rHCaBP; and spectrum 4, 8 μM S-nitrosated *apo*rHCaBP. (B) 8 μM *holo*rHCaBP in the absence (solid line) and presence of 160 μM $NaNO_2$ (dashed line). (C) 10 μM free tryptophan before (solid line) and after incubation with 160 μM CysNO for 30 min (dashed line). (D) 6.8 μM *holo*rHCaBP incubated with 240 μM NEM for 30 min (upper solid line), then 160 μM CysNO for 30 min (upper dashed line); 7.0 μM *apo*rHCaBP incubated with 240 μM NEM for 30 min (lower solid line) and then 160 μM CysNO for 30 min (lower dashed line). (A–D) Spectra were recorded in 5 mM TrisHCl buffer (pH 7.4) with 80 μM $Ca(Oac)_2$ for *holo*rHCaBP, and 200 μM EGTA for *apo*rHCaBP samples. S-nitrosation of rHCaBP was carried out in a 30-min incubation with CysNO in 5 mM TrisHCl (pH 7.4). (E) rHCaBP (5 μM) before (solid line) and after (dashed line) incubation with an NO-saturated solution (100 μM) in 10 mM ammonium acetate buffer with 1 mM EDTA at pH 4.0 for 40 min at room temperature. All of the spectra were recorded in a 1-cm cuvette at 25°C.

Since it is not stable at pH 7, excess CysNO in the reaction solution will form NO_2^- as proposed by Pietraforte and coworkers (*67*):

$$2RSNO \rightarrow RSSR + 2NO^{\bullet}$$

$$2\ NO^{\bullet} + O_2 \rightarrow 2\ ^{\bullet}NO_2$$

$$^{\bullet}NO_2 + NO^{\bullet} \rightarrow N_2O_3$$

$$N_2O_3 + H_2O \rightarrow 2NO_2^- + 2H^+$$

Free NO_2^- has been shown to be an efficient quencher of horse liver alcohol dehydrogenase, alkaline phosphatase and *N*-acetyltryptophanamide fluorescence (*124*) at higher concentration (~50 mM). Figure 4.3B shows that micromolar NO_2^- does not quench rHCaBP fluorescence under our experimental conditions. To investigate the possible quenching effect of other NO-modified species, such as nitroso-tryptophan and tyrosine-NO_2, both *holo-* and *apo*rHCaBP were incubated with NEM for 30 min before incubation with CysNO to block the cysteine residues in rHCaBP. The effects of CysNO on the intrinsic fluorescence of NEM-treated rHCaBP is negligible (Figure 4.3D).

The mass spectra discussed later revealed the presence of one mixed disulfide in S-nitrosated rHCaBP. Since tryptophan fluorescence can be quenched by nearby disulfides (*38*), we sought to distinguish between S–NO and S–S quenching. Exposure to the oxidized form of glutathione (GSSG) resulted in a single disulfide bond formation between glutathione and a protein cysteine residue, but this S-S bond formation did not quench the intrinsic fluorescence of rHCaBP (data not shown). The mass spectrum (Figure 4.5B) of rHCaBP mixed with a NO-saturated solution revealed that two S-NO bonds formed in the protein at pH 4.0. The corresponding fluorescence spectra, also recorded at pH 4.0 (Figure 4.3E), revealed extensive fluorescence quenching and a red-

shift of the emission maximum from 329 to 333 nm, which indicated that the tryptophan residues become more exposed at low pH. The extent of rHCaBP S-nitrosation and protein quenching is less in the NO-treated sample compared to the CysNO-treated samples. Taken together, these results indicate that efficient Trp→CysNO energy transfer occurs in S-nitrosated rHCaBP due to the spectral overlap between tryptophan emission at 329 nm and CysNO absorption at 334 nm. The strong quenching of fluorescence in S-nitrosated rHCaBP is consistent with efficient Trp→GSNO Förster energy transfer which exhibits a J of 8.82×10^{-16} (cm^3M^{-1}) and a R_0 of 17 Å. Also, Trp→CysNO energy transfer is more efficient in *apo*- than in *holo*rHCaBP (Figure 4.3A), indicating greater S-nitrosation of cysteine residues within quenching distance of the two tryptophan residues in *apo*rHCaBP (Trp20 and Trp107).

4.4.2 Mass spectrometry

ESI mass spectra were obtained to determine if incubation with the S-nitrosothiols or NO caused any spectroscopically silent alterations in rHCaBP. The deconvoluted ESI mass spectrum of our rHCaBP exhibits a single peak with M_r 31722 ± 2 Da (Figure 4.4A). This corresponds to the average mass predicted for rHCaBP from the native HCaBP sequence (*3*) plus the His-tag ($MATSH_6IEGRAS$) minus the initial methionine (M). As expected, Ca^{2+}-binding was not detected under the experimental conditions used to record the mass spectrum (75% acetonitrile/0.05% TFA, positive-ion mode). Following incubation with a 33-fold molar excess of NEM, labelling of rHCaBP with 3–5 NEM is seen in Figure 4.4B, confirming the results in Table 4.1 that 5 free cysteine residues are present in rHCaBP.

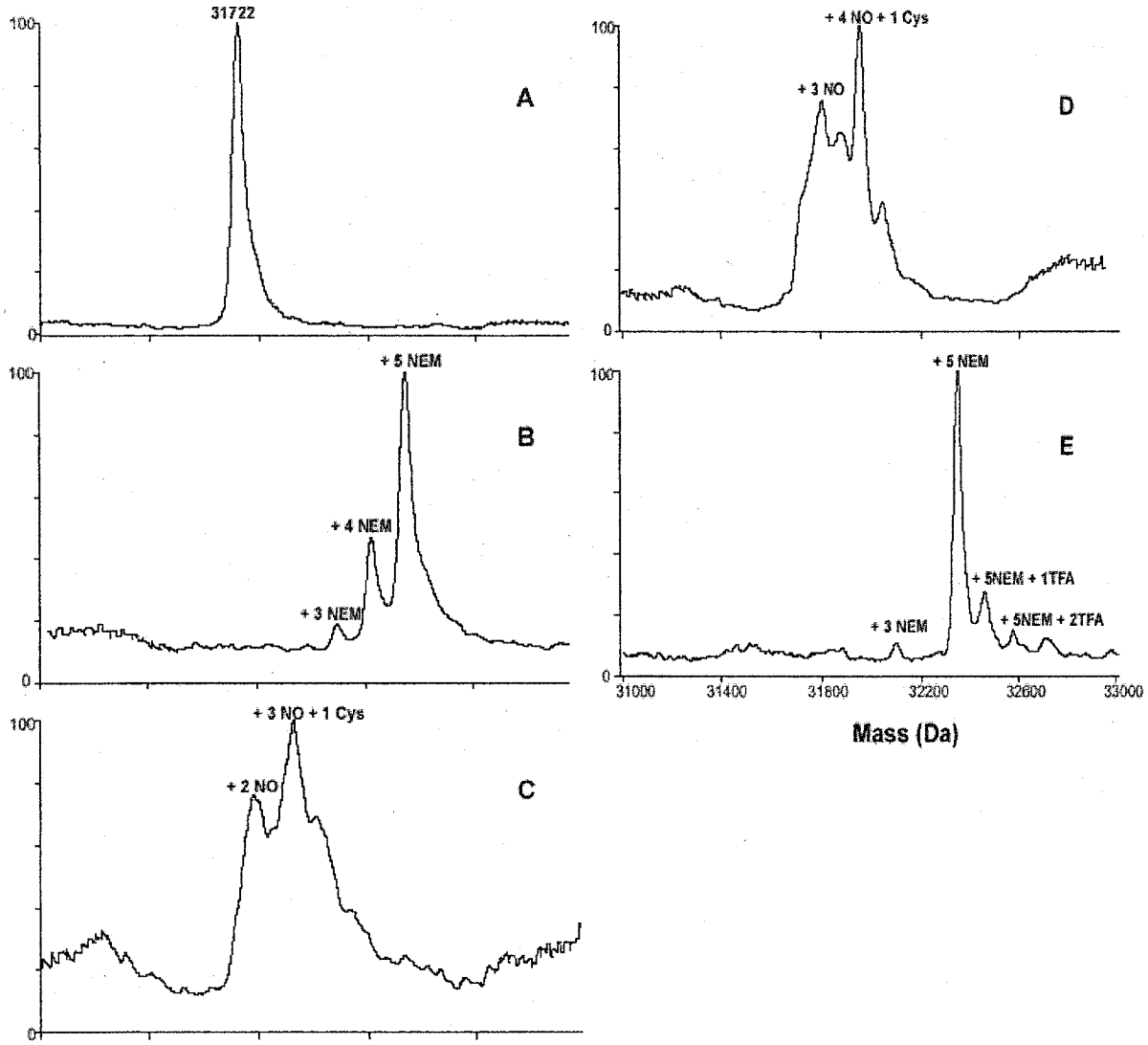

Figure 4.4. **ESI-MS analysis of rHCaBP S-nitrosation.** (A) *holo*rHCaBP; (B) NEM-labeled *holo*rHCaBP; (C) S-nitrosated *holo*rHCaBP; (D) S-nitrosated *apo*rHCaBP; (E) NEM-labeled *apo*rHCaBP after a 30-min incubation with 10-fold molar excess CysNO. Experimental conditions: All samples were in 5 mM TrisHCl (pH 7.4) and the S-nitrosated samples contained 0.5% TFA to stabilize the S-NO bond. NEM-labeled *holo*rHCaBP (B) and *apo*rHCaBP (E) were prepared by incubating the protein with 33-fold molar excess NEM for 5 and 30 min, respectively, at 25°C, and the samples were frozen at –80°C until use. The S-nitrosated proteins were prepared as described in Figure 4.1. Samples for MS analysis were diluted 20-fold into 75% acetonitrile/0.05% TFA and directly infused at a flow rate of 5 μL/min into the ESI source of the mass spectrometer with capillary temperatures of 250°C (A, B), or 180°C (C–E), a spray voltage of 4.5 kV and a sheath gas pressure of 30 psi.

Mass spectrometry was also used to confirm the chemical nature of the species formed during the incubation of rHCaBP with CysNO. Since the S-NO bond is thermally labile, altering the temperature of the metal capillary transfer tube can alter the intensity of S-nitrosated species in the mass spectrum (*125*). At a capillary temperature of 180°C, the spectrum of *holo*rHCaBP is dominated by peaks with M_r values that are 59 ± 3 Da and 206 ± 3 Da higher than those of untreated rHCaBP (Figure 4.4C). These mass shifts (ΔM_r) are assigned to rHCaBP modified with two NO groups and three NO plus one Cys, respectively. For *apo*rHCaBP, two dominant species were also detected with ΔM_r of 87 ± 3 and 235 ± 3 Da, which corresponds to protein derivatized with three NO groups, and protein derivatized with four NO plus one Cys (Figure 4.4D).

To determine whether CysNO incubation resulted in modification of only cysteine residues, the protein was first treated with 33-fold molar excess of NEM for 30 min. A 30-min incubation of NEM-treated rHCaBP with 10-fold excess of CysNO was then carried out before the mass spectra were recorded. Figure 4.4E shows a single dominant peak with a ΔM_r of 625 Da higher than untreated rHCaBP, which reveals labelling with five NEM groups. There are also minor peaks corresponding to protein labeled with three NEM, and TFA adducts of the dominant (rHCaBP-NEM_5) species. These results indicate that a 33-fold excess of NEM blocks all five cysteine residues in rHCaBP and that CysNO does not modify the protein at other residues such as tryptophan or tyrosine under the experimental conditions used in this work.

Because the GSNO is likely the dominant intracellular S-nitrosothiol, *holo*rHCaBP was incubated with a 10-fold excess of GSNO. The mass spectrum (Figure 4.5A) revealed that, despite the larger size of GSNO, up to three cysteine residues were

S-nitrosated and a glutathione adduct was also formed. The mass increase of 306 Da for the glutathione adduct resulted in much better peak separation compared to that in the CysNO-modified protein (Figure 4.5A vs 4.4C). A comparison of the peptide mass maps obtained by MALDI-TOF for modified and unmodified rHCaBP indicated that most likely the Cys187 is the S-thiolation site and Cys100 is one of the S-nitrosation sites (data not shown).

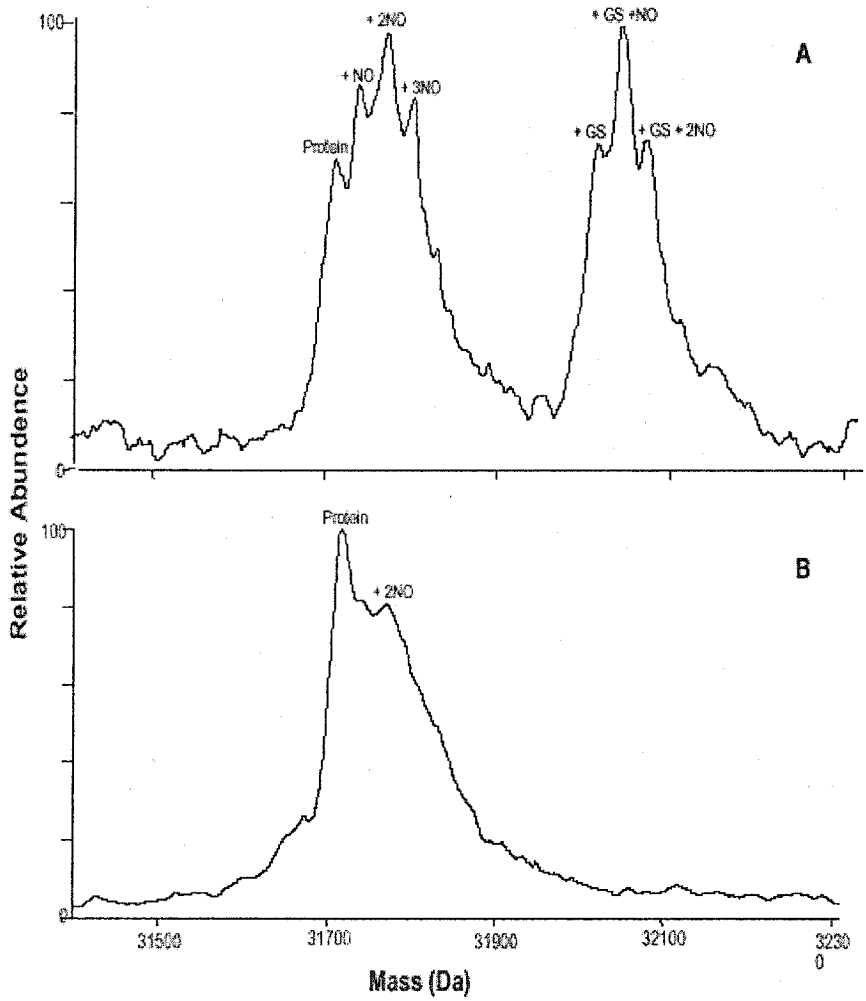

Figure 4.5. **ESI-MS of GSNO- and NO-treated rHCaBP.** (A) *holo*rHCaBP treated with a 10-fold molar excess GSNO for 30 min in 5 mM TrisHCl (pH7.4) at room temperature. (B) *holo*rHCaBP treated with a 20-fold molar excess NO for 30 min in 10 mM ammonium acetate buffer (pH 4.0) at room temperature. The mass spectrometry conditions were the same as in Figure 4.4.

4.4.3 Determination of S-nitrosothiols in rHCaBP by Saville assay

The spectroscopic and mass spectral results all show that *apo*rHCaBP undergoes greater S-nitrosation than the *holo*protein on treatment with CysNO. To confirm this important conclusion, the Saville assay for nitrosothiol quantification was selected as the method of choice. The numbers of S-nitrosothiols per protein molecule determined by the Saville assay (Table 4.2) show that in *holo*rHCaBP and *apo*rHCaBP about two to four cysteine residues are S-nitrosated, with a greater extent of S-nitrosation in *apo*rHCaBP.

Table 4.2. **Determination of CysNO in rHCaBP by the Saville assay** [a]

protein	CysNO/protein (mol/mol) [b]
*Holo*rHCaBP	2.6 ± 0.05
*Apo*rHCaBP	3.4 ± 0.09

[a] See experimental procedures

[b] The molar ratios given represent the mean ± RMSD (root mean square deviation) of three to four determinations

4.5 Discussion

The reaction with the thiol-specific reagents, DTNB and ODNB, shows that rHCaBP possesses five free cysteines (Table 4.1). This is consistent with the fact that most members of the troponin C superfamily of proteins do not contain disulfide bonds (*126*). The cytosol provides a reducing environment that prevents the formation of

disulfide linkages by maintaining cysteine residues in their reduced form (*24*). Mass spectrometry revealed that five NEM adducts are formed (Figure 4.4E), confirming that rHCaBP has five reactive cysteines. Since the rHCaBP species labeled with three and four NEM groups also show quite strong signals (Figure 4.4B), the mass spectral data additionally indicate that one cysteine residue is likely buried in the protein and a second semiburied. The Saville assay demonstrates that 2.6 ± 0.05 S–NO groups are present in *holo*rHCaBP and 3.4 ± 0.09 in *apo*rHCaBP after incubation with CysNO (Table 4.2).

Modified rHCaBP exhibited UV absorbance at ~ 333 nm, which confirms the presence of the S–NO group. S-nitrosated *holo*rHCaBP and *apo*rHCaBP possess ε_{333} values of 2.7 ± 0.3 and 3.3 ± 0.2 $mM^{-1}cm^{-1}$, respectively. From the published values of 0.87 and 0.76 $mM^{-1}cm^{-1}$ for BSA-SNO (*127*) and GSNO (*45*), respectively, which each possess only one free thiol, the average ε_{333} per S–NO group is 0.82 $mM^{-1}cm^{-1}$. Based on this number, S-nitrosated *holo*rHCaBP possesses 3.3 SNO groups and S-nitrosated *apo*rHCaBP 4.0. These estimates of SNO groups per rHCaBP are in agreement with the results from the Saville assay (Table 4.2) and mass spectrometry (Figure 4.4C and D).

Mohney and Walker (*74*) demonstrated that changes in the Cys34-NO CD signals of BSA can be correlated with conformational change in the protein. The SNO CD absorption band at 545 nm of S-nitrosated *holo*rHCaBP decreases in intensity and red-shifts by 9 nm when the pH is dropped from 7.4 to 3 (Figure 4.2). In contrast, the CD signal of Cys34-NO in BSA is stronger under acidic conditions. Interpretation of the visible CD spectra of S-nitrosated rHCaBP is more complicated since it has about three to four SNO groups compared to the single SNO group in S-nitrosated BSA. Nonetheless, the 4-nm red-shift for *apo*rHCaBP compared to *holo*rHCaBP at pH 7.4, as well as the 9-

nm red-shift in *holo*rHCaBP on lowering the pH to 3, indicates that the CysNO residues are more buried on average in the *holo*protein at pH 7.4 than in the *apo*form at pH 7.4 or the *holo*form at pH 3. Thus, removal of Ca^{2+} or decreasing the pH to 3 (which may also result in loss of Ca^{2+}) leads to more exposed CysNO groups in rHCaBP.

ESI-MS is a useful method for the study of S-nitrosation. In addition to accurate mass measurements, the ESI-source conditions can be varied to cleave the labile S–NO bond during the analysis (*125*). Thus, S-NO bonds formed in reactions between NO donors and proteins or peptides can be distinguished from other bonds such as disulfides formed on S-thiolation (*128*). In this study, we varied the temperature of the metal capillary transfer tube to distinguish between S–NO bond formation, which is observed only at low capillary temperatures due to its lability, and other modifications. The mass spectra reveal that in addition to S-nitrosation, a single cysteine residue of rHCaBP is S-thiolated on incubation with CysNO (Figure 4.4C and D) or GSNO (Figure 4.5A). With S-nitrosothiols as NO donors, the formation of mixed disulfides has been reported in a number of other studies (*123, 128, 129*). NO or NO donors can also modify tyrosine or tryptophan residues in proteins (*125, 130, 131*). However, the combined mass spectrometry (Figure 4.4) and fluorescence (Figure 4.3) data on NEM-labeled rHCaBP confirm that under the present experimental conditions, CysNO targets only the protein's cysteine residues. NEM-blocked rHCaBP exhibits no peaks due to additional adducts in its mass spectrum and negligible quenching of intrinsic fluorescence following incubation with CysNO.

Because of spectral overlap between tryptophan emission at 320-340 nm and SNO absorption at 330-340 nm, efficient energy transfer is expected. Our experimental

data (Figure 4.3A) confirm this, and a R_0 value of ~17 Å was estimated for S-nitrosated rHCaBP on the basis of Trp/GSNO spectral overlap (eq 4.2). Efficient intramolecular Förster energy transfer is also seen in other small S-nitrosothiols, such as N-dansyl-S-nitrosohomocysteine (*132*) and other fluorophore-labeled S-nitrosothiols (*50*). For proteins that contain tryptophan residues, quenching of intrinsic fluorescence provides a rapid and sensitive method to detect S-nitrosation of cysteine residues.

Two cysteine residues were S-nitrosated in the reaction of rHCaBP with NO (Figure 4.5B). At low GSNO to rHCaBP molar ratios (1–5 : 1), about one to two cysteine residues were also the targets of S-nitrosation (data not shown). Interestingly, two of the five cysteine residues (Cys100 and Cys219) of rHCaBP fall within putative S-nitrosation consensus motifs (*112*). Peptide mass mapping of modified rHCaBP revealed that Cys100 is S-nitrosated and Cys187 S-thiolated. Extensive attempts at peptide mass mapping using Glu-C, pepsin, and cyanogen bromide digests and both MALDI and ESI sources failed to identify other S-nitrosation sites in rHCaBP. The reasons for the instability of the other S-nitrosated peptides under the peptide mass mapping conditions are not clear. Further analysis using Cys → Ser mutants of rHCaBP is needed to investigate the other site(s) of S-nitrosation as well as mechanism of S-nitrosation and S-thiolation of the protein.

In conclusion, this study reports that HCaBP can be easily S-nitrosated. Hence rHCaBP may act not only as a Ca^{2+} buffer but also as a NO buffer or reservoir in mammalian brain and sensory neurons. Furthermore, since Ca^{2+}-binding affects the extent of S-nitrosation of rHCaBP, there is likely crosstalk between these two buffering capacities of the protein. Accessibility of cysteine residues may be different in the *apo-*

and *holo*protein, as suggested by the CD results, and/or ligation of carboxylate residues by Ca^{2+} may affect the reactivity of cysteine residues towards S-nitrosation. This posttranslational modification is reportedly identified by an "acid-base consensus motif" where cysteine is flanked by acidic and/or basic residues (*112*), (*133*). We are currently studying the relationships between Ca^{2+}-binding, S-nitrosation, and S-thiolation in rHCaBP and its mutants.

Note added to thesis: It was found following publication that the difference between the results of Berggard *et al.* (*114*) and our results comes from the different experimental conditions used. In our experiments, 0.15 M KCl was not present. The lower ionic strength of our solutions causes the fluorescence spectra to differ from that published (*114*).

5.0 Mechanism of S-nitrosation of recombinant human brain calbindin D_{28K} (rHCaBP)

5.1 Abstract

Mass spectrometry and UV–vis absorption results support a mechanism for NO donation by GSNO to rHCaBP that requires the presence of trace copper, added as either Cu,Zn-superoxide dismutase (CuZnSOD) or $CuSO_4$. The extent of copper-catalyzed rHCaBP S-nitrosation depends on the ratio of protein to GSNO and on the reaction time, and NO-transfer is prevented when copper chelators are present. CuZnSOD is an efficient catalyst of rHCaBP S-nitrosation, and the mechanism of CuZnSOD-catalyzed S-nitrosation involves reduction of the active-site Cu^{II} by a number of the five free thiols in rHCaBP, giving rise to thiyl radicals. The Cu^{I}ZnSOD formed catalyzes the reductive cleavage of GSNO present in solution to give GSH and release NO. rHCaBP thiyl radicals react with NO to yield the S-nitrosoprotein. Cu^{II}ZnSOD is also reduced by GSH in a concentration-dependent manner up to 5 mM, but not at higher GSH concentrations. However, unlike the rHCaBP thiyl radicals, $GS^{\bullet}$ radicals dimerize to GSSG faster than their reaction with NO. The data presented here provide a biologically relevant mechanism for protein S-nitrosation by small S-nitrosothiols. S-nitrosation is rapidly gaining recognition as a major form of protein posttranslational modification, and the efficient S-nitrosation of HCaBP by CuZnSOD/GSNO is speculated to be of neurochemical importance given that CaBP and CuZnSOD are abundant in neurons.

5.2 Introduction

NO is a molecule that has, in recent years, been shown to play many roles in bioregulation. It is known to be involved in vasodilation, platelet aggregation, inflammation, and neuronal communication (*4*). In addition, NO has been implicated in many neurodegenerative diseases such as AIDS dementia and Huntington's and Parkinson's diseases (*5*). Since NO is a labile free radical, the way it exerts its biological effects has become the focus of intense research. Recently, it has been reported that NO can react with the thiol groups of small molecules such as glutathione or cysteine to form S-nitroso compounds, which in turn can donate NO to protein thiols (*67*). S-Nitrosothiols are believed to be prevalent in the body (*4*), having been detected in the human airway, plasma, platelets, and neutrophils (*15, 134*). They can confer NO-like biological activities (*135*), and are thought to facilitate NO transport, to prolong its life in blood and tissues, to target its delivery, and to mitigate its cytotoxic potential (*8*). S-Nitrosothiols have also been shown to regulate protein function in numerous systems (*14, 136*). For example, sulfhydryl S-nitrosation (*123*) has been reported to affect the function of serum albumin (*8*), tissue-type plasminogen activator (*137*), gyceraldehyde-3-phosphate dehydrogenase (*138*) and protein-phosphotyrosine phosphatase (*139*). The latter two enzymes are inactivated by S-nitrosation of their active-site cysteine residues.

The mechanisms of formation of low- and high-molecular-weight S-nitroso compounds *in vivo* are still incompletely understood. Attention has focused to date on the reactivity of NO with molecules such as glutathione, cysteine and BSA. It has been reported that S-nitrosothiols are formed by the autoxidation of NO to higher oxides of nitrogen (NOx) (*140*), by metal catalysis (*19*), by the action of dinitrosyl-iron complexes (*17*), or by direct reaction between NO and thiols in the presence of electron acceptors

(*20*). Low-molecular-weight compounds are generally thought to undergo "instantaneous" *trans*-S-nitrosation or SNO-SH exchange reactions (*127, 141*), but the mechanism of NO donation from small S-nitrosothiols to protein thiols has received little attention. Previous results from our lab (*63*) have shown that S-nitrosation of hemoglobin by GSNO, unlike *trans*-S-nitrosation (*142*), requires the presence of redox-active copper:

$$GSNO + Cu^{I} + H^{+} \rightleftharpoons GSH + NO + Cu^{II} \qquad (5.1)$$

$$\text{protein-SH} + NO + Cu^{II} \rightleftharpoons \text{protein-SNO} + Cu^{I} + H^{+} \qquad (5.2)$$

Questions arise as to whether copper catalysis is a general mechanism of protein S-nitrosation, and if it can occur *in vivo* where there is less than one free copper ion per cell (*143*). Interestingly, it has been reported that CuZnSOD catalyzes the decomposition of S-nitrosothiols in the presence of a reductant such as GSH (*60*).

In the present study, the mechanism of rHCaBP S-nitrosation by GSNO is investigated in detail. CaBP is a Ca^{2+}-binding protein noted for its abundance and specific distribution in mammalian brain and sensory neurons. Previously, we reported that rHCaBP has five free thiols and is readily S-nitrosated and S-thiolated (*144*). GSNO, which has been identified as a low-molecular-weight NO carrier *in vivo* (*12, 145*), was used as an NO donor. We now report that the redox turnover of trace copper is required for S-nitrosation of rHCaBP by GSNO and that CuZnSOD is a likely catalyst *in vivo*. Cu^{II}ZnSOD is reduced first by free thiols to give thiyl radicals and Cu^{I}ZnSOD. The latter catalyzes the reductive cleavage of GSNO to release NO, and rHCaBP-based thiyl radicals react with the nascent NO to give the S-nitrosated protein.

5.3 Materials and methods

Materials: Recombinant human brain calbindin D_{28K} (rHCaBP) was prepared as described previously (*144*). Glycine *N*-(*N*-L-γ-glutamyl-S-nitroso-L-cysteinyl) (GSNO) was obtained from Cayman; diethylenetriaminepentaacetic acid (DTPA) from ICN Pharmaceuticals and $CuSO_4 \cdot 5H_2O$ from Anachemia. 2,9-Dimethyl-1,10-phenanthroline hydrochloride (neocuproine) and nitrosonium tetrafluoroborate (BF_4NO) were purchased from Fluka; copper, zinc-superoxide dismutase (CuZnSOD) and bovine serum albumin (BSA) from Roche Molecular Biochemicals; reduced glutathione (GSH), and horse heart myoglobin from Sigma. Nanopure water (MilliQ) from a Millipore system was used to prepare all solutions.

Aerobic modification of rHCaBP by GSNO: rHCaBP (17.2 μM) was incubated with different molar ratios of GSNO in 1 mM TrisHCl buffer (pH 7.4) for 5 to 180 min at room temperature in the presence or absence of chelators (200 μM DTPA and 1 mM neocuproine), 50 μM $CuSO_4$ or 40 μM CuZnSOD.

Anaerobic modification of rHCaBP by GSNO: Anaerobic manipulations were performed under a nitrogen atmosphere (< 2 ppm O_2) in a glove box (Mbraun UniLab Workstation) at 25°C. rHCaBP (20 μM) was incubated with 2.5-fold molar excess GSNO in 1 mM TrisHCl buffer (pH 7.4) for 20 min in the presence of 40 μM CuZnSOD.

Modification of rHCaBP by BF_4NO: A stock solution of BF_4NO (15 mM) was prepared just prior to use in 0.2 M HCl since NO^+ is stable under acidic conditions. An aliquot (0.5 μL) of the BF_4NO stock was added to 19 μM rHCaBP in 10 mM TrisHCl buffer (pH 7.4) to give to a final molar ratio of 1:20 (rHCaBP: BF_4NO). Addition of this

quantity of BF_4NO did not alter the pH of the buffer. The reactions were carried out for 30 min at 30°C in the presence or absence of chelators.

Myoglobin assay for free NO: A solution of horse heart oxymyoglobin (~1.6 mM) in 100 mM potassium phosphate buffer (pH 7.4), was prepared by dithionite reduction of metmyoglobin followed by desalting in air on a G25 NAP-10 1.3 X 2.6-cm column (Amersham Pharmacia Biotech) equilibrated with 100 mM phosphate buffer (pH 7.4). The oxymyoglobin solution was aliquoted and stored at –80°C until needed (*12*). Release of NO from 250 μM GSNO was monitored by following the conversion of oxymyoglobin to metmyoglobin spectrophotometrically in solutions containing 10 μM myoglobin and 50 μM CuZnSOD in 10 mM PBS/1 mM EDTA with or without free thiols. Spectra were recorded in a 1-cm pathlength cuvette at 37°C.

Reduction of CuZnSOD: Conversion of active-site Cu^{II} to Cu^{I} was monitored using the characteristic visible absorption peak of $Cu^{II}ZnSOD$ at 680 nm (*146*). $Cu^{II}ZnSOD$ (0.93 mM) was incubated with or without free thiols (2.0 mM GSH, 2.0 mM Cys, 2.0 mM BSA or 0.5 mM rHCaBP) in 50 mM phosphate buffer/0.2 mM EDTA (pH 7.4) over 30 min at 37°C. Spectra were recorded immediately in a 1-cm pathlength cuvette and again every 3 min over ~ 35 min. The time course of 1 mM CuZnSOD reduction by different concentrations of GSH was also examined. For each concentration of GSH used, spectra were recorded every 0.5 min over 30 min. The data presented are the average of triplicate measurements.

Mass spectrometry: Electrospray ionization mass spectrometry (ESI-MS) was carried out on a ThermoFinnigan SSQ7000 mass spectrometer. Samples for protein mass spectra (10 μL) in TrisHCl buffer (pH 7.4) were desalted using C18 pipette tips

(ZipTip$_{C18}$; Millpore) and eluted from the tips with 50% acetonitrile/0.05% TFA. The eluate (10 μL) was mixed with 200 μL of 75% acetonitrile/0.2% formic acid, and directly infused at a flow rate of 3 μL/min into the ESI source of the mass spectrometer with source and capillary temperatures of 70 and 185°C, respectively, a spray voltage of 4.0 kV and a sheath-gas pressure of 35 psi. Spectra were scanned over an m/z range of 700-1800 at a rate of 5s/scan. The low-mass range (m/z 300–700) of the spectra was examined following sample (100 μL) infusion into the ESI source of the mass spectrometer by flow injection from a 100-μL loop (but no column) attached to the HPLC (Agilent 1090) at 50 μL/min with 75% acetonitrile/0.05% trifluoroacetic acid as a mobile phase. The mass-scale calibration was carried out using myoglobin and L-methionyl-arginyl-phenylalanyl-alanine acetate (MRFA) as reference compounds. Protein mass spectra were deconvoluted using BioWorks software (ThermoFinnigan).

ICP-MS analysis: The copper content in 5 mM rHCaBP and 25 mM Tris-HCl was determined using previously published procedures (*27*).

5.4 Results

The number of cysteine residues in a protein that are S-nitrosated or converted to protein-mixed disulfides can be readily established from accurate mass measurements. To determine the time course and concentration dependence of S-nitrosation and S-glutathiolation of rHCaBP, the protein was incubated with GSNO at different molar ratios for 5–180 min. The mass spectra in Figures 5.1A–C show that at a molar ratio of 1:10 rHCaBP/GSNO, the extent of S-nitrosation is incubation-time dependent. When the incubation time was increased from 5 min (Figure 5.1A) to 180 min (Figure 5.1C), the

major species in solution changed from native protein to doubly NO-labeled protein. Figures 5.1A–C also reveal that, although GSNO is in 10-fold excess, after 180 min some of the thiols in the protein are not modified, which may be due to their lower accessibility or reactivity. When the incubation time was fixed at 20 min, the extent of rHCaBP S-nitrosation increased with the molar ratio of rHCaBP to GSNO (Figures 5.1B,D–E).

Copper is known to catalyze the breakdown of GSNO with NO release (*147*). The metal (1.5 μM) was detected in 5 mM rHCaBP in 25 mM Tris-HCl by ICP-MS (data not shown). Thus, the effects of copper chelators on rHCaBP modification were examined. In the presence of both DTPA (a Cu^{II}-specific chelator) and neocuproine (a Cu^{I}-specific chelator), only the GS adduct of rHCaBP was detected in the mass spectrum after 20 min incubation of the protein with 5-fold excess GSNO (Figure 5.1F), suggesting that S-nitrosation but not S-glutathiolation is a metal-catalyzed process. However, DTPA or neocuproine alone did not completely prevent S-nitrosation (data not shown), revealing that both chelators are necessary to fully inhibit turnover of the trace copper present in solution. This would explain why S-nitrosothiol formation is observed in the presence of the commonly used Cu^{II}-chelators, DTPA and EDTA (*19, 123*). Examination of the low m/z range of the mass spectra showed that incubation with GSNO did not modify the chelators (data not shown).

Could Cu-catalyzed rHCaBP S-nitrosation (eqs 5.1 and 5.2) occur *in vivo*? The catalyst would likely have to be protein-bound copper since there is essentially no free aqueous copper in cells (e.g., yeast contain ≤ 1 copper ion per cell) (*59, 143*). The dominant copper-containing enzyme in cells is CuZnSOD with reported concentrations of 10 μM in yeast, 10-30 μM in erythrocytes and hepatocytes, and immunostaining revealed

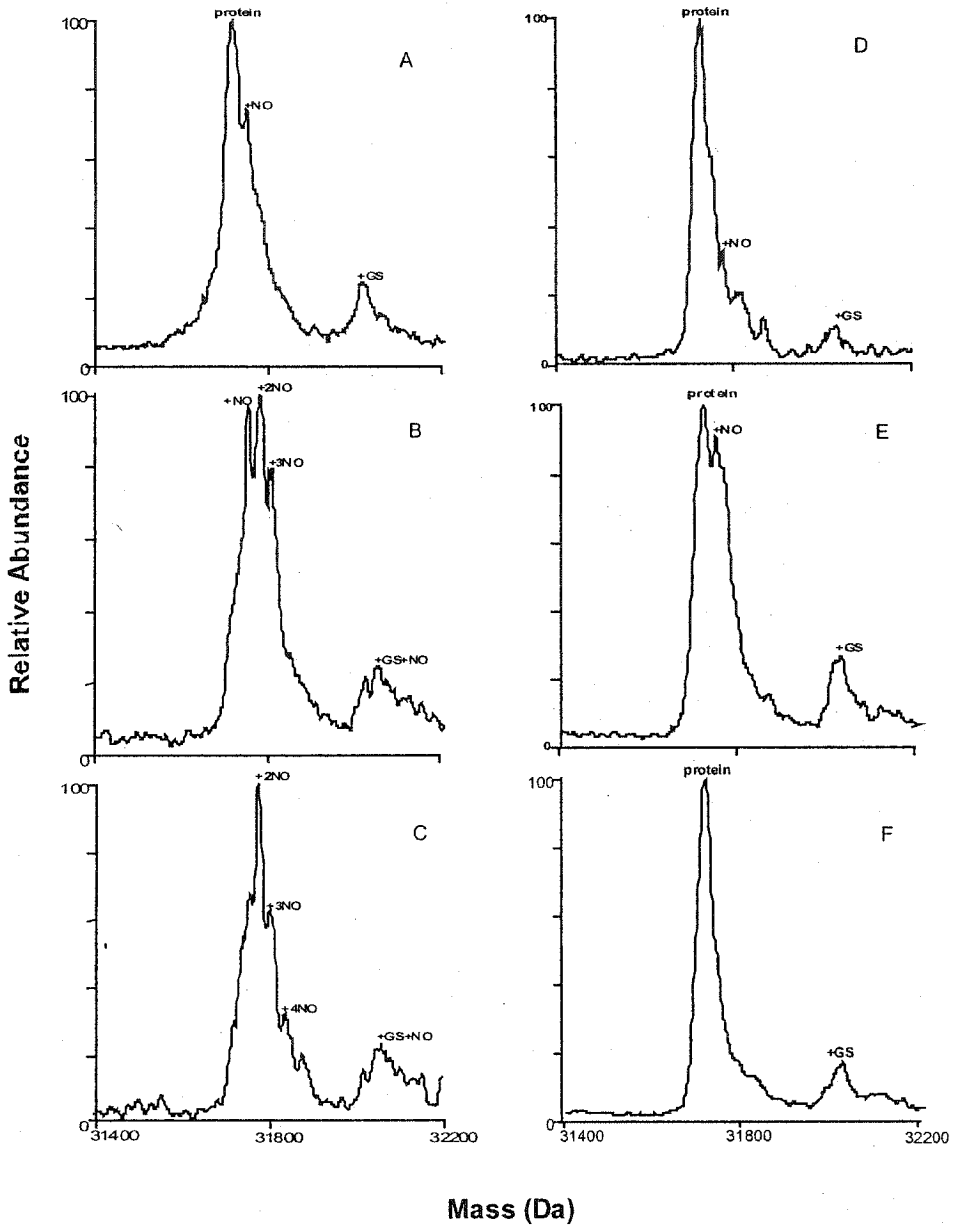

Figure 5.1. **Effects of incubation time, GSNO/rHCaBP molar ratio, and metal chelators on the S-nitrosation of rHCaBP.** Mass spectra of rHCaBP treated with 10-fold molar excess of GSNO for **(A)** 5 min, **(B)** 20 min and **(C)** 180 min, and rHCaBP treated with **(D)** 2.5-fold and **(E)** 5-fold molar excess of GSNO. **(F)** Same as sample E but with 200 μM DTPA and 1 mM neocuproine added. rHCaBP (17.2 μM) was incubated with GSNO in 1 mM Tris-HCl buffer (pH 7.4) at room temperature. Prior to MS analysis, the samples were desalted and diluted into 50% acetonitrile/0.2% formic acid, and directly infused at a flow rate of 3 μL/min into the ESI source of the mass spectrometer with a capillary temperature of 185°C, a spray voltage of 4.0 kV and a sheath-gas pressure of 30 psi.

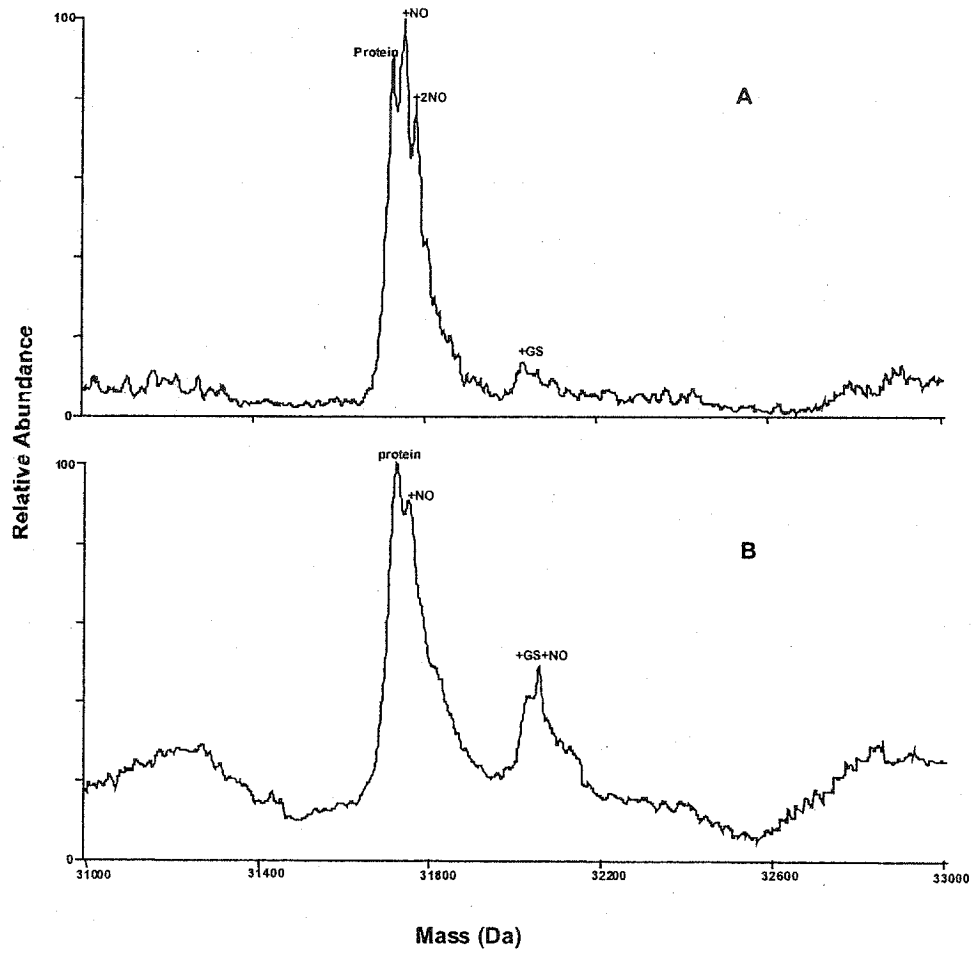

Figure 5.2. **Effects of CuZnSOD and $CuSO_4$ on the S-nitrosation of rHCaBP.** Mass spectra of rHCaBP treated with **(A)** 2.5-fold molar excess of GSNO with 40 μM CuZnSOD and **(B)** 2.5-fold molar excess of GSNO with 50 μM $CuSO_4$ for 20 min in 1 mM Tris-HCl buffer (pH 7.4) at room temperature. The mass spectral conditions are given in Figure 5.1.

exceptionally high concentrations in motor neurons (*59*). Thus, the effects of bovine CuZnSOD on rHCaBP modification by GSNO was examined. After 20-min incubation of rHCaBP with 2.5-molar excess GSNO, the protein was extensively NO-labeled in the presence but not in the absence of CuZnSOD (Figure 5.2A vs Figure 5.1D). In contrast, CuZnSOD had little effect on the extent of rHCaBP S-glutathiolation (Figure 5.2A vs Figure 5.1D). Interestingly, when copper was added as $CuSO_4$, the yields of rHCaBP S-nitrosation are clearly lower than in the presence of CuZnSOD (Figure 5.2B vs Figure 5.2A). This reveals that free copper is a less selective catalyst than CuZnSOD; thus, copper released from the enzyme is unlikely a cocatalyst in CuZnSOD-catalyzed rHCaBP S-nitrosation (Figure 5.2A).

It has been proposed that S-nitrosothiols such as GSNO act as NO^+ donors and undergo direct *trans*-S-nitrosation with thiols such as cysteine (CysH) (*93, 148*):

$$GSNO + CysH \rightleftharpoons GSH + CysNO \qquad (5.3)$$

BF_4NO is exclusively an NO^+ donor that can force S-nitrosoprotein generation by direct attack of NO^+ on free thiols. Thus, to distinguish between NO^+ and NO release from GSNO, BF_4NO-treated rHCaBP was examined by ESI-MS in the presence and absence of copper chelators. Although the mass spectra are noisy due to salt effects and not all peaks can be identified, the results reveal that S-nitrosation of rHCaBP by BF_4NO is actually more extensive in the presence of the chelators (Figure 5.3B) than in their absence (Figure 5.3A). Since copper-chelation prevents protein S-nitrosation by GSNO (Figure 5.1F) but not by NO^+ (Figure 5.3B), this eliminates direct NO^+ transfer from GSNO to rHCaBP as shown for free CysH in reaction 5.3.

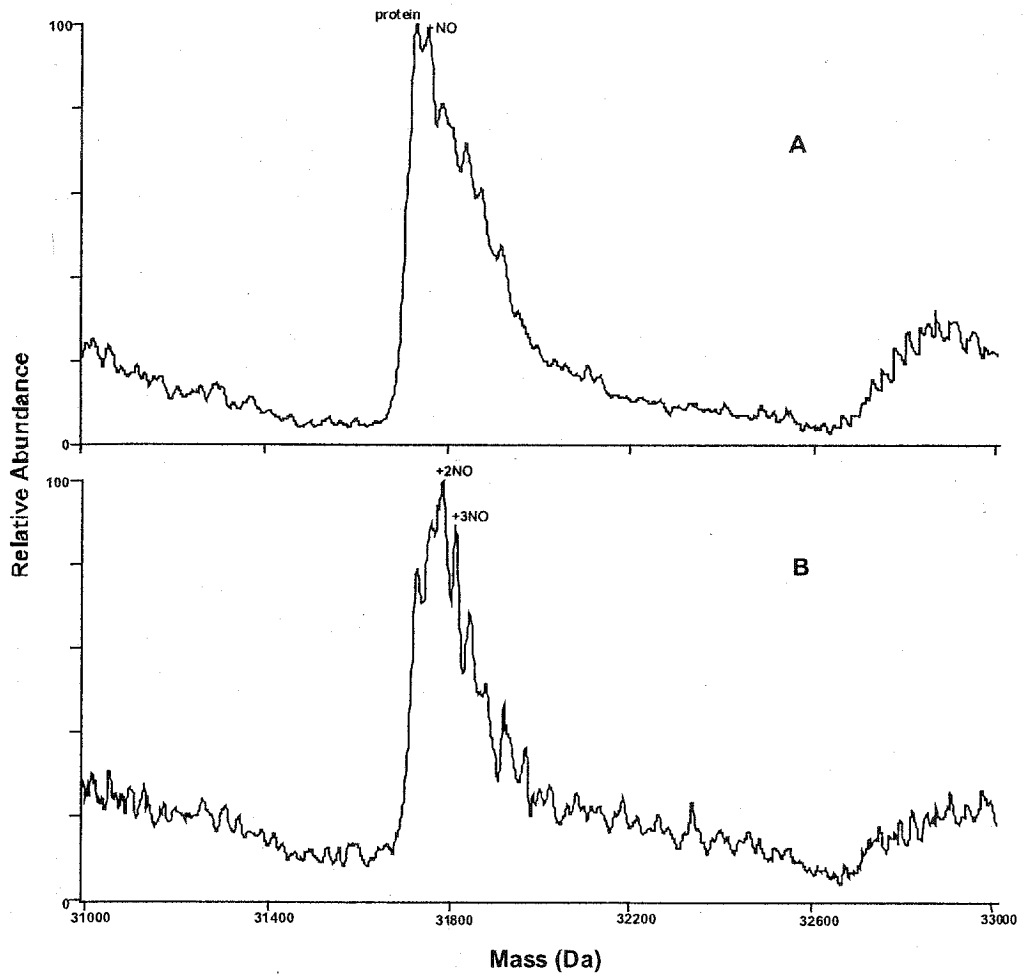

Figure 5.3. **Effects of chelators on the S-nitrosation of rHCaBP by BF_4NO.** Mass spectra of BF_4NO-treated rHCaBP in the **(A)** absence and **(B)** presence of chelators. rHCaBP was incubated with 20-fold molar excess of BF_4NO for 30 min in 10 mM Tris-HCl buffer (pH 7.4) at 30°C with or without 200 μM DTPA and 1 mM neocuproine. The mass spectral conditions are given in Figure 5.1.

What is the mechanism of CuZnSOD-catalyzed rHCaBP S-nitrosation? Incubation of rHCaBP/GSNO/CuZnSOD under anaerobic conditions gives rise to a protein product with a mass spectrum very similar to that in Figure 5.2A (data not shown), revealing that O_2 does not play a role in this S-nitrosation process. Does CuZnSOD act as an NO transferase? Oxymyoglobin ($MbFe^{II}O_2$) was used as a scavenger to detect if any NO was released during the incubation. NO is quickly scavenged [$k = (43.6 \pm 0.5) \times 10^6$ $M^{-1}s^{-1}$ at pH 7.0] (*149*) by $MbFe^{II}O_2$ to give metmyoglobin ($MbFe^{III}$):

$$MbFe^{II}O_2 + NO \rightleftharpoons MbFe^{III} + NO_3^- \qquad (5.4)$$

Reaction 5.4 can be readily monitored spectrophotometrically since a decrease in absorbance at 542 and 580 nm ($MbFe^{II}O_2$ decay) is accompanied by increased absorbance at 632 and 502 nm ($MbFe^{III}$ growth), and the Soret band at 416 nm ($MbFe^{II}O_2$) shifts to 408 nm ($MbFe^{III}$). Figure 5.4A shows that CuZnSOD and GSNO together have negligible effect on the Mb absorption spectra, but when a free thiol, such as GSH (Figure 5.4B) or rHCaBP (Figure 5.4C) is added, absorbance changes consistent with $MbFe^{II}O_2$ decay and $MbFe^{III}$ formation are observed, indicating that NO was released from GSNO and scavenged by $MbFe^{II}O_2$ (eq 5.4).

Reduction of Cu^{II}ZnSOD to Cu^{I}ZnSOD by the free thiols was detected by directly monitoring the visible spectrum of the protein. A band centered at 680 nm has been assigned to the *d-d* absorption of Cu^{II} at the active site of CuZnSOD (*146*). When Cu^{II} is reduced to Cu^{I}, the 680-nm band disappears. The inset to Figure 5.5 reveals that in the absence of free thiols, the Cu^{II}ZnSOD absorbance at 680 nm was essentially constant over 30 min at 37°C but decreased on a similar time scale when free thiols, such as GSH (Figure 5.5A) or rHCaBP (Figure 5.5B), were added. Since rHCaBP has five free thiols

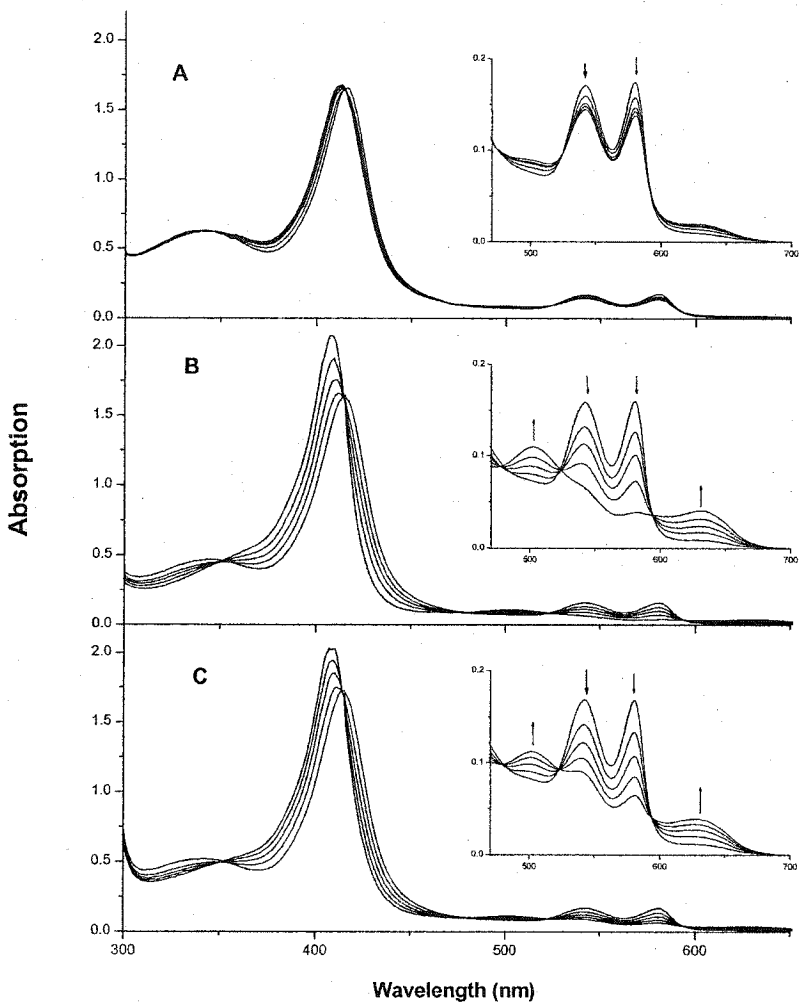

Figure 5.4. **Time-dependent spectral changes in $MbFe^{II}O_2$ because of NO scavenging.** Absorbance decreases at 416, 542 and 580 nm ($MbFe^{II}O_2$ decay) are accompanied by increases at 408, 502 and 632 nm ($MbFe^{III}$ growth). **(A)** Mb + CuZnSOD + 250 μM GSNO; **(B)** Mb + CuZnSOD + 125 μM GSNO + 0.5 mM GSH; **(C)** Mb + CuZnSOD +125 μM GSNO + 0.1 mM rHCaBP. All solutions contained 10 μM $MbFe^{II}O_2$ and 50 μM CuZnSOD in 10 mM PBS with 1 mM EDTA at 37°C. Spectra were recorded at 0, 5, 10, 15, and 20 min in a 1-cm pathlength cuvette.

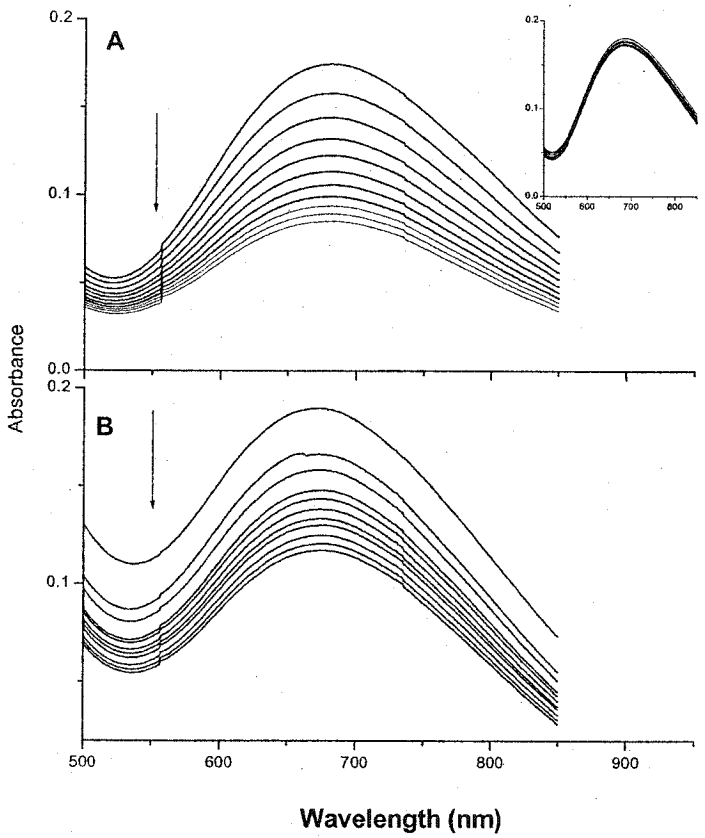

Figure 5.5. **Effects of GSH and rHCaBP on the visible absorption spectrum of 0.93 mM Cu^{II}ZnSOD.** **(A)** CuZnSOD with 2 mM GSH, **(B)** CuZnSOD with 0.5 mM rHCaBP, and CuZnSOD alone (inset, panel A). Incubations were in 50 mM phosphate buffer/0.2 mM EDTA (pH 7.4) over 30 min at 37°C. Spectra were recorded at 0, 3, 9, 15, 18, 21, 24, 27, 30, 33, and 36 min in a 1-cm pathlength cuvette.

(*144*), four of which are exposed based on DTNB titrations (data not shown), a 4-fold molar excess of GSH over rHCaBP was used. Since the time scale of NO scavenging (Figure 5.4) is similar to that of active-site Cu^{II} reduction (Figure 5.5), the latter must be the rate-limiting step in Cu^{I}ZnSOD-catalyzed reductive cleavage of GSNO.

The reduction of Cu^{II}ZnSOD at higher concentrations of GSH was investigated since GSH levels are usually 2-10 mM *in vivo* (*150*). At $\leq$ 5 mM GSH, the reaction showed a free-thiol concentration-dependence, which disappeared above 5 mM (Figure 5.6A). Moreover, Cu^{II}ZnSOD was never reduced fully by physiological concentrations of GSH even after 3 h incubation (data not shown).

Free cysteine and BSA were used to further probe the efficiency of various free thiols as donors to Cu^{II}ZnSOD. On addition of cysteine, the absorbance at 680 nm decreased to almost zero within 10 min as reported (*151*), followed by a slow increase, indicating reoxidation of the active-site copper in air (Figure 5.6B, trace 5). No absorbance loss at 680 nm was observed in the presence of BSA (Figure 5.6B, trace 2), although titration with DTNB revealed that ~ 40% of BSA possessed a free thiol (data not shown).

To fully investigate the mechanism of CuZnSOD-catalyzed rHCaBP S-nitrosation, it is necessary to also know the species produced from GSNO. After a 20-min incubation of rHCaBP with 2.5-fold molar excess of GSNO in the presence of CuZnSOD, only GSH was detected by mass spectrometry (Figure 5.7A).

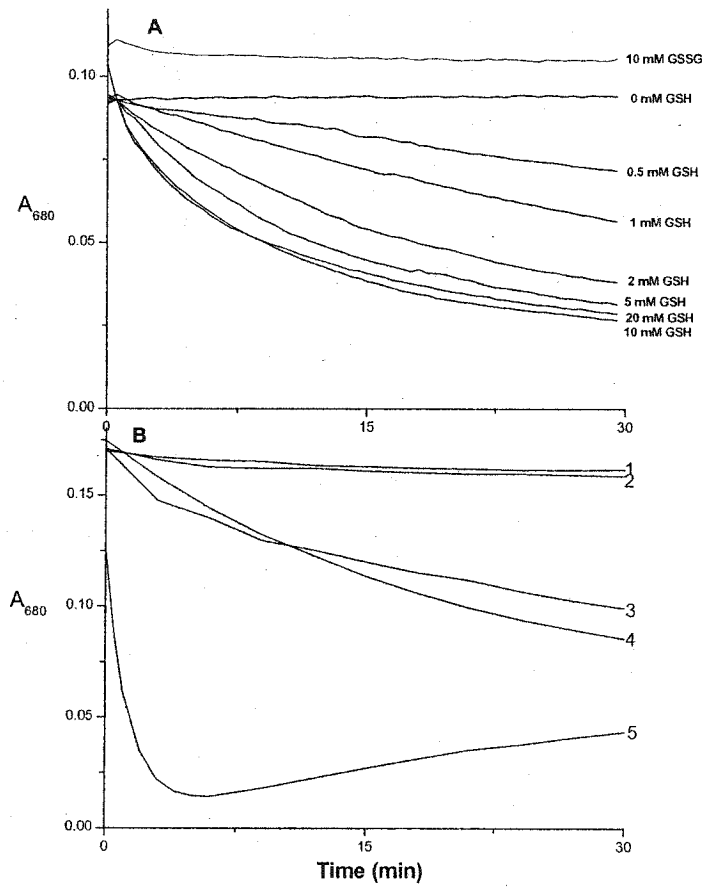

Figure 5.6. **Plot of Cu^{II} *d-d* absorption at 680 nm vs time on incubation of Cu^{II}ZnSOD with thiols. (A)** 0.58 mM Cu^{II}ZnSOD with 10 mM GSSG or 0.5 mM Cu^{II}ZnSOD with the GSH concentrations indicated on the traces. The data are the averages of triplicate experiments. **(B)** 0.93 mM Cu^{II}ZnSOD only (trace 1), and Cu^{II}ZnSOD with: 2 mM BSA (trace 2), 0.5 mM rHCaBP (trace 3), 2 mM GSH (trace 4), and 2 mM cysteine (trace 5). Samples were in 50 mM phosphate buffer/0.2 mM EDTA (pH 7.4) at 37°C. Absorbances at 680 nm were recorded immediately after thiol addition to Cu^{II}ZnSOD and repeated every 0.5 min over 30 min.

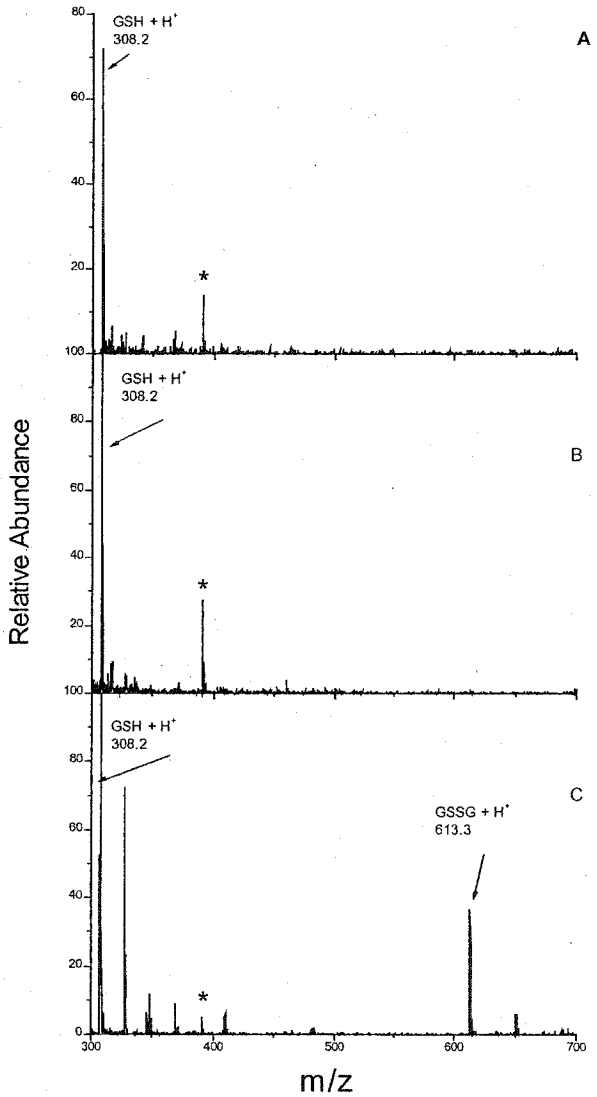

Figure 5.7. **Mass spectra in the low m/z range.** (**A**) rHCaBP (~15 μM) was incubated with 2.5-fold molar excess of GSNO in the presence of 40 μM CuZnSOD for 20 min in 1 mM Tris-HCl buffer (pH 7.4) at room temperature. (**B**) 0.5 mM or (**C**) 20 mM GSH was incubated with 1 mM CuZnSOD in the absence of GSNO for 2 h in 50 mM phosphate buffer/0.2 mM EDTA (pH 7.4) at 37°C. Samples (100 μL) were infused into the electrospray source of the mass spectrometer by flow injection at 50 μL/min with 75% acetonitrile/0.05% trifluoroacetic acid as a mobile phase. The capillary temperature was 180°C, and the spray voltage 4.0 kV. The mass spectrum of the mobile phase was recorded and subtracted from the spectra of the samples. The peak at m/z 391 marked with an asterisk is due to a bis(2-ethyl-hexyl) phthalate impurity in the system (*152*).

5.5 Discussion

The extent of rHCaBP S-nitrosation by GSNO depends on the incubation time and rHCaBP/GSNO ratio (Figure 5.1). After 20 min, ~1-2 cysteine residues were S-nitrosated (rHCaBP/GSNO = 1:10), which increased to ~3-4 after 180 min. These results are consistent with a number of studies that demonstrated that enzymes with active-site cysteines are inhibited by NO donors in a time- and concentration-dependent manner (*128*). rHCaBP S-nitrosation occurs only in the presence of redox-active copper (e.g., Figure 5.1E vs Figure 1F). Turnover of copper by redox cycling is required (eqs 5.1 and 5.2) and the present results suggest that both Cu^{I}- and Cu^{II}-chelators are necessary to fully inhibit this turnover. Previous results from our lab (*142*) indicated that S-nitrosation of oxyhemoglobin at Cysβ93 by GSNO also requires redox-active copper. In contrast to S-nitrosation, S-thiolation of rHCaBP by GSNO occurred within 5 min and only slightly increased after 25 min. This mirrors the reported time course of S-glutathiolation of glyceraldehyde-3-phosphate dehydrogenase (*64*).

The presence of CuZnSOD dramatically increases rHCaBP S-nitrosation (Figure 5.2A). Because free copper also catalyzes rHCaBP S-nitrosation (Figure 5.2B), it is important to establish whether CuZnSOD-catalyzed S-nitrosation is due to its active-site copper or to copper non-specifically associated with the enzyme. Since copper added as $CuSO_4$ is a less selective catalyst than CuZnSOD (Figure 5.2B vs Figure 5.2A), the S-nitrosation activity of the enzyme must be associated with its active-site copper. This was confirmed by pretreating CuZnSOD with DTPA to remove free copper (*151*), which did not diminish the ability of the enzyme to promote NO release from GSNO as detected by the Mb assay (eq 5.4) (data not shown). Furthermore, Figures 5.5 A and B show that both

GSH and rHCaBP reduce the active-site copper, thus allowing its redox turnover. Combined, these data establish that S-nitrosation of rHCaBP is mediated by the active-site copper in CuZnSOD rather than free copper. Nonetheless, the possibility exists that free copper may be a much more rapid catalyst of *both* S-nitrosothiol formation and breakdown (i.e., eq 5.2) (*59*), thereby decreasing the yield of protein S-nitrosation compared to that in the CuZnSOD-catalyzed reaction. Chelation of free Cu^{II} by GSSG (*147*) or rHCaBP would also explain the lower yield of S-nitrosation in incubates containing $CuSO_4$ (Figure 5.2B).

Using $MbFe^{II}O_2$ as an NO scavenger (eq 5.4), it was found that CuZnSOD catalyzes NO release from GSNO in the presence of GSH or rHCaBP (Figure 5.4). Since electron donors such as thiols are required for the reductive cleavage of GSNO, formation of Cu^{I}ZnSOD in the presence of various free thiols was investigated. By monitoring the time course of decay of the Cu^{II} *d-d* absorption at 680 mm, the ability of free thiols to reduce Cu^{II}ZnSOD was found to be different (Figures 5.5 and 5.6). Cysteine, the smallest thiol used, was the fastest reductant, whereas no reduction was observed with BSA (Figure 5.6B). Thus, steric control of access to the catalytic site may be a critical factor in CuZnSOD-mediated S-nitrosation. For example, the active-site Cu^{II} appears to be accessible to ~2 of the five thiols in rHCaBP (*144*) and to Cysβ93 of oxyhemoglobin (A. Romeo, personal communication) but not to the single free thiol (Cys34) of BSA. The intrinsic reactivity of a protein thiol depends on its pK_a value since the thiolate anion is much more reactive towards S-nitrosation than the thiol (*153*). Cys34, which contains the single sulfhydryl group of BSA, has a low pK_a (4.5) compared to GSH (8.75) (*12, 154*), and the X-ray structure of human serum albumin (*155*) showed that Cys34 is partially

solvent exposed. BSA is readily S-nitrosated at Cys34 by free copper and NO (*19*), so its lack of reactivity in CuZnSOD–catalyzed S-nitrosation indicates that selectivity is dictated by specific protein-protein interactions. Thus, sites of protein S-nitrosation *in vivo* will likely depend not only on concentration, but also on access to catalysts such as CuZnSOD, giving rise to specificity. Unfortunately, the crystal structure of rHCaBP is not yet known, so modeling its interaction with CuZnSOD is not now possible.

The rate of Cu^{II}ZnSOD reduction by GSH (Figure 5.6A) was found to be concentration dependent up to 5 mM. Negligible increased reduction was observed above 5 mM GSH, which suggests product inhibition. Figure 5.7C shows that GSSG is present in the products, and more GSSG was formed at higher concentrations of GSH (Figures 5.7C vs Figure 5.7B). GSSG chelates free Cu^{II} (*147*) but Figure 5.6A shows that 10 mM GSSG causes negligible change in the 680-nm absorbance of Cu^{II}ZnSOD, indicating that it does not remove Cu^{II} from the enzyme. GSSG may block the active-site crevice and inhibit further reduction of the Cu^{II} center by GSH. This would allow CuZnSOD to function as a superoxide dismutase in the presence of high cytosolic GSH. Due to the activity of glutathione reductase (*156*), GSSG levels *in vivo* are < 5% those of GSH, but they may be sufficient to inhibit reduction of Cu^{II}ZnSOD by GSH.

Taking all the present results into consideration, the following mechanism for CuZnSOD-catalyzed protein S-nitrosation is proposed:

$$Cu^{II}ZnSOD + CaBP\text{-}SH \rightleftharpoons Cu^{I}ZnSOD + CaBP\text{-}S^{\bullet} + H^{+} \qquad (5.5)$$

$$Cu^{I}ZnSOD + GSNO + H^{+} \rightleftharpoons GSH + NO^{\bullet} + Cu^{II}ZnSOD \qquad (5.6)$$

$$NO^{\bullet} + CaBP\text{-}S^{\bullet} \rightleftharpoons CaBP\text{-}SNO \qquad (5.7)$$

The active-site Cu^{II} in CuZnSOD is first (partially) reduced to Cu^{I} by free protein thiols, such as those of rHCaBP (eq 5.5). Then Cu^{I} catalyzes the reductive cleavage of GSNO (eq 5.6), and the nascent NO radical is scavenged by a protein-based thiyl radical such as CaBP-S$^{\bullet}$ yielding the S-nitrosated protein (eq 5.7). A role for any oxygen-derived species in CuZnSOD-mediated S-nitrosation is excluded since the yields of S-nitroso-rHCaBP were the same in the absence or presence of O_2. Furthermore, NO gas added to anaerobic rHCaBP/CuZnSOD incubation did not lead to detectable nitrosation of rHCaBP (data not shown). This supports the mechanism given in eqs 5.5-5.7 since the thiyl radical yield would be low in the absence of a reaction that regenerates Cu^{II}ZnSOD (eq 5.6).

Cu-catalyzed dimerization of low-molecular-weight thiyl radicals such as GS$^{\bullet}$ is efficient and competes with their reaction with NO (*19*). However, no CuZnSOD-catalyzed dimerization of rHCaBP was detected by SDS-PAGE (data not shown), presumably because steric hindrance prevents rHCaBP cross-linking via the thiyl radicals formed. Thus, protein thiyl radicals undergo reaction 5.7, whereas GS$^{\bullet}$ radicals dimerize to GSSG (Figure 5.7C) following their production when GSH is a donor as shown for CaBP in reaction 5.5.

Since CaBP, Ca^{2+}, NO and CuZnSOD are implicated in neurodegenerative disorders such as Parkinson's and Huntington's diseases (*5, 39*), a full understanding of their chemistry *in vitro* is crucial to understanding their possible interactions *in vivo*. For example, as shown here and elsewhere (*59*), CuZnSOD catalyzes GSNO breakdown (reaction 5.6), but we have not yet established if and under what conditions CuZnSOD will catalyze S-nitroso-rHCaBP breakdown and NO release.

We speculate that CuZnSOD is an efficient catalyst of CaBP S-nitrosation *in vivo*. CaBP levels in auditory neurons are estimated to reach 2 mM (*157*). Muller and co-workers (*158*) report that granule cells most likely contain several hundred micromolar CaBP, which controls calcium microdomains in hippocampal neurons and acts as a freely diffusible intracellular calcium buffer. Thus, high local concentrations of CaBP would compete with millimolar GSH (*67*) as a reductant of Cu^{II}ZnSOD. The thiyl radicals formed would efficiently trap any NO released from GSNO or other nitrosothiol, allowing CaBP to serve as an NO buffer in addition to its function as a calcium buffer (*38*). In this context, it is of note that the prototypical calcium-sensor protein, calmodulin, does not possess a single cysteine residue (*159*) in contrast to the five free cysteine residues present in CaBP (*144*).

6.0 Protein S-glutathiolation triggered by decomposed S-nitrosoglutathione

6.1 Abstract

Recombinant human brain calbindin D_{28K} (rHCaBP), human Cu,Zn-superoxide dismutase (HCuZnSOD), rabbit muscle glyceraldehyde-3-phosphate dehydrogenase (GAPDH), and bovine serum albumin (BSA) were found to be S-glutathiolated in decomposed S-nitrosoglutathione (GSNO) solutions. Tryptic or Glu-C digestion and MALDI-TOF-MS analyses of the digests are consistent with S-thiolation of Cys111 and Cys187 of HCuZnSOD and rHCaBP, respectively, on exposure to decomposed GSNO. GAPDH activity analysis reveals that S-glutathiolation most likely occurs on the active-site Cys149, and the single free Cys34 is assumed to be the site of S-glutathiolation in BSA. The yields of S-glutathiolation of rHCaBP, GAPDH and BSA were much higher than that of HCuZnSOD. The latter is limited by accessibility of Cys111 to the glutathiolating reagent in the HCuZnSOD dimer. Unlike decomposed GSNO, fresh GSNO, reduced glutathione (GSH) or oxidized glutathione (GSSG) are not efficient S-glutathiolating agents for the proteins examined here. Based on analysis by mass spectrometry and UV-visible absorption, GSNO decomposition in the dark at room temperature yields glutathione disulfide S-oxide [GS(O)SG], glutathione disulfide S-dioxide (GSO_2SG), and GSSG as products. GS(O)SG is the efficient protein S-glutathiolating agent in GSNO solutions, not GSNO, which does not efficiently carry out S-glutathiolation of rHCaBP, HCuZnSOD or GAPDH *in vitro*. A hydrolysis pathway yielding GSOH and nitroxyl HNO/NO^- as intermediates is proposed for GSNO

decomposition in the dark. This is based on inhibition of GSNO breakdown by dimedone, a reagent specific for sulfenic acids, and nitroxyl scavenging by metmyoglobin. The results presented here are contrary to numerous reports of protein S-thiolation by low-molecular-weight S-nitrosothiols.

6.2 Introduction

Protein S-thiolation is a reversible oxidative modification that involves disulfide linkage of GSH (S-glutathiolation), or related low-molecular-weight thiols such as cysteine, to proteins *in vivo* (*160, 161*). Protein S-glutathiolation was introduced into the field of redox biochemistry almost 50 years ago as a possible mechanism of protein regulation in response to changes in the intracellular redox status (*31*). Currently, protein S-glutathiolation is being reinvestigated as a mechanism of redox- and NO-mediated signal transduction as well as a cellular response to oxidative and/or nitrosative stress (*145, 162*). Interrelations between S-glutathiolation, thiol oxidation and S-nitrosation leading to the formation of mixed disulfides between protein thiols and the tripeptide GSH may serve to transduce oxidative and nitrosative stimuli into a functional response at various levels of cellular signalling (*31*).

Stress-induced protein S-thiolation is poorly understood. Several mechanisms have been proposed for protein S-glutathiolation including: (a) thiol-disulfide exchange between a protein thiol and GSSG (*163*), (b) oxidation of a protein thiol by oxy radicals or H_2O_2 to form a thiyl radical or sulfenic acid that reacts with GSH to produce a mixed disulfide (*164*), (c) oxidation of GSH to the sulfenic acid GSOH that reacts with a protein thiol to form a mixed disulfide (*165*), (d) nucleophilic attack of a protein thiolate on

GSNO to produce a mixed disulfide (*64, 128, 145, 165*), and (e) S-nitrosation of a protein thiol followed by reaction with GSH to yield a mixed disulfide (*145, 165*).

Numerous groups have reported protein S-thiolation by low-molecular-weight S-nitrosothiols (RSNO) (*64, 128, 145, 165-167*). The list includes many proteins that contain activated cysteine residues such as aldose reductase (*166*), cathepsin K (*128*), glyceraldehyde-3-phosphate dehydrogenase (GAPDH) (*64*), papain (*123*) and caspase-3 (*167*). It has also been proposed (*156*) that a product of GSNO decomposition, GS(O)SG, is a protein glutathiolating agent. In this study, we compare protein S-glutathiolation in fresh and aged GSNO solutions. We recently reported that recombinant human brain calbindin D_{28k} (rHCaBP), a Ca^{2+}-binding protein noted for its abundance and specific distribution in mammalian brain and sensory neurons, has five free thiols and is readily S-glutathiolated *in vitro* (*144*). Since rHCaBP has not been reported to be S-glutathiolated *in vivo*, modifications of human Cu,Zn-superoxide dismutase (HCuZnSOD), GAPDH and BSA triggered by GSNO were also investigated. S-thiolated forms of HCuZnSOD have been isolated from normal cells and from cells of individuals with amyotrophic lateral sclerosis (*168-170*). GAPDH has been identified as a major S-glutathiolated protein in endothelial cells and in rat heart under oxidative stress (*171, 172*), and was reported to be S-glutathiolated by GSNO *in vitro* as well as in endothelial cells (*64*). Serum albumin is the most abundant protein in plasma and is assumed to play an antioxidant role because of its scavenging of reactive oxygen and nitrogen species (*173-175*). The group responsible for this property is its only free thiol on Cys34, which comprises ~80% of the total free thiols in plasma (*173*).

A mechanism for rHCaBP, HCuZnSOD, GAPDH and BSA S-glutathiolation trigged by GSNO breakdown is proposed here. GSNO is hydrolyzed to glutathione sulfenic acid, GSOH, and the nitroxyl (HNO/NO^-). The reaction of GSOH with GSNO or dimerization of GSOH yields glutathione disulfide S-oxide [GS(O)SG], which is the active protein S-glutathiolating agent (*156*) in GSNO solutions. The results obtained upon addition of sulfenic acid and nitroxyl scavengers support the proposed mechanism.

6.3 Materials and methods

Materials: Recombinant His-tagged human brain calbindin D_{28K} (rHCaBP) was prepared as described previously (*144*). The Ni-NTA-purified protein was dialyzed against 20 mM TrisHCl (pH 7.4) containing 100 mM NaCl and 2 mM $CaCl_2$, and then digested with 1:100 (w/w) factor Xa (Promega) for 18 h at room temperature to cleave the His-tag. Any remaining His-tagged rHCaBP was removed by rebinding the sample to the Ni-NTA beads. S-nitrosoglutathione (GSNO) was obtained from Cayman; diethylenetriaminepentaacetic acid (DTPA) from ICN Pharmaceuticals; 2,9-dimethyl-1,10-phenanthroline (neocuproine) from Fluka; 5,5-dimethyl-1,3-cyclohexanedione (dimedone) from Aldrich; glutathione (GSH), glutathione disulfide (GSSG), 5,5'-dithio-bis(2-nitrobenzoic acid) (DTNB), human Cu,Zn-superoxide dismutase (HCuZnSOD), catalase, horse heart myoglobin, bovine serum albumin (BSA) and *dl*-dithiothreitol (DTT), human [Glu^1]-fibrinopeptide B, α-cyano-4-hydrooxycinnamic acid, ACTH, rennin and angiotensin I. were from Sigma. Trypsin (modified sequencing grade), bovine CuZnSOD and rabbit muscle GAPDH were from Roche; 2-propanol was from Fisher

Scientific. Nanopure water (MilliQ) from a Millipore system was used to prepare all solutions.

Preparations of HCuZnSOD stock solutions: Commercial HCuZnSOD was reduced by incubating 1 mg/ml with 5 mM DTT in 50 mM phosphate buffer (pH 7.4) at 30°C for 1.5 h. The small reagents were removed on a NAP-5 1.3-cm × 2.6-cm G25 column (Amersham Pharmacia Biotech) pre-equilibrated with N_2-saturated 50 mM TrisHCl buffer (pH 7.4) or 50 mM ammonium acetate buffer (pH 4.0) for 1 h just before use. Reduced HCuZnSOD was concentrated by ultrafiltration using an Ultrafree-0.5 centrifugal filter (Millipore) and incubated immediately after preparation with fresh or decomposed GSNO. The number of free cysteine residues was determined by monitoring on a Cary Varian spectrophotometer the absorbance at 412 nm (ε=14.15 $mM^{-1}cm^{-1}$) of the 5-thio-2-nitrobenzoate dianion (TNB^{2-}) generated by the reaction of 200 μM DTNB with the free SH groups of 40 μM HCuZnSOD (*116*) in 100 mM potassium phosphate buffer (pH 7.27) containing 1 mM EDTA.

Preparation of GAPDH stock solutions: An ammonium sulphate suspension of GAPDH was diluted 2-fold with water and dialyzed (6,000-8,000–Da cut-off dialysis tubing) against water for 3 h, followed by three changes of 50 mM TrisHCl buffer (pH 7.4) over a total of 48 h. The concentration of the resulting protein solution was determined spectrophotometrically (ε_{280} = 149 $mM^{-1}cm^{-1}$) (*176*).

Preparation of BSA stock solutions: The number of free cysteine residues in BSA was determined as described above for HCuZnSOD. BSA was incubated with 2 mM DTT for 3 h at room temperature, and excess DTT was removed by dialysis (12,000-14,000 Da cut-off dialysis tubing) against 100 μM DTPA for 48 h with three changes.

This procedure increased the number of free cysteines from 0.33 to 0.86 per BSA molecule.

Fresh and decomposed GSNO stock solutions: Fresh GSNO solutions were prepared in MilliQ water just before being used and kept on ice. The GSNO concentration was determined spectrophotometrically (ε_{330nm} = 767 $M^{-1}cm^{-1}$) (*65*)]. Decomposed GSNO was prepared by storage of aqueous solutions at room temperature in the dark until no SNO absorption (334 nm) was detected (~60 h). Note that the GSNO solutions were always protected from light.

Nitroxyl scavenging: Metmyoglobin was prepared (*12*) by oxidizing myoglobin with a 5% molar excess of potassium ferricyanide in 100 mM potassium phosphate buffer (pH 7.0). The low-molecular-weight products were removed on a NAP-10 column equilibrated with MilliQ water, and metmyoglobin at a final concentration of 185 μM was incubated with 5 mM GSNO with and without 5 mM dimedone in water at 20°C in the dark. The reaction solutions were diluted 10-fold into degassed 100 mM potassium phosphate (pH 7.0) in a sealed 0.4-cm cuvette, and the spectrum of myoglobin was recorded. To measure the amount of GSNO remaining, myoglobin was removed by ultrafiltration using Ultrafree-0.5 centrifugal filters, and the absorbance at 330 nm was recorded in a 1-cm cuvette.

Reactivity of proteins with GSNO, GSH or GSSG: rHCaBP was incubated with different molar ratios of GSNO, GSH, or GSSG in 50 mM TrisHCl buffer (pH 7.4) for 20 min at 37°C or room temperature. HCuZnSOD, GADPDH and BSA were incubated in GSNO solutions under the conditions given in the figure legends.

UV-vis spectrophotometric analyses: UV-vis measurements were used to investigate the decomposition of GSNO in the presence and absence of metal chelators or dimedone. Spectra were recorded in 1-cm cuvettes at 25°C on a Beckman DU 650 spectrophotometer. Appropriate blanks, run under the same conditions, were subtracted from the sample spectra.

Mass spectrometry: Electrospray ionization mass spectrometry (ESI-MS) was carried out on a Waters Micromass QTOF2 mass spectrometer. Protein samples (except BSA) were exchanged into water on NAP-5 columns, concentrated by ultrafiltration using Ultrafree-0.5 centrifugal filters, and added to 60 μL of 50% acetonitrile/0.2% formic acid mixture to give final protein concentrations of 1-2 μM. BSA was purified by dialysis against MilliQ water for 48 h with three changes, and diluted ~15-fold into 20% methanol/5% acetic acid mixture to a final concentration of 5-10 μM. Samples were directly infused into the Z-spray source of the QTOF2 apparatus at a flow rate of 1 μL/min. Mass calibration was carried out using human [Glu^1]-fibrinopeptide B. Protein mass spectra were deconvoluted using MaxEnt 1 software (Waters Micromass).

Peptide mass mapping: HCuZnSOD (~20 μg) was dissolved in a 60% acetonitrile/0.1% TFA mixture and dried on a Speed Vac. This step improved the digestion efficiency probably because HCuZnSOD is irreversibly unfolded to some extent in 60% acetonitrile/0.1% TFA mixture, making the digestion sites more accessible. The sample was resuspended in 20 μL of 100 mM TrisHCl (pH 8.8) and heated to ~90°C for 5 min to further denature the protein (*177*). After the sample had cooled in an ice-water bath, 2 μL of trypsin (0.5 μg/μL in 1% acetic acid) was added, the solution was incubated at 37°C for 18 h, and digestion was stopped by freezing to –80°C. Peptides

were desalted using C18 tips ($ZipTip_{C18}$, Millipore) and eluted from the tips with a 60% acetonitrile/0.1% TFA mixture. The eluate (1.5 μL) was mixed with 1.5 μL of matrix solution [100 μL α–cyano-4-hydroxycinnamic acid (40 mg/mL in acetone), 10 μL nitrocellulose (20 mg/mL in acetone), 40 μL acetone, and 50 μL 2-propanol], and 1.5 μL of the peptide/matrix mixture was spotted onto a 96-well MALDI plate and air-dried. Samples were analyzed using a Waters Micromass M@LDI-TOF mass spectrometer equipped with an N_2 laser (335 nm). The spectrometer was mass calibrated externally using ACTH, rennin, and angiotensin I.

6.4 Results

S-glutathiolation of rHCaBP: We have shown previously that Cys187 is readily S-thiolated but not the four other cysteine residues in His-tagged rHCaBP (*144*). After addition of GSNO to His-tagged rHCaBP, S-glutathiolation occurred rapidly and was independent of the incubation time over 5-180 min with GSNO (*144*). The His-tag was cleaved from rHCaBP used in the present study since we have evidence that this N-terminal modification may alter the dimerization state and accessibility of the thiols in the protein (L. Tao, unpublished observations). Please see the note on page 152. It was reported that decomposed GSNO is a more effective S-glutathiolation reagent and less effective S-nitrosation reagent than fresh GSNO of glycogen phosphorylase b (*165*). To establish if this is the case with other proteins, a 5-mM solution of GSNO was left standing at room temperature in the dark until the SNO absorption at 334 nm was close to the baseline (Figure 6.1A, inset). Non-tagged rHCaBP was incubated with the decomposed GSNO for 20 min, and although a negligible amount GSNO remained in

solution, rHCaBP was S-glutathiolated (+GS) to a much greater extent in decomposed than in fresh GSNO solutions (panel B vs panel A). On the other hand, S-nitrosation (+NO) is detected only in the presence of fresh GSNO (Figure 6.1A).

S-nitrosothiols are unstable species. On the basis of published results (*178*), we assumed initially that decomposition in the dark would result in the metal-catalyzed conversion of 2 mol of GSNO to 1 mol of GSSG (with no formation of $GS^{\bullet}$ thiyl radicals) and 2 mol of NO. Hence, different molar ratios of GSSG and/or GSH were added to a solution of fresh GSNO and rHCaBP but protein S-glutathiolation (data not shown) never reached the level seen in Figure 6.1B. GSSG is not an effective S-glutathiolation agent as what demonstrated by the presence of only unmodified rHCaBP in Figure 6.1C, where a 50-fold excess GSSG was added to the protein. Changing the pH [ammonium acetate buffer (pH 4) or ammonium bicarbonate buffer (pH 8)] or adding NO_x (formed on exposure of NO-saturated buffer to air) to fresh GSNO did not significantly alter the level of rHCaBP S-thiolation (data not shown). rHCaBP also was incubated with fresh GSNO in the presence and absence of bovine CuZnSOD or catalase to eliminate possible effects of $O_2^{\cdot}$ and H_2O_2, but no increase in S-thiolation level over that seen in Figure 6.1A was detected (data not shown).

Mechanism of GS(O)SG formation: Li and co-workers (*156*) recently reported that GS(O)SG is a decomposition product of GSNO and a potent glutathiolating agent. Figure 6.2 compares the ESI mass spectra of fresh and decomposed GSNO solutions. The spectrum of fresh GSNO is dominated by peaks at m/z 307.1 and 337.1 (Figure 6.2A). The base peak at m/z 307.1 is assigned to $GS^{\bullet}$ with a proton ($GSH^{\bullet+}$). Since this species has an odd number of nitrogen atoms (three) and an odd mass (307.1), it must be an odd-

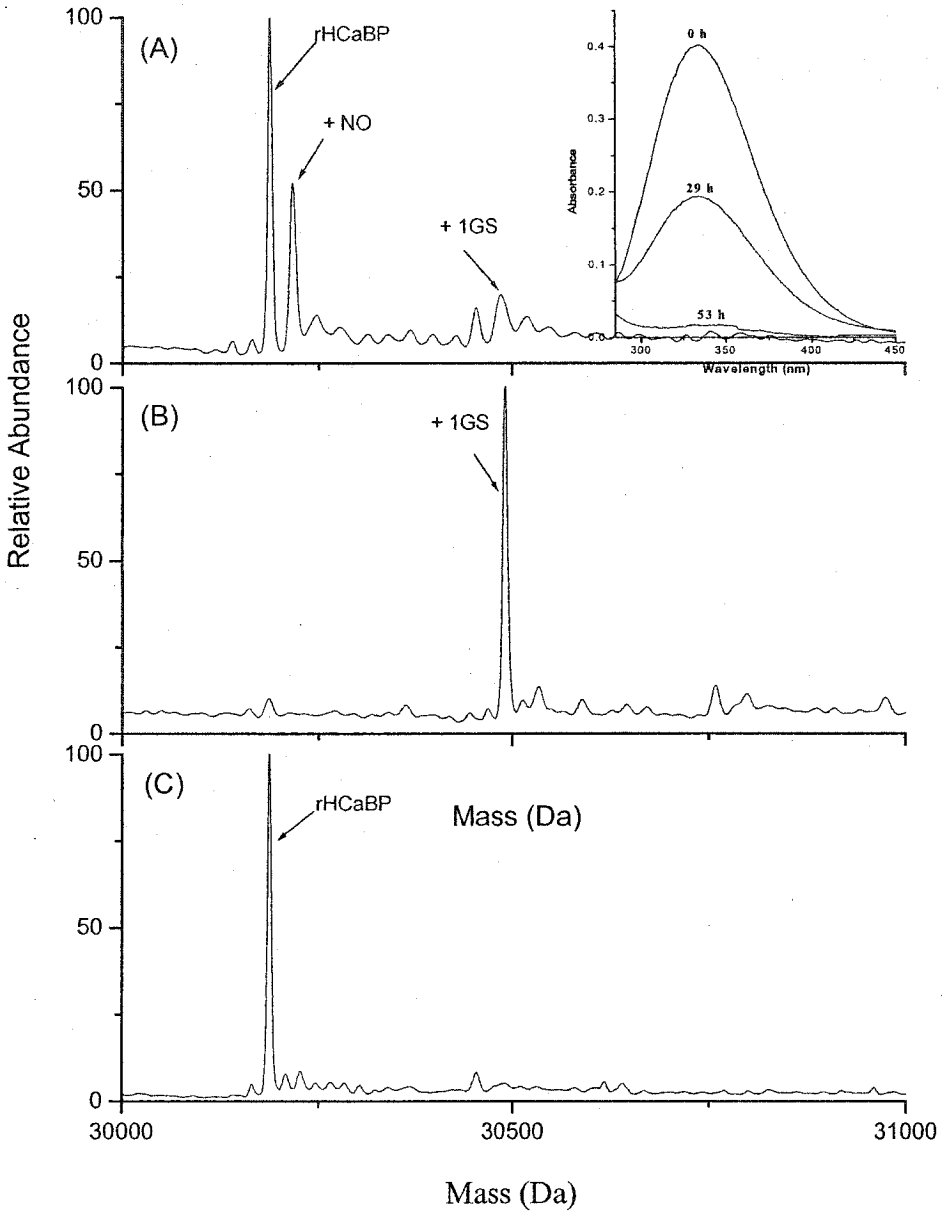

Figure 6.1. **Effects of GSNO and GSSG on the S-glutathiolation of rHCaBP.** rHCaBP was incubated with 100-fold molar excess of **(A)** fresh GSNO or **(B)** decomposed GSNO and **(C)** a 50-fold excess GSSG for 20 min at 37°C in 50 mM Tris-HCl buffer (pH 7.4). Samples for MS analysis were exchanged into water on a NAP-5 column, concentrated by ultrafiltration and added to 60 µL of 50% acetonitrile/0.2% formic acid to give a final protein concentration of 1-2 µM. Samples were directly infused into the Z-spray source of the QTOF2 mass spectrometer at a flow rate of 1 µL/min. The instrumental parameters were: capillary voltage 3.8 kV, cone voltage 45 V, multiplier 550 V, MCP 2100 V and TOF –9.1 kV. The Inset shows UV-Vis absorption of fresh and aged GSNO solutions. GSNO (5 mM) in water was allowed to stand at room temperature in the dark over 3 days. Aliquots were diluted 10-fold with water and the spectra recorded in a 1-cm cuvette at 25°C after 0, 29 and 53 h are shown.

electron ion (*179*) that arises from GSNO homolysis (GSNO $\rightarrow$ $GS^{\bullet}$ + $NO^{\bullet}$) and protonation in the ESI source. $GS^{\bullet}$ dimerization followed by protonation would give rise to the relatively abundant peak at m/z 613.2 assigned to $GSSGH^{+}$. The peaks at m/z 337 and 673 are assigned to the protonated ions (MH^{+}) of GSNO and its dimer, $(GSNO)_2H^{+}$. There is also a minor peak arising from the MH^{+} ion of GS(O)SG (m/z 629), which is a decomposition product present in commercial GSNO. This ion dominates the spectrum of GSNO that was allowed to decompose over the course of 63 h in the dark. The peak at m/z 306 is assigned to GS^{+}, which likely arises from heterolysis of GS(O)SG [GS(O)SG + H^{+} $\rightarrow$ GS^{+} + GSOH] in the ESI source since no peak at m/z 306 is observed in the mass spectrum of fresh GSNO solutions (Figure 6.2A). Other abundant peaks are those at m/z 613 and 645 assigned to the MH^{+} ions of GSSG and GSO_2SG, respectively, which are formed on GS(O)SG dimerization (see below).

Although Li and co-workers (*156*) identified GS(O)SG as a potent S-glutathiolation agent, the mechanism of its formation from GSNO was not examined. Hence, GSNO decomposition was monitored in the presence of metal chelators (neocuproine and DTPA) and dimedone to probe the pathway of its conversion to GS(O)SG. RSNOs give rise to an absorption band centered at ~335 nm (ε = 890 $cm^{-1}M^{-1}$) and a second, nearly electric-dipole forbidden, band at ~550 nm (ε = 16 $cm^{-1}M^{-1}$) (*74*). Since neocuproine and dimedone both absorb at 335 nm, the weak 550-nm band was used here to monitor GSNO decomposition. Decomposition of GSNO slowed down dramatically when dimedone was present in solution, and only ~10% loss of SNO absorbance was observed after 51 h (Figure 6.3). In contrast, the metal chelators had no

effects on GSNO stability indicating that GSNO decomposition in the dark over 51 h is not a copper-catalyzed process (*93*).

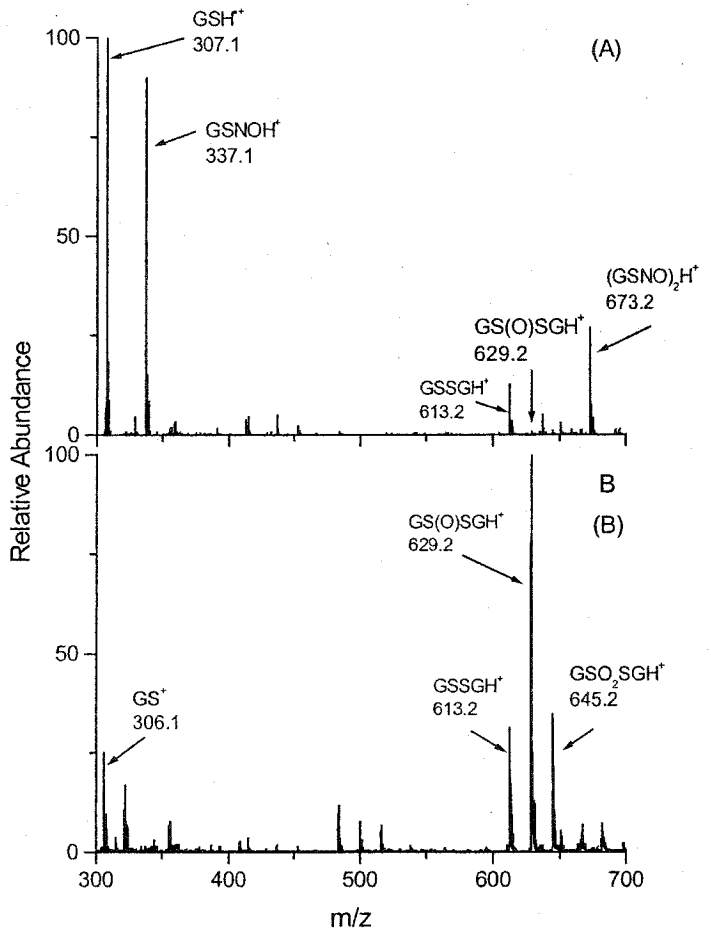

Figure 6.2. **ESI mass spectra of (A) fresh GSNO and (B) decomposed GSNO.** GSNO (5 mM) in water without added metal-ion chelators was allowed to stand at room temperature in the dark for 0 h (fresh GSNO) and 63 h (decomposed GSNO). Samples were diluted into 50% acetonitrile/0.2% formic acid to a final concentration of ~100 μM, and directly infused into the Z-spray source of the QTOF2 mass spectrometer at a flow rate of 1 μL/min. Experimental conditions are given in the caption to Figure 6.1.

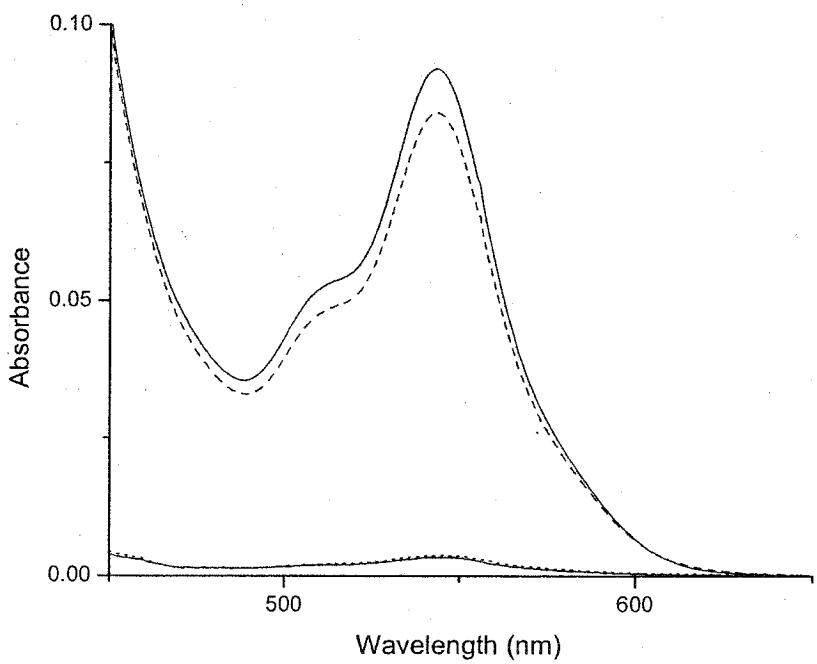

Figure 6.3. **Effects of metal-ion chelators and dimedone on the decomposition of 5-mM GSNO.** Absorbance between 450 and 650 nm of GSNO in water after standing at room temperature in the dark for 0 h in the presence or absence of added reagents (top solid line); for 51 h in the presence of 10 mM dimedone (top dashed line); for 51 h in the presence of 200 μM neocuproine and 200 μM DTPA (bottom dotted line); and for 51 h in the absence of added reagents (bottom solid line). Spectra were recorded in a 1-cm cuvette at 25°C.

Nitroxyl scavenging: Metmyoglobin exhibits different spectral properties when the Fe^{III} in the protein binds different axial ligands in the distal cavity (*180*). Since metmyoglobin was shown to be an efficient scavenger of nitroxyl released from S-nitroso-dithiothreitol (*12*), it was used here to probe the release of nitroxyl on GSNO hydrolysis. After incubation for 24 h in the dark of substoichiometric metmyoglobin with GSNO and dimedone, the Fe^{III} heme is fully converted to the nitrosyl form (Fe^{II}-NO) (Figure 6.4, top solid line). However, in the absence of dimedone, only a fraction of heme is transformed to the Fe^{II}-NO form (Figure 6.4, dashed line). Interestingly, when metmyoglobin is present in solution, dimedone promotes GSNO decomposition (Figure 6.5, bottom solid line *vs* dashed line), whereas in the absence of metmyoglobin, dimedone strongly inhibits GSNO breakdown (Figure 6.3). These suggest that nitroxyl reacts with the GS-dimedone thioether to re-form GSNO as discussed below.

S-glutathiolation of HCuZnSOD: Unlike rHCaBP, S-glutathiolated HCuZnSOD has been isolated from cells (*168*), and the structure of CuZnSOD from various sources has been determined to high resolution (*181-183*). Thus, S-glutathiolation of HCuZnSOD by decomposed GSNO was investigated to provide insight into why certain cysteine residues are S-glutathiolated *in vivo*. DTNB titration revealed ~0.15 free thiol per HCuZnSOD dimer and its ESI mass spectrum uncovered two major components (Figure 6.6A). The lighter component corresponds to the unmodified metal-free or apoHCuZnSOD monomer (theoretical mass 15,844.6 Da), and the heavier component (M+32 Da) is assigned to the apoHCuZnSOD monomer with a bound S^0 atom. Briggs and co-workers showed that sulfhydryl groups in HCuZnSOD react with zero-valence

sulfur during the purification procedure to yield a product with a 325-nm absorption band (*184*) that is seen in the insert to Figure 6.6 (solid line).

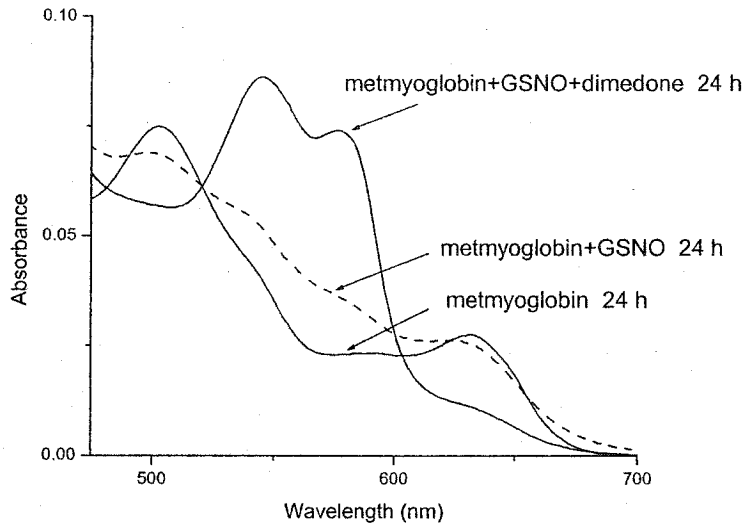

Figure 6.4. **Conversion of metmyoglobin (Fe^{III}) to nitrosyl-myoglobin (Fe^{II}-NO) by GSNO.** GSNO (5 mM) and metmyoglobin (185 μM) were incubated in the presence (top solid line) or absence (dashed line) of 5 mM dimedone in water at 20°C for 24 h under anaerobic conditions in the dark. The reaction solution was diluted 10-fold into degassed 100 mM potassium phosphate buffer (pH 7.0) in a sealed 0.4-cm cuvette just before the absorption spectrum was recorded. The bottom solid line is 18.5 μM metmyoglobin alone.

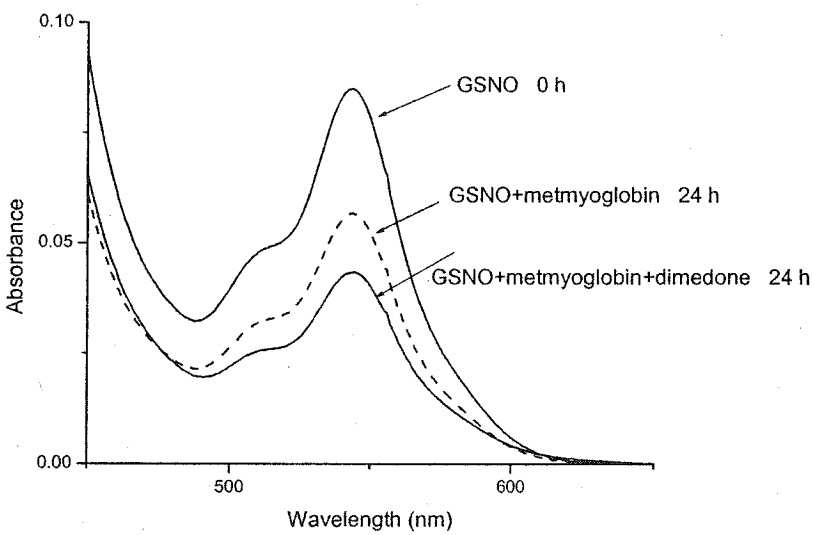

Figure 6.5. **Effects of dimedone on the decomposition of GSNO in the presence of metmyoglobin.** GSNO (5 mM) and metmyoglobin (185 μM) were incubated in the presence (bottom solid line) or absence (dashed line) of 5 mM dimedone in water at 20°C for 24 h under anaerobic conditions in the dark. Metmyoglobin was removed by ultrafiltration before recording the absorbance of GSNO. The top solid line is freshly prepared 5 mM GSNO in water. Spectra were recorded in a 1-cm cuvette.

The 325-nm absorption disappears after HCuZnSOD protein is reduced by DTT (Figure 6.6A inset, dashed line), as does the M+32 Da peak in the mass spectrum (Figure 6.6B). Moreover, a peak at M+129 Da is uncovered in the mass spectrum of the DTT-reduced protein (Figure 6.6B), and is assigned to a monomer with one Zn (65.4 u) and one Cu (63.5 u) bound. Peaks corresponding to metal-loaded monomer are also seen in Figure 6.7. Reduced HCuZnSOD was incubated with fresh and decomposed GSNO, but only the latter is an effective glutathiolating agent (panel A *vs* panel B of Figure 6.7). This mirrors the results obtained for rHCaBP (panel A *vs* B of Figure 1), although the yield of rHCaBP glutathiolation is greater than that of HCuZnSOD (Figure 6.1B *vs* 6.7B). The yield of glutathiolated HCuZnSOD was less in TrisHCl buffer (pH 7.4) (data not shown) compared to that in ammonium acetate buffer (pH 4.0) (Figure 6.7). Additionally, GSSG does not effectively glutathiolate HCuZnSOD (data not shown).

Identification of the modification site on HCuZnSOD: To identify the glutathiolated amino-acid residue, tryptic digests of HCuZnSOD were analyzed by MALDI-TOF. Although the sequence coverage was only ~42% (Table 6.1), the peptide mass fingerprints revealed that peptide DGVADVSIEDSVISLSGDHCIIGR (D93-R116) has an increased mass of 305 Da in the sample exposed to decomposed GSNO (panel A vs panel B of Figure 6.8). Since this is consistent with the addition of a single GS group, as observed for intact HCuZnSOD (Figure 6.7), Cys111 in D93-R116 is identified as the likely site of S-glutathiolation. Moreover, a peak with m/z 2489 corresponding to the MH^+ ion of peptide D93-R116 with an increased mass of 32 Da is present in the mass fingerprints of the digests of both untreated HCuZnSOD and reduced HCuZnSOD that was exposed to decomposed GSNO (Figure 6.8). A comparison of panel A and B of

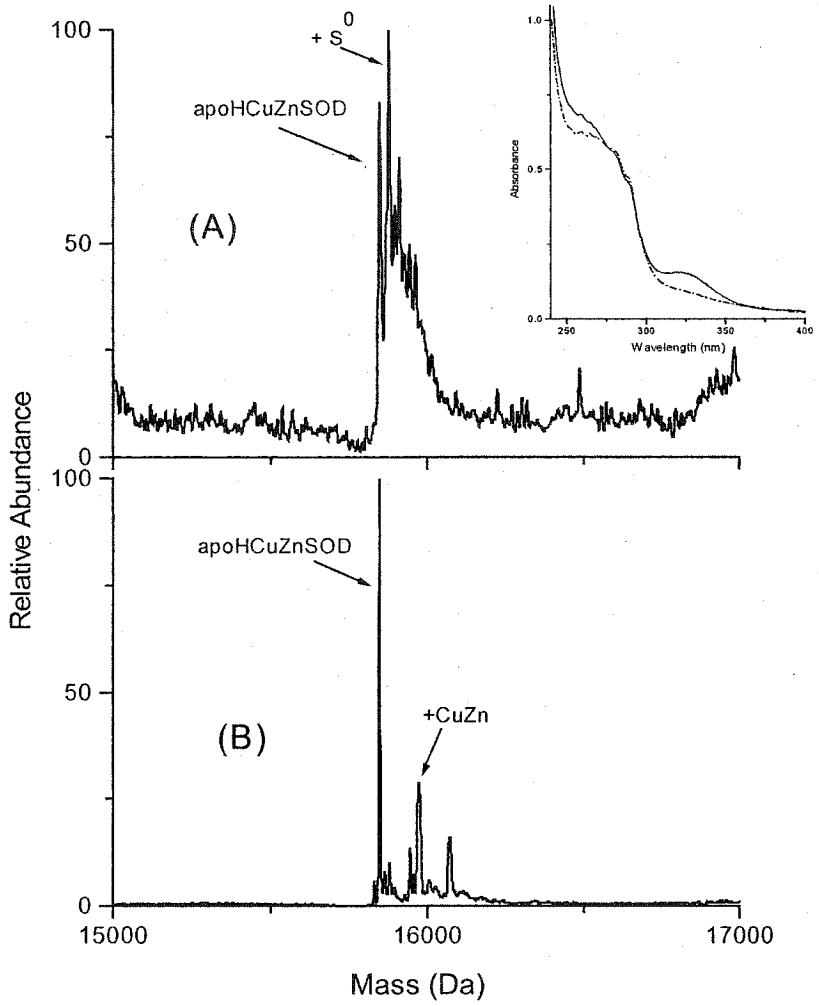

Figure 6.6. **Deconvoluted ESI mass spectra of HCuZnSOD. (A)** Untreated HCuZnSOD and **(B)** DTT-reduced HCuZnSOD. The arrows point to peaks at 15,845, 15,877 and 15,974 Da corresponding to the metal-free (apoHCuZnSOD), the S^0-derivatized metal-free ($+S^0$), and the metal-loaded (+CuZn) protein monomer, respectively. Experimental conditions are given in the legend of Figure 6.1. The Inset shows UV-vis absorption of HCuZnSOD in 50 mM ammonium bicarbonate buffer (pH 7.8) at room temperature in 1-cm cuvette. Solid line: 66 μM untreated HCuZnSOD. Dashed line: 61 μM DTT-reduced HCuZnSOD.

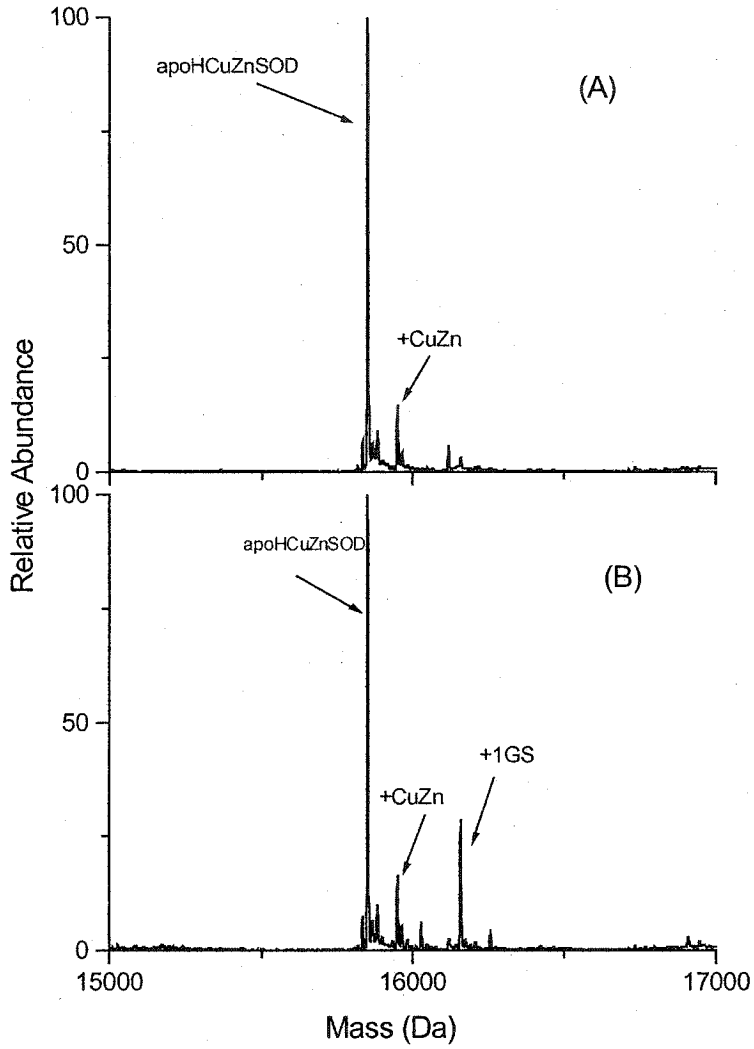

Figure 6.7. **Effects of GSNO on the S-glutathiolation of HCuZnSOD.** Deconvoluted ESI mass spectra of DTT-reduced HCuZnSOD following incubation of 66 μM protein with 100-fold molar excess **(A)** fresh GSNO and **(B)** decomposed GSNO in 50 mM ammonium acetate buffer (pH 4) for 30 min at 37°C in the dark. The arrows point to peaks with masses of 15,845, 15,974 and 16150 Da corresponding to the metal-free (apoHCuZnSOD), metal-loaded (+CuZn) and singly S-glutathiolated metal free (+1GS) protein, respectively. Experimental conditions are given in the caption to Figure 6.1.

Figure 6.8 indicates that the peak corresponding to D93-R116 + S^0 (m/z 2489) is much less intense than the D93-R116 peak (m/z 2457) following reduction of HCuZnSOD. Hence, Cys111 is also likely the residue that is linked to the single zero-valence sulfur atom found in HCuZnSOD. Although linking of an S^0 atom to the extra sulfhydryl in HCuZnSOD was suggested over 20 years ago (*184, 185*), the evidence provided in Figure 6.8 is the first to support this assignment.

Table 6.1. **Tryptic peptides in MALDI mass fingerprint of S-glutathiolated HCuZnSOD** [a]

Residues	Peptide sequence	MH^+ [b] observed mass	MH^+ [c] calculated mass	Chemical Modification [d]
117-123	TLVVHEK	825.3	825.5	
38-46	GLTEGLHGF	930.4	930.5	
81-92	HVGDLGNVTADK	1225.5	1225.6	
11-24	GDGPVQGIINFEQK	1501.6	1501.8	
93-116	DGVADVSIEDSVISLSGDHCIIGR	2457.4	2457.2	
93-116	DGVADVSIEDSVISLSGDHCIIGR	2489.7	2489.3	S^0
93-116	DGVADVSIEDSVISLSGDHCIIGR	2762.6	2762.2	GS

[a] HCuZnSOD was incubated with 100-fold molar excess decomposed GSNO in 50 mM ammonium acetate buffer (pH 4.0) for 30 min at 37°C. Tryptic digestion was carried out as described in the Experimental Section and the tryptic peptides were analyzed by MALDI-TOF-MS.

[b] Observed monoisotopic masses of the singly protonated ions (MH^+) of the tryptic peptides.

[c] Calculated monoisotopic masses of the MH^+ ions of the tryptic peptides.

[d] Chemical modification of Cys111 based on the mass shift in peptide D93-R116 (see the text).

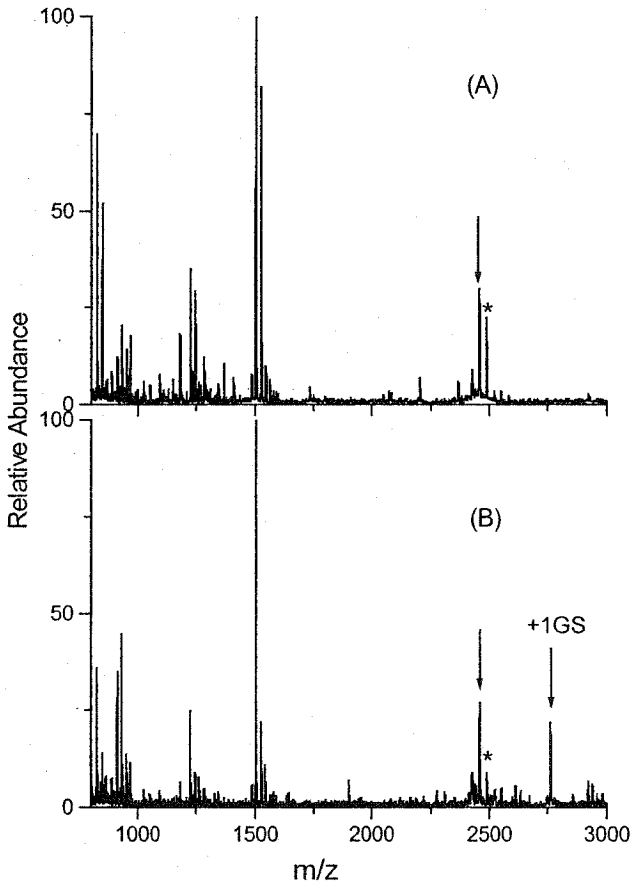

Figure 6.8. **MALDI-TOF mass fingerprints of the tryptic digests of HCuZnSOD. (A)** Untreated HCuZnSOD and **(B)** DTT-reduced HCuZnSOD following incubation with decomposed GSNO. The arrows point to peaks at m/z 2457.4 and 2762.6 corresponding to unmodified and GS-derivatized peptide D93-R116, respectively. The asterisk denotes the peak at m/z 2489.7 containing S^0-derivatized peptide D93-R116. Cys111 is assumed to be the site of derivatization in each case (see Table 6.1).

S-glutathiolation of GAPDH: The effects of fresh and decomposed GSNO on GAPDH are also of interest since it was found to be a target for S-glutathiolation *in vivo* and *in vitro* following exposure to oxidative stress (*64, 171, 186, 187*). Thus, examination of S-glutathiolation of rabbit muscle GAPDH, a homotetramer (*188*), was carried out to provide further insight into protein S-glutathiolation *in vitro* and *in vivo*. GAPDH was incubated with a 50-fold molar ratio of fresh or decomposed GSNO for 20 min at room temperature. The mass spectrum of GAPDH exposed to fresh GSNO (Figure 6.9A) shows a major peak at 35,691 Da, which corresponds to the reported mass of the monomer (*189*), and minor peaks at M+32 and M+305 Da (+GS). The singly GS-labeled monomer is the major species in the mass spectrum following exposure to decomposed GSNO (Figure 6.9B). Moreover, a peak at M+610 Da (+ 2 GS) is also observed in Figure 6.9B. Therefore, GAPDH is glutathiolated to a much greater extent in decomposed than in fresh GSNO solutions (panel A *vs* panel B of Figure 6.9). The M+32 species, which is also present in untreated GAPDH samples (data not shown), has not been identified but may result from addition of two oxygen atoms to the GADPH monomer. Exposure to fresh *vs* decomposed GSNO does not appear to alter the relative abundance of the M+32 species (Figure 6.9).

S-glutathiolation of BSA: Serum albumin is the most abundant protein in plasma and is proposed to have an antioxidant role (*173*). Hence, it is of interest to establish if this protein is S-glutathiolated in decomposed GSNO solutions on its single free cysteine residue, Cys34. The mass spectrum of BSA after the commercial protein was dialyzed against MilliQ water shows a major peak at 66,430 Da (Figure 6.10A), which corresponds to the reported mass of the protein (*190*). Singly GS-labeled BSA is the

major species in the mass spectrum (Figure 6.10B) after the DTT-reduced protein was exposed to a 100-fold molar excess of decomposed GSNO for 20 min at room temperature.

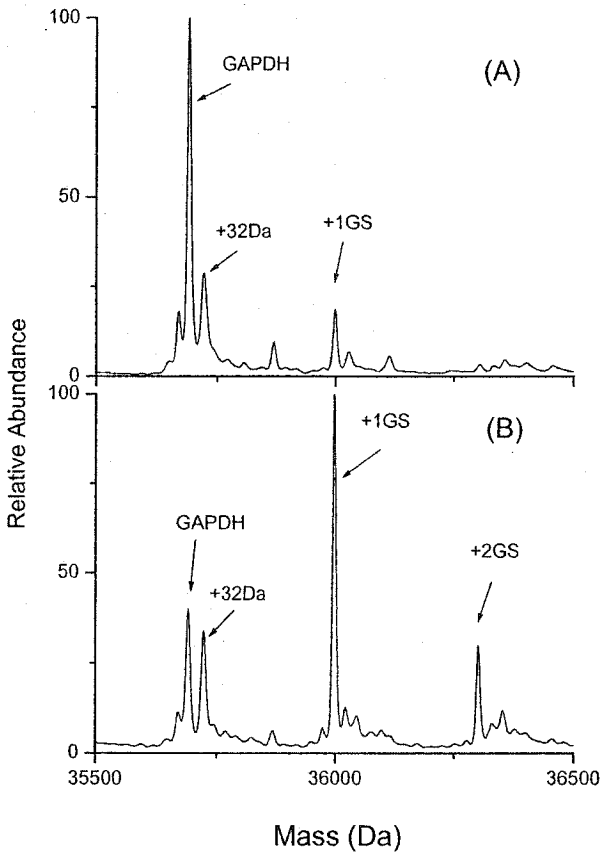

Figure 6.9. **Effects of GSNO on the S-glutathiolation of GAPDH.** Deconvoluted ESI mass spectra of the GAPDH monomer after incubation with a 50-fold molar excess **(A)** fresh GSNO and **(B)** decomposed GSNO in 50 mM TrisHCl buffer (pH 7.4) for 20 min at room temperature in the dark. Arrows point to peaks at 35,691 (M), M + 32, M + 305 and M + 610 Da corresponding to unmodified (GAPDH), possibly oxidized (+32 Da), and singly (+GS) and doubly (+2GS) GS-labeled protein monomer, respectively. Experimental conditions are given in the caption to Figure 6.1.

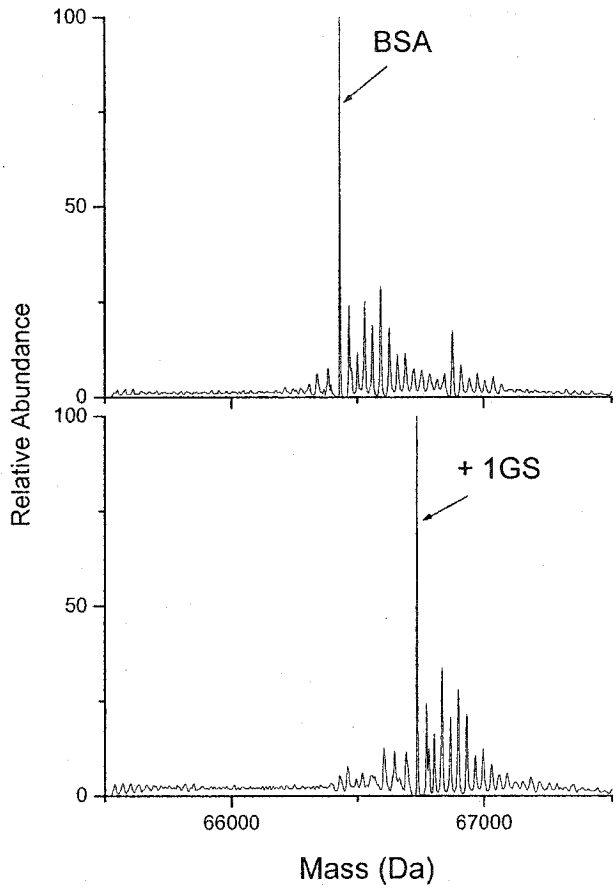

Figure 6.10. **BSA S-glutathiolation by decomposed GSNO.** Deconvoluted ESI mass spectra of **(A)** DTT-reduced BSA and **(B)** DTT-reduced BSA following incubation with a 100-fold molar excess of decomposed GSNO in 100 mM TrisHCl buffer (pH 7.4) for 20 min at room temperature in the dark. Arrows point to peaks at 66430 and 66735 Da corresponding to unmodified and singly GS-labeled (+1GS) BSA, respectively. Samples for MS analysis were exchanged into water by dialysis, added to a 20% methanol/5% acetic acid to a final protein concentration of 5-10 μM, and directly infused into the Z-spray source of the QTOF2. Experimental conditions are given in the caption to Figure 6.1.

6.5 Discussion

Protein S-glutathiolation has been observed *in vivo* and *in vitro* (*31, 162, 165, 191*). This oxidative modification is recognized as one of the physiological responses to nitrosative and oxidative stress, but how proteins are S-glutathiolated *in vivo* is not clear. GSH alone reportedly does not S-glutathiolate proteins such as cathepsin (*128*) and GAPDH (*64*), and protein S-thiolation occurred without GSSG in neutrophil-treated hepatocytes (*162*). It has been deduced that S-glutathiolation of proteins by GSSG *in vivo* likely is not an efficient process (*156*). Clearly, GSSG is not an effective S-glutathiolating agent of rHCaBP (Figure 6.1C) and HCuZnSOD (data not shown) *in vitro,* consistent with observations on glycogen phosphorylase b (*165*) and aldose reductase (*166*). Recently, it was reported that GSNO S-glutathiolates proteins *in vivo* and *in vitro* (*64, 128, 145, 165-167, 187*), but the present results reveal that decomposed GSNO solutions contain a much more effective S-glutathiolating reagent for rHCaBP, HCuZnSOD and GAPDH than fresh solutions (Figures 6.1, 6.7 and 6.9). Similar results were obtained by Li *et al.* for neurogranin and neuromodulin (*156*), and by Ji *et al.* for glycogen phosphorylase b (*165*). Interestingly, the formation of P-SSG (S-glutathiolated protein) did not lead to the detection here of cross-linked protein (P-SS-P) in any of the mass spectra recorded.

GS(O)SG, a GSNO decomposition product (Figure 6.2), was suggested to be a potent S-glutathiolating agent for proteins (*156*). However, it is not clear from the published work on protein S-glutathiolation triggered by GSNO whether NO or GSNO plays a role since residual GSNO was present in the decomposed GSNO solutions (*156*). Also, the mechanism of GSNO decomposition to GS(O)SG has not been determined,

although Huang and co-workers speculated that GSNO decomposition was likely catalyzed by copper ions (*192*).

In the work presented here, GSNO decomposition in the dark was monitored by the loss of its SNO absorption at 335 nm (Figure 6.1A, inset). A GSNO decomposition product is an efficient protein S-glutathiolation agent (Figures 6.1B, 6.7B, 6.9B and 6.10B) in the absence of any detectable GSNO (Figure 6.2B). On the other hand, in fresh GSNO solutions containing only trace GS(O)SG as monitored by ESI-MS (Figure 6.2A), little S-glutathiolation of rHCaBP, HCuZnSOD and GAPDH occurred (Figures 6.1A, 6.7A and 6.9A). Moreover, addition of solutions of NO_x from aerobic NO decomposition ($NO \rightarrow NO_x$) did not alter the extent of rHCaBP S-glutathiolation (data not shown). These results indicate that neither GSNO nor NO_x is directly involved in S-glutathiolation of rHCaBP, HCuZnSOD or GAPDH *in vitro*.

As reported by Li *et al.* (*156*), the major decomposition products of GSNO were found to be GS(O)SG, GSO_2SG and GSSG (Figure 6.2B). How is GSNO converted to these products? Thermal and photochemical homolysis pathways have been proposed for RSNO decomposition (*193*):

$$2RSNO \overset{h\nu \text{ or } \Delta}{\rightleftharpoons} RSSR + 2NO \qquad (6.1)$$

Also, copper-catalyzed reductive cleavage (eqs 6.2 and 6.3) results in the rapid breakdown of many RSNOs at ambient temperatures in the dark, under which conditions homolysis (eq 6.1) is highly inefficient (*147*).

$$2RS^- + 2Cu^{II} \rightleftharpoons RSSR + 2Cu^{I} \qquad (6.2)$$

$$Cu^{I} + RSNO \rightleftharpoons Cu^{II} + RS^- + NO \qquad (6.3)$$

Figure 6.3 shows that the presence of dimedone, but not metal chelators, prevents GSNO decomposition. Thus, metal ions are not involved in GSNO decomposition under the conditions used here. This is consistent with the results of Williams and co-workers who have shown that copper-catalyzed decomposition of GSNO is efficient at low concentrations (~3 μM) but is prevented at high GSNO concentrations due to product inhibition (*147*). The GSSG produced on copper-catalyzed GSNO breakdown (eq 6.2) forms a stable Cu^{II} chelate and inhibits further redox turnover of the metal (eq 6.3) required for catalytic RSNO cleavage (*147*).

Dimedone has been shown to react specifically with sulfenic acids to form a stable thioether product (*128, 194*):

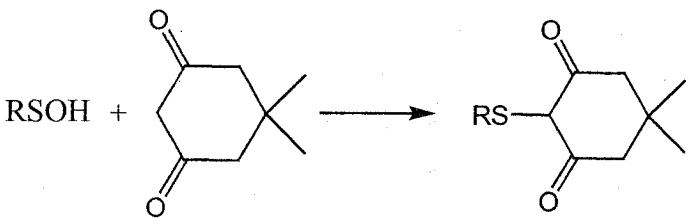

(6.4)

Since dimedone is a scavenger of GSOH and strongly inhibits GSNO breakdown (Figure 6.3C), the following mechanism for GS(O)SG formation from GSNO is proposed:

$$GSNO + H_2O \rightleftharpoons GSOH + NO^- + H^+ \rightleftharpoons HNO \quad (6.5)$$

$$GSOH + GSNO \rightleftharpoons GS(O)SG + NO^- + H^+ \rightleftharpoons HNO \quad (6.6)$$

$$GSOH + GSOH \rightleftharpoons GS(O)SG + H_2O \quad (6.7)$$

$$2GS(O)SG \rightleftharpoons GSO_2SG + GSSG \quad (6.8)$$

$$2HNO \rightleftharpoons N_2O + H_2O \quad (6.9)$$

In this scheme, GSNO hydrolysis generates GSOH and HNO/NO^- (eq 6.5). GSOH further reacts with GSNO to give GS(O)SG and HNO (eq 6.6). GSOH can also

undergo self-condensation (*195*) to yield GS(O)SG (eq 6.7), which dimerizes to yield GSO_2SG and GSSG as products (eq 6.8) (*196*). Presumably, Reaction 6.5 is rate-limiting and Reactions 6.6 and 6.7 drive GSNO breakdown by consuming GSOH.

When dimedone is present, it traps GSOH (eq 6.10) and prevents its further reaction with GSNO (eq 6.6) or self-condensation (eq 6.7). However, since <10% of GSNO is consumed in the presence of dimedone (Figure 6.3), most of the thioether formed in Reaction 6.10 must be reconverted to GSNO. The rate of reaction 6.9, which removes HNO from solution by dimerization and dehydration, is dependent on the square of the HNO concentration. Trapping of GSOH by dimedone will decrease the HNO concentration by inhibiting reaction 6.6, and nitroxyl attack on the GS-dimedone adduct to re-form GSNO (eq 6.11) will be favoured over HNO dimerization (eq 6.9). Breakdown of thiol-dimedone adducts has been previously proposed by Benitez *et al.* under acidic conditions (*197*).

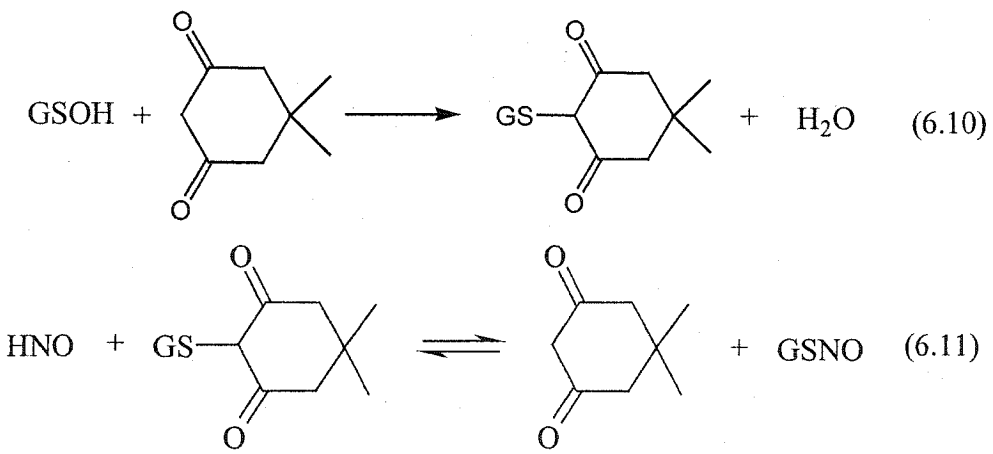

To obtain further evidence that HNO/NO^- is released upon GSNO decomposition, metmyoglobin was added as a nitroxyl scavenger (*12*). In the presence of dimedone,

metmyoglobin was fully converted into its nitrosyl (Fe^{II}-NO) form (Figure 6.4, solid line) confirming that nitroxyl is released on GSNO hydrolysis. Moreover, dimedone inhibits GSNO consumption in the absence (Figure 6.3) but *not* in the presence of metmyoglobin (Figure 6.5, bottom solid line), revealing that nitroxyl scavenging prevents regeneration of GSNO as predicted (eq 6.11). However, GSOH is free to react with GSNO (eq 6.6) when dimedone is absent, and the lower scavenging yield (Figure 6.4) probably reflects an increased rate of HNO dimerization (eq 6.9).

GS(O)SG formed on GSNO decomposition reacts with free thiols such as GSH and certain protein thiols (PSH) (*156*):

$$PSH + GS(O)SG \rightarrow PSSG + GSOH \qquad (6.12)$$

GSOH produced *in situ* in reaction 6.12 may act also as a protein S-glutathiolating agent (*128*) depending on the relative rates of reaction 6.7 and 6.13.

$$PSH + GSOH \rightarrow PSSG + H_2O \qquad (6.13)$$

No GSOH was detected here in the decomposed GSNO solutions by mass spectrometry, which is consistent with the known instability of sulfenic acids to dimerization and dehydration (*195*) (reaction 6.7). Interestingly, many of the proteins that are susceptible to mixed disulfide formation in response to nitrosative stress (*31*) have been reported to undergo S-thiolation under oxidative conditions (*30, 64, 198, 199*). What determines the susceptibility of protein thiols to S-glutathiolation? For example, of the five free cysteine residues in rHCaBP, S-glutathiolation of Cys187 is preferred (*144*). Since the structure of rHCaBP is not yet known, HCuZnSOD was chosen as another model protein in this study. CuZnSODs from different species possess three conserved cysteine residues per monomer (*168*). Two of them form an intrasubunit disulfide bridge and the side chain of

the third highly conserved cysteine points toward the interior of the protein. In addition to the conserved cysteines, a few CuZnSODs possess exposed free thiols, referred to as extra sulfhydryl or extra cysteine residues. HCuZnSOD is among the extra-cysteine-containing enzymes. The extra Cys111 causes the observed heterogeneity of HCuZnSOD preparations since it is derivatized in both the wild-type and recombinant protein (*200, 201*). Cys111 is also the site modified naturally or artificially by mixed disulfide formation with free cysteine or glutathione (*202, 203*).

Here we report that peptide D93-R116, which contains Cys111, is labeled with the single zero-valence sulfur atom formed in commercial HCuZnSOD preparations. Cys111 is also the site of S-glutathiolation (Figure 6.8). However, the yield of S-glutathiolated HCuZnSOD is much lower than that of rHCaBP (Figures 6.1B *vs* Figure 6.7B), but comparable to that of the enzyme isolated from cells (*169, 170*). Liu *et al.* found that only ~50% of HCuZnSOD was modified by 4-vinylpyridine or DTNB although 100- or 1000-fold molar excess reagent over protein sulfhydryl was employed (*202*). Cys111 is near the dimer interface and the distance between the two sulfhydryl groups is ~10 Å as estimated from the crystal structure of HCuZnSOD (*204*). Because of their close proximity (*202*), modification of Cys111 on one subunit of the dimer likely impedes access of the modifying reagent to Cys111 on the other subunit. The yield of S-glutathiolated HCuZnSOD at pH 4.0 (Figure 6.5B) was higher than that at pH 7.4 (data not shown), which suggests that HCuZnSOD has greater conformational flexibility at lower pH making Cys111 more accessible.

GAPDH is a homotetramer and each monomer contains 4 free cysteine residues. On the basis of DTNB reactivity, the four thiols have been classified into three groups:

one fast reacting thiol, which is most likely the active-site Cys149 (*205-207*); one thiol that reacts at an intermediate rate, and two slow reacting thiols (*205, 208*). GAPDH is found to be S-glutathiolated by decomposed GSNO to a large extent on one cysteine and to a lesser extent on a second cysteine (Figure 6.9B). After S-glutathiolation, ~90% of the GAPDH activity is lost (data not shown), so it is likely that the active-site Cys149 is S-glutathiolated. The cysteine residue with lower GS(O)SG reactivity is probably that with intermediate DTNB reactivity.

BSA has 35 cysteine residues, but 34 are involved in disulfide bridges. Only Cys34 possesses a free thiol, which can partake in thiol-specific reactions (*173, 209*). *In vivo,* Cys34 is in the free thiol form, but once extracted and purified from plasma it is partially involved in intermolecular disulfide bond formation or in mixed disulfides with other low-molecular-weight thiols (*173*). Here we report that DTT-reduced BSA, which possesses 0.86 free thiols per molecule, undergoes a mass increase of 305 Da on incubation with decomposed GSNO (Figure 6.10B). This indicates that BSA is efficiently S-glutathiolated by GS(O)SG presumably on Cys34.

The active-site structure of the GAPDH tetramer is conserved (*210*). The distance between two active-site Cys149 side chains in *bacillus stearothermophilus* GAPDH is ~35 Å (*211*), which is much larger than the ~10-Å separation between the Cys111 residues in HCuZnSOD. Also, the X-ray structure of human serum albumin (*155*) showed that Cys34 is partially solvent exposed. Therefore, accessibility to the glutathiolating reagent and a cavity that can accommodate the GS group are likely prerequisites for protein S-glutathiolation. Although no structural properties that render accessible protein sulfhydryls equally reactive to S-glutathiolation have been identified (*160*), cysteines

with depressed pK_a values due to the proximity of basic amino acid residues are preferentially S-glutathiolated. Examples include Cys298 in aldose reductase and Cys269 in c-Jun (*166, 187*).

6.6 Conclusions

GS(O)SG is an efficient S-glutathiolation reagent unlike GSNO, GSH or GSSG. GS(O)SG can be formed by the treatment of GSH with H_2O_2 (*212*), by bubbling GSH or GSSG solutions with NO gas (*156*), and from decomposed GSNO. Interestingly, GS(O)SG was found to be present at low levels in rat brain slices and its concentration increased under oxidative stress (*156*). Thus, oxidative or nitrosative stress may promote protein S-glutathiolation *in vivo*, with GS(O)SG acting as a thiolating agent in this process. It is also possible that the slow GSNO hydrolysis to GSOH observed here is enzymatically catalyzed *in vivo,* but such activity remains to be identified.

6.7 Acknowledgements

We thank David Yong-Hoi Yeung and Biao Shen for their assistance with the preparation of rHCaBP and BSA. Lekha Sleno and Dominic Cuerrier are thanked for helpful discussions on GAPDH modification.

Note added to thesis: After publication we found no difference between HCaBP with and without a His-tag. The previous observation is due to differece in purification process (chapter 2). Cleavage of the His-tag by factor Xa requires removal of thiol reductants which results in oxidation of some of the cysteine residues of HCaBP. However, thrombin cleavage can be carried out in the presence of reductants and oxidation of HCaBP thiols was not observed in the thrombin-cleaved protein.

7.0 Conclusions and suggestions for future work

7.1 Chapter 2

Our results support a free-radical mechanism (*16*) for CysNO formation from NO and cysteine in air-saturated buffers. This involves $Cys^{\bullet}$ generation by reaction with $^{\bullet}NO_2$ at higher NO concentrations and with copper ions at lower NO concentrations. We propose that CysNO formation is catalyzed by copper *in vivo*, because (i) the concentration of NO is low *in vivo* (0.1-1.0 μM) and (ii) the non-copper-catalyzed pathway consumes three molecules of NO to form CysNO, which is not efficient compared to the copper-catalyzed reaction that only consumes one molecule of NO to form CysNO.

By monitoring O_2 consumption, it is also clearly demonstrated in Chapter 2 that DTPA does not fully inhibit the redox turnover of copper in air-saturated cysteine solutions. This key observation is overlooked in many studies on NO/thiol chemistry, where addition of DTPA is assumed to inhibit all metal-catalyzed processes. Of further interest is the nature of the copper complexes formed on NO addition to cysteine solutions. These complexes rapidly lose the ability to consume oxygen, unlike the copper species present in cysteine solutions without NO.

7.2 Chapters 3 and 4

A very efficient expression and purification system was set up for rHCaBP by subcloning the HCaBP gene into the pET15b vector and expressing the protein in BL21(DE3)pLysS host cells. A yield of >30 mg/L culture with >95% purity was obtained.

Moreover, all five free thiols were protected from oxidation by using this purification process. This work provides a strong foundation for further research on the biological function of HCaBP (Chapter 3).

We have demonstrated that HCaBP can be easily S-nitrosated. Since up to four cysteine residues can be S-nitrosated in HCaBP and it is abundant in the brain, we proposed that the protein may act as a NO buffer or reservoir in the brain in a manner similar to serum albumin in blood. It was reported that NO circulates in the plasma of healthy humans primarily as S-nitrosoalbumin (*8*). Furthermore, since Ca^{2+}-binding affects the extent of S-nitrosation of rHCaBP, there is likely crosstalk between these two buffering capacities of the protein. This could allow for crosstalk between NO and Ca^{2+} signaling in the brain.

Several techniques for detecting S-nitrosated protein such as HCaBP were evaluated, including UV-vis and circular dichroism absorption, intrinsic fluorescence and mass spectrometry measurements, as well as the Saville assay. It was demonstrated here for the first time that intrinsic protein fluorescence is a sensitive probe of protein S-nitrosation. This is due to efficient Förster energy transfer ($R_0 \sim 17$ Å) between tryptophan donors and S-nitrosothiol acceptors. Mass spectrometry is the most efficient and convincing tool to detect RSNO formation. The Saville assay is a valuable but indirect method to quantify the extent of S-nitrosation. S-NO formation in HCaBP also gives circular dichroism absorption, which could be further explored as a tool to investigate conformational changes around the SNO group under different conditions. UV-vis absorption is a convenient method for detecting RSNO formation, but care has to

be taken since all RSNOs absorb within the same range and the SNO absorbance is low ($\varepsilon_{340} \sim 10^3\ M^{-1}cm^{-1}$ and $\varepsilon_{540} \sim 20\ M^{-1}cm^{-1}$) (*93*).

7.3 Chapter 5

It was found that NO donation by GSNO to rHCaBP requires the presence of trace copper, added as either Cu,Zn-superoxide dismutase (CuZnSOD) or $CuSO_4$. CuZnSOD is an efficient catalyst of rHCaBP S-nitrosation. Similar to the mechanism given in Chapter 2 for CysNO formation, rHCaBP S-nitrosation by GSNO follows a copper-catalyzed thiyl-radical pathway except that GSNO is both an oxidant and source of NO, and the copper catalyst (CuZnSOD) and cysteine are protein-bound. The mechanism involves reduction of the active-site Cu^{II} by a number of the five free thiols in rHCaBP, giving rise to thiyl radicals. The Cu^{I}ZnSOD formed catalyzes the reductive cleavage of GSNO present in solution to give GSH and release NO. rHCaBP thiyl radicals react with NO to yield the S-nitrosoprotein.

The data presented provide a biologically relevant mechanism for protein S-nitrosation by small S-nitrosothiols. This mechanism requires interaction of 2 proteins, HCaBP and CuZnSOD for reduction of copper to its active cuprous (Cu^{I}) form. Since protein-protein interactions occur with high specificity *in vivo*, the mechanism for protein S-nitrosation proposed here should lead to S-nitrosation of specific thiols. Only protein thiols that interact with and donate an electron to a catalyst such as CuZnSOD will be S-nitrosated. S-nitrosation by NO_x species such as $^{\bullet}NO_2$ and N_2O_3 is expected to be less specific since these are small diffusive species that can probably access many protein thiols.

S-nitrosation is rapidly gaining recognition as a major form of protein post-translational modification, and the efficient S-nitrosation of HCaBP by CuZnSOD/GSNO is speculated to be of neurochemical importance given that CaBP and CuZnSOD are abundant in neurons.

7.4 Chapter 6

It was determined that rHCaBP, HCuZnSOD, GAPDH, and BSA were S-glutathiolated in decomposed GSNO solutions, in which GS(O)SG is the efficient S-glutathiolating reagent. GSNO, GSH or GSSG are not efficient protein S-glutathiolating reagents. The results in this chapter are contrary to numerous reports of protein S-thiolation by low-molecular-weight S-nitrosothiols. In these reports the impurities in the GSNO solutions used were not examined.

It was found that GSNO decomposition in the dark at room temperature yields glutathione disulfide S-oxide [GS(O)SG], glutathione disulfide S-dioxide (GSO_2SG), and GSSG as products. Based on the inhibition of GSNO breakdown by dimedone, a reagent specific for sulfenic acids, and nitroxyl scavenging by metmyoglobin, a hydrolysis pathway yielding GSOH and nitroxyl HNO/NO^- as intermediates for GSNO decomposition in the dark is proposed.

S-glutathiolation sites were identified or proposed in the proteins exposed to decomposed GSNO. The yields of S-glutathiolation of rHCaBP, GAPDH and BSA were much higher than that of HCuZnSOD. The accessibility of the S-glutathiolation site (Cys111) to the glutathiolating reagent in the HCuZnSOD dimer limits the extent of modification.

7.5 Suggestions for future work

(1) The nature of the copper species formed in air-saturated cysteine solutions following NO addition are of interest. As seen in Chapter 2, these species lose the ability to consume O_2, and may contain ligands derived from NO or $^{\bullet}NO_2$ such as NO_2^-.

(2) Although up to 4 cysteine residues are S-nitrosated in rHCaBP, at low GSNO to rHCaBP molar ratios, only 1-2 cysteines are S-nitrosated. To determine the preferred S-nitrosation sites is important for understanding the mechanism of rHCaBP S-nitrosation and the possible physiological roles of rHCaBP. The preparation of five site-directed mutants, in which each cysteine is replaced individually by serine, would help identify the reactivities to S-nitrosation of the different cysteines in rHCaBP .

(3) It was reported that CaBP exhibits a dramatic neuroprotective effect in motor neurons (*213*) under stressful conditions. After the S-nitrosation sites are found by mutation, expression vectors encoding interesting HCaBP mutants could be microinjected into motor neurons using wild-type HCaBP as a control. Thus, it could be established if any of the HCaBP mutants with altered nitrosation potential offer less neuroprotection under stressful conditions (such as glutamate exposure) than the wild-type protein. Single motor neurons from fetal mice spinal cords could be microinjected with a cocktail that contains the HCaBP construct and a fluorescently labelled protein to identify cells that have been injected, and the number of neurons that survive counted over ten days. This assay would provide a quantitative handle on the effects of overexpression of HCaBP mutants on neuronal survival, and the role if any of HCaBP as a NO buffer.

(4) The conformations of HCaBP before and after S-nitrosation or S-glutathiolation should be investigated. This would shed light on how HCaBP S-modification affects its Ca^{2+}-binding properties.

(5) HCaBP, HCuZnSOD, GAPDH and BSA from the S-glutathiolation reactions should be sequenced by MS/MS to identify the modification sites. Sequencing by MS can be carried out using a QTof mass spectrometer.

(6) Very recently, a new player in NO research has emerged, HNO (*214*). In the past few years, a growing number of researchers has come to believe that HNO may play a significant role in biology and pharmacology, protecting the cardiovascular system, interacting with enzymes, and suggesting new drug possibilities (*214*). In Chapter 6, HNO was found to be one of the GSNO hydrolysis products (eq 6.5). RSNO hydrolysis may be a physiologically important route to HNO generation and needs to be further investigated. Also, the GS-dimedone adduct was found to be a good trap for the highly unstable HNO (eq 6.11) since GSNO decomposition was essentially eliminated in the presence of dimedone (Figure 6.3) due to the reverse of reaction 6.11. Thus, dimedone thioethers should be explored as tools for the study of nitroxyl biochemistry.

8.0 References

1. Leone, A. M., Palmer, R. M., Knowles, R. G., Francis, P. L., Ashton, D. S., and Moncada, S. (1991) *J Biol Chem 266*, 23790-5.
2. Williams, D. L. (2003) *Org Biomol Chem 1*, 441-9.
3. Snyder, S. H. (1992) *Science 257*, 494-6.
4. Sampath, V., Zhao, X. J., and Caughey, W. S. (1994) *Biochem Biophys Res Commun 198*, 281-7.
5. Rang, H. P., Dale, M. M., Ritter, J. M. and Gardner, P. (1995) in *Pharmacology*, Churchill livingstone Inc., New York.
6. Kerwin, J. F., Jr., Lancaster, J. R., Jr., and Feldman, P. L. (1995) *J Med Chem 38*, 4343-62.
7. Kelm, M. (1999) *Biochim Biophys Acta 1411*, 273-89.
8. Stamler, J. S., Jaraki, O., Osborne, J., Simon, D. I., Keaney, J., Vita, J., Singel, D., Valeri, C. R., and Loscalzo, J. (1992) *Proc Natl Acad Sci U S A 89*, 7674-7.
9. Girard, P., and Potier, P. (1993) *FEBS Lett 320*, 7-8.
10. Rassaf, T., Kleinbongard, P., Preik, M., Dejam, A., Gharini, P., Lauer, T., Erckenbrecht, J., Duschin, A., Schulz, R., Heusch, G., Feelisch, M., and Kelm, M. (2002) *Circ Res 91*, 470-7.
11. Myers, P. R., Minor, R. L., Jr., Guerra, R., Jr., Bates, J. N., and Harrison, D. G. (1990) *Nature 345*, 161-3.
12. Arnelle, D. R., and Stamler, J. S. (1995) *Arch Biochem Biophys 318*, 279-85.
13. Bauer, J. A., and Fung, H. L. (1991) *J Pharmacol Exp Ther 256*, 249-54.

14. Stamler, J. S., Simon, D. I., Osborne, J. A., Mullins, M. E., Jaraki, O., Michel, T., Singel, D. J., and Loscalzo, J. (1992) *Proc Natl Acad Sci U S A 89*, 444-8.

15. Gaston, B., Reilly, J., Drazen, J. M., Fackler, J., Ramdev, P., Arnelle, D., Mullins, M. E., Sugarbaker, D. J., Chee, C., Singel, D. J., Loscalzom J. and Stamlerm J. S. (1993) *Proc Natl Acad Sci U S A 90*, 10957-61.

16. Jourd'heuil, D., Jourd'heuil, F. L., and Feelisch, M. (2003) *J Biol Chem 278*, 15720-6.

17. Wink, D. A., Nims, R. W., Darbyshire, J. F., Christodoulou, D., Hanbauer, I., Cox, G. W., Laval, F., Laval, J., Cook, J. A., Krishna, M. C., and et al. (1994) *Chem Res Toxicol 7*, 519-25.

18. Pryor, W. A., Church, D. F., Govindan, C. K., and Crank, G. (1982) *J Org Chem 47*, 159-161.

19. Stubauer, G., Giuffre, A., and Sarti, P. (1999) *J Biol Chem 274*, 28128-33.

20. Gow, A. J., Buerk, D. G., and Ischiropoulos, H. (1997) *J Biol Chem 272*, 2841-5.

21. Kharitonov, V. G., Sundquist, A. R., and Sharma, V. S. (1995) *J Biol Chem 270*, 28158-64.

22. Wade, R. S., and Castro, C. E. (1990) *Chem Res Toxicol 3*, 289-91.

23. Boese, M., Mordvintcev, P. I., Vanin, A. F., Busse, R., and Mulsch, A. (1995) *J Biol Chem 270*, 29244-9.

24. Hogg, N. (1999) *Anal Biochem 272*, 257-62.

25. Hogg, N. (2002) *Annu Rev Pharmacol Toxicol 42*, 585-600.

26. Houk, K. N., Hietbrink, B. N., Bartberger, M. D., McCarren, P. R., Choi, B. Y., Voyksner, R. D., Stamler, J. S., and Toone, E. J. (2003) *J Am Chem Soc 125*, 6972-6.

27. Romeo, A. A., Capobianco, J. A., and English, A. M. (2002) *J Biol Chem 277*, 24135-24141.

28. Martinez-Ruiz, A., and Lamas, S. (2004) *Cardiovasc Res 62*, 43-52.

29. Wong, P. S., Hyun, J., Fukuto, J. M., Shirota, F. N., DeMaster, E. G., Shoeman, D. W., and Nagasawa, H. T. (1998) *Biochemistry 37*, 5362-71.

30. Klatt, P., Pineda Molina, E., Lacoba, M. G., Padilla, C. A., Martinez Galisteo, E., Barcena, J. A., and Lamas, S. (1999) *FASEB J 13*, 1481-1490.

31. Klatt, P., and Lamas, S. (2000) *Eur J Biochem 267*, 4928-44.

32. Hemmingsen, C. (2000) *Pharmacol Toxicol 87 Suppl 3*, 5-30.

33. Christakos, S., Gabrielides, C., and Rhoten, W. B. (1989) *Endocr Rev 10*, 3-26.

34. Akerfeldt, K. S., Coyne, A. N., and Wilk, R. R., Thulin, E., Linse, S. (1996) *Biochemistry 35*, 3662-3669.

35. Berggard, T., Szczepankiewicz, O., Thulin, E., and Linse, S. (2002) *J Biol Chem 277*, 41954-9.

36. Veenstra, T. D., Gross, M. D., Hunziker, W., and Kumar, R. (1995) *J Biol Chem 270*, 30353-8.

37. Pansini, A. R., and Christakos, S. (1984) *J Biol Chem 259*, 9735-41.

38. Parmentier, M., Lawson, D. E., and Vassart, G. (1987) *Eur J Biochem 170*, 207-15.

39. Miller, R. J. (1995) *Biochem Soc Trans 23*, 629-32.

40. Christakos, S., Gabrielides, C., and Rhoten, W. B. (1989) *Endocr Rev 10*, 3-26.

41. Alexianu, M. E., Ho, B. K., Mohamed, A. H., La Bella, V., Smith, R. G., and Appel, S. H. (1994) *Ann Neurol 36*, 846-58.

42. Seto-Ohshima, A., Emson, P. C., Lawson, E., Mountjoy, C. Q., and Carrasco, L. H. (1988) *Lancet 1*, 1252-5.

43. Guo, Q., Christakos, S., Robinson, N., and Mattson, M. P. (1998) *Proc Natl Acad Sci U S A 95*, 3227-32.

44. Lukas, W., and Jones, K. A. (1994) *Neuroscience 61*, 307-16.

45. Gross, M. D., Nelsestuen, G. L., and Kumar, R. (1987) *J Biol Chem 262*, 6539-45.

46. Winsky, L., and Kuznicki, J. (1995) *J Neurochem 65*, 381-8.

47. Berggard, T., Miron, S., Onnerfjord, P., Thulin, E., Akerfeldt, K. S., Enghild, J. J., Akke, M., and Linse, S. (2002) *J Biol Chem 277*, 16662-72.

48. Norman, A. W., and Leathers, V. (1982) *Biochem Biophys Res Commun 108*, 220-6.

49. Morgan, D. W., Welton, A. F., Heick, A. E., and Christakos, S. (1986) *Biochem Biophys Res Commun 138*, 547-53.

50. Bellido, T., Huening, M., Raval-Pandya, M., Manolagas, S. C., and Christakos, S. (2000) *J Biol Chem 275*, 26328-32.

51. Lutz, W., Frank, E. M., Craig, T. A., Thompson, R., Venters, R. A., Kojetin, D., Cavanagh, J., and Kumar, R. (2003) *Biochem Biophys Res Commun 303*, 1186-92.

52. Jaffrey, S. R., Erdjument-Bromage, H., Ferris, C. D., Tempst, P., and Snyder, S. H. (2001) *Nat Cell Biol 3*, 193-7.

53. Bruning, G. (1993) *J Neurosci Res 36*, 580-7.

54. Alonso, J. R., Sanchez, F., Arevalo, R., Carretero, J., Aijon, J., and Vazquez, R. (1992) *Neuroreport 3*, 249-52.

55. Willmott, N. J., Wong, K., and Strong, A. J. (2000) *FEBS Lett 487*, 239-47.

56. Lai, T. S., Hausladen, A., Slaughter, T. F., Eu, J. P., Stamler, J. S., and Greenberg, C. S. (2001) *Biochemistry 40*, 4904-10.

57. Fridovich, I. (1995) *Annu Rev Biochem 64*, 97-112.

58. Bounds, P. L., Sutter, B., and Koppenol, W. H. (2002) *Methods Enzymol 349*, 115-23.

59. Johnson, M. A., Macdonald, T. L., Mannick, J. B., Conaway, M. R., and Gaston, B. (2001) *J Biol Chem 276*, 39872-8.

60. Jourd'heuil, D., Laroux, F. S., Miles, A. M., Wink, D. A., and Grisham, M. B. (1999) *Arch Biochem Biophys 361*, 323-30.

61. Perutz, M. F. (1996) *Nature 380*, 205-6.

62. Klotz, L. O., and Sies, H. (2002) *Methods Enzymol 349*, 101-6.

63. Barnett, D. J., McAninly, J., and Williams, D. L. H. (1994) *J Chem Soc Perkin Trans 2*, 1131-1133.

64. Mohr, S., Hallak, H., Boitte, A., Lapetina, E. G., and Brune, B. (1999) *J Biol Chem 274*, 9427-9430.

65. Mathews, W. R., and Kerr, S. W. (1993) *J Pharmacol Exp Ther 267*, 1529-37.

66. Komiyama, T., and Fujimori, K. (1997) *Bioorg Medicinal Chem Lett 7*, 175-180.

67. Pietraforte, D., Mallozzi, C., Scorza, G., and Minetti, M. (1995) *Biochemistry 34*, 7177-85.

68. Wink, D. A., Darbyshire, J. F., Nims, R. W., Saavedra, J. E., and Ford, P. C. (1993) *Chem Res Toxicol 6*, 23-7.

69. Hogg, N., Singh, R. J., and Kalyanaraman, B. (1996) *FEBS Lett 382*, 223-8.

70. Buettner, G. R., Oberley, L. W., and Leuthauser, S. W. (1978) *Photochem Photobiol 28*, 693-5.

71. Pires, M., Rossi, M. J., and Ross, D. S. (1994) *International J Chem Kinetics 26*, 1207-1227.

72. Vanin, A. F., Malenkova, I. V., and Serezhenkov, V. A. (1997) *Nitric Oxide 1*, 191-203.

73. Koppenol, W. H. (1998) *Free Radic Biol Med 25*, 385-91.

74. Mohney, B. K., and Walker, G. C. (1997) *J Am Chem Soc 119*, 9311-9312.

75. DeMaster, E. G., Quast, B. J., Redfern, B., and Nagasawa, H. T. (1995) *Biochemistry 34*, 11494-9.

76. Ford, P. C., Wink, D. A., and Stanbury, D. M. (1993) *FEBS Lett 326*, 1-3.

77. Wink, D. A., Grisham, M. B., Mitchell, J. B., and Ford, P. C. (1996) *Methods Enzymol 268*, 12-31.

78. Gratzel, M., Taniguchi, S., and Henglein, A. (1970) *Ber Bunserges Phys Chem 74*, 488-492.

79. Keshive, M., Singh, S., Wishnok, J. S., Tannenbaum, S. R., and Deen, W. M. (1996) *Chem Res Toxicol 9*, 988-93.

80. Goldstein, S., and Czapski, G. (1995) *J. Am. Chem. Soc. 118*, 3419-3425.

81. Lewis, R. L., Tannenbaum, S. R., and Deen, W. M. (1995) *J Am Chem Soc 117*, 3933-3939.

82. Ford, E., Hughes, M. N., and Wardman, P. (2002) *Free Radic Biol Med 32*, 1314-23.

83. Gratzel, M., Henglein, A., Lilie, J., and Beck, G. (1969) *Ber Bunserges Phys Chem 73*, 646-653.

84. Mezyk, S. P. (1996) *J. Phys. Chem. 100*, 8861-8866.

85. Wardman, P., and von Sonntag, C. (1995) *Methods Enzymol 251*, 31-45.

86. Swaddle, T. W. (1990) *Applied Inorganic Chemistry*, University of Calgary Press, Calgary.

87. Cavallini, D., De Marco, C., Dupre, S., and Rotilio, G. (1969) *Arch Biochem Biophys 130*, 354-61.

88. Tanaka, N., Kolthoff, I. M., and Stricks, W. (1955) *J Am Chem Soc 77*, 1996-2004.

89. Liochev, S. I., and Fridovich, I. (2001) *J Biol Chem 276*, 35253-7.

90. Liochev, S. I., and Fridovich, I. (2002) *Arch Biochem Biophys 402*, 166-71.

91. Budavari, S., and O'Neil, M. J. (2001) *The Merck Index*, 13th ed., Merck, Whitehouse Station, N.J.

92. Huie, R. E., and Padmaja, S. (1993) *Free Radic Res Commun 18*, 195-9.

93. Williams, D. L. H. (1999) *Acc. Chem. Res. 32*, 869-876.

94. QIAexpressionist. (June 2003) *A handbook for high-level expression and purification of 6xHis-tagged proteins*, 5th Edition.

95. Karginov, A. V., Karginova, O. A., Spiridonova, V. A., and Kopylov, A. M. (1995) *FEBS Lett 369*, 158-60.

96. Steipe, B., Pluckthun, A., and Huber, R. (1992) *J Mol Biol 225*, 739-53.

97. Janknecht, R., de Martynoff, G., Lou, J., Hipskind, R. A., Nordheim, A., and Stunnenberg, H. G. (1991) *Proc Natl Acad Sci U S A 88*, 8972-6.

98. http://www-structure.llnl.gov/internal/his/histag.htm.

99. Kumar, R., Hunziker, W., Gross, M., Naylor, S., Londowski, J. M., and Schaefer, J. (1994) *Arch Biochem Biophys 308*, 311-7.

100. Venters, R. A., Benson, L. M., Craig, T. A., Paul, K. H., Kordys, D. R., Thompson, R., Naylor, S., Kumar, R., and Cavanagh, J. (2003) *Anal Biochem 317*, 59-66.

101. Thulin, E., and Linse, S. (1999) *Protein Expr Purif 15*, 265-70.

102. Rintoul, G. L., Raymond, L. A., and Baimbridge, K. G. (2001) *Cell Calcium 29*, 277-87.

103. Steffensen, B., Wallon, U. M., and Overall, C. M. (1995) *J Biol Chem 270*, 11555-66.

104. (1998) *Catalogue of Amersham Pharmacia Biotech.*

105. Fritz, G., Heizmann, C. W., and Kroneck, P. M. (1998) *Biochim Biophys Acta 1448*, 264-76.

106. (2001) *Factor Xa kits*, Novagen.

107. Berggard, T., Thulin, E., Akerfeldt, K. S., and Linse, S. (2000) *Protein Sci 9*, 2094-108.

108. Sambrook, J., and Russell, D. W. (2001) *Molecular Cloning*, Vol. 1, 3. ed., Cold Spring Harbor Laboratory Press, Cold Spring Harbor, N.Y.

109. Sambrook, J., and Russell, D. W. (2001) *Molecular Cloning*, Vol. 3, 3. ed., Cold Spring Harbor Laboratory Press, Cold Spring Harbor, N.Y.

110. http://www.stratagene.com/manuals/200132.pdf. 3.

111. Meier, T. J., Ho, D. Y., and Sapolsky, R. M. (1997) *J Neurochem 69*, 1039-47.

112. Stamler, J. S., Toone, E. J., Lipton, S. A., and Sucher, N. J. (1997) *Neuron 18*, 691-6.

113. Lee, S. J., Beckingham, K., and Stull, J. T. (2001) *Biochem Biophys Res Commun 284*, 526-30.

114. Berggard, T., Silow, M., Thulin, E., and Linse, S. (2000) *Biochemistry 39*, 6864-73.

115. Ferranti, P., Mamone, G., and Malorni, A. (2000) *Methods Mol Biol 146*, 147-65.

116. Riddles, P. W., Blakeley, R. L., and Zerner, B. (1983) *Methods Enzymol 91*, 49-60.

117. Saville, B. (1958) *Analyst 83*, 670-672.

118. Campbell, I. D., and Dwek, R. A. (1984) *Biological Spectroscopy*, Benjamin Cummings, Menlo Park, CA.

119. Haas, E., Katchalski-Katzir, E., and Steinberg, I. Z. (1978) *Biochemistry 17*, 5064-70.

120. Stryer, L. (1978) *Annu Rev Biochem 47*, 819-46.

121. Teale, F. W. J., and Weber, G. (1957) *Biochem J 65*, 476-480.

122. Faulstich, H., Tews, P., and Heintz, D. (1993) *Anal Biochem 208*, 357-62.

123. Xian, M., Chen, X., Liu, Z., Wang, K., and Wang, P. G. (2000) *J Biol Chem 275*, 20467-73.

124. Calhoun, D. B., Vanderkooi, J. M., and Englander, S. W. (1983) *Biochemistry 22*, 1533-9.

125. Mirza, U. A., Chait, B. T., and Lander, H. M. (1995) *J Biol Chem 270*, 17185-8.

126. Linse, S., Thulin, E., and Sellers, P. (1993) *Protein Sci 2*, 985-1000.

127. Meyer, D. J., Kramer, H., Ozer, N., Coles, B., and Ketterer, B. (1994) *FEBS Lett 345*, 177-80.

128. Percival, M. D., Ouellet, M., Campagnolo, C., Claveau, D., and Li, C. (1999) *Biochemistry 38*, 13574-83.

129. Xian, M., Wang, Q. M., Chen, X., Wang, K., and Wang, P. G. (2000) *Bioorg Med Chem Lett 10*, 2097-100.

130. Zhang, Y. Y., Xu, A. M., Nomen, M., Walsh, M., Keaney, J. F., Jr., and Loscalzo, J. (1996) *J Biol Chem 271*, 14271-9.

131. Nedospasov, A., Rafikov, R., Beda, N., and Nudler, E. (2000) *Proc Natl Acad Sci U S A 97*, 13543-8.

132. Ramachandran, N., Jacob, S., Zielinski, B., Curatola, G., Mazzanti, L., and Mutus, B. (1999) *Biochim Biophys Acta 1430*, 149-54.

133. Sun, J., Xin, C., Eu, J. P., Stamler, J. S., and Meissner, G. (2001) *Proc Natl Acad Sci U S A 98*, 11158-62.

134. Rockett, K. A., Awburn, M. M., Cowden, W. B., and Clark, I. A. (1991) *Infect Immun 59*, 3280-3.

135. Ignarro, L. J., Lippton, H., Edwards, J. C., Baricos, W. H., Hyman, A. L., Kadowitz, P. J., and Gruetter, C. A. (1981) *J Pharmacol Exp Ther 218*, 739-49.

136. Simon, D. I., Mullins, M. E., Jia, L., Gaston, B., Singel, D. J., and Stamler, J. S. (1996) *Proc Natl Acad Sci U S A 93*, 4736-41.

137. Stamler, J. S., Simon, D. I., Jaraki, O., Osborne, J. A., Francis, S., Mullins, M., Singel, D., and Loscalzo, J. (1992) *Proc Natl Acad Sci U S A 89*, 8087-91.

138. Mohr, S., Stamler, J. S., and Brune, B. (1994) *FEBS Lett 348*, 223-7.

139. Caselli, A., Camici, G., Manao, G., Moneti, G., Pazzagli, L., Cappugi, G., and Ramponi, G. (1994) *J Biol Chem 269*, 24878-82.

140. Oae, S., and Shinhama, K. (1983) *Org Prep Proced Int 15*, 165-198.

141. Park, J. W. (1988) *Biochem Biophys Res Commun 152*, 916-20.

142. Romeo, A. A., Filosa, A., Capobianco, J. A., and English, A. M. (2001) *J Am Chem Soc 123*, 1782-3.

143. Rae, T. D., Schmidt, P. J., Pufahl, R. A., Culotta, V. C., and O'Halloran, T. V. (1999) *Science 284*, 805-8.

144. Tao, L., Murphy, M. E., and English, A. M. (2002) *Biochemistry 41*, 6185-92.

145. Padgett, C. M., and Whorton, A. R. (1998) *Arch Biochem Biophys 358*, 232-42.

146. Lyons, T. J., Liu, H., Goto, J. J., Nersissian, A., Roe, J. A., Graden, J. A., Cafe, C., Ellerby, L. M., Bredesen, D. E., Gralla, E. B., and Valentine, J. S. (1996) *Proc Natl Acad Sci U S A 93*, 12240-4.

147. Noble, D. R., and Williams, D. L. (2000) *Nitric Oxide 4*, 392-8.

148. Williams, D. L. H. (1996) *Chem Commun*, 1085-1091.

149. Herold, S., Exner, M., and Nauser, T. (2001) *Biochemistry 40*, 3385-95.

150. Torchinsky, Y. M. (1981) *Sulphur in Proteins*, Pergamon Press, Oxford.

151. Winterbourn, C. C., Peskin, A. V., and Parsons-Mair, H. N. (2002) *J Biol Chem 277*, 1906-11.

152. Verge, K. M., and Agnes, G. R. (2002) *J Am Soc Mass Spectrom 13*, 901-905.

153. Rossi, R., Milzani, A., Dalle-Donne, I., Giannerini, F., Giustarini, D., Lusini, L., Colombo, R., and Di Simplicio, P. (2001) *J Biol Chem 276*, 7004-10.

154. Di Simplicio, P., Lusini, L., Giannerini, F., Giustarini, D., Bellelli, A., Boumis, G., Amiconi, G., and and Rossi, R. (1998) *in Nitric Oxide and the Cell: Proliferation and Death (Moncada, S., Nistico, G., Bagetta, G., and Higgs, E.A, ds.)*, pp. 47-59, Portland Press Ltd., London.

155. He, X. M., and Carter, D. C. (1992) *Nature 358*, 209-15.

156. Li, J., Huang, F. L., and Huang, K. P. (2001) *J Biol Chem 276*, 3098-105.

157. Oberholtzer, J. C., Buettger, C., Summers, M. C., and Matschinsky, F. M. (1988) *Proc Natl Acad Sci U S A 85*, 3387-90.

158. Muller A., Muller W., and Dietrich D. (2002) *7th European Symposium on Calcium Binding Proteins in Normal and Transformed Cells*, 266-267.

159. Gardner, M. J., Hall, N., Fung, E., White, O., Berriman, M., Hyman, R. W., Carlton, J. M., Pain, A., Nelson, K. E., Bowman, S., Paulsen, I. T., James, K., Eisen, J. A., Rutherford, K., Salzberg, S. L., , Craig, A., Kyes, S., Chan, M. -S., Nene, V., Shallom, S. J., , Suh, B., Peterson, J., Angiuoli, S., , and Pertea, M., Allen, J., Selengut, J., Haft, D., Mather, M. W., Vaidya, A. B., Martin, D. M. A., Fairlamb, A. H., Fraunholz, M. J., Roos, D. S., Ralph, S. A., McFadden, G. I., Cummings, L. M., Subramanian, G. M., Mungall, C., Venter, J. C., Carucci, D. J., Hoffman, S. L., Newbold, C., Davis, R. W., Fraser, C. M. and Barrell, B. (2002) *Nature 419*, 498-511.

160. Thomas, J. A., Poland, B., and Honzatko, R. (1995) *Arch Biochem Biophys 319*, 1-9.

161. Ward, N. E., Stewart, J. R., Ioannides, C. G., and O'Brian, C. A. (2000) *Biochemistry 39*, 10319-29.

162. Chai, Y. C., Hendrich, S., and Thomas, J. A. (1994) *Arch Biochem Biophys 310*, 264-72.

163. Gilbert, H. F. (1990) *Adv Enzymol Relat Areas Mol Biol 63*, 69-172.

164. Park, E. M., and Thomas, J. A. (1988) *Biochim Biophys Acta 964*, 151-60.

165. Ji, Y., Akerboom, T. P., Sies, H., and Thomas, J. A. (1999) *Arch Biochem Biophys 362*, 67-78.

166. Chandra, A., Srivastava, S., Petrash, J. M., Bhatnagar, A., and Srivastava, S. K. (1997) *Biochemistry 36*, 15801-15809.

167. Zech, B., Wilm, M., Eldik, R. V., and Brune, B. (1999) *J Biol chem 274*, 20931-20936.

168. Schinina, M. E., Carlini, P., Polticelli, F., Zappacosta, F., Bossa, F., and Calabrese, L. (1996) *Eur J Biochem 237*, 433-9.

169. Marklund, S. L., Andersen, P. M., Forsgren, L., Nilsson, P., Ohlsson, P. I., Wikander, G., and Oberg, A. (1997) *J Neurochem 69*, 675-81.

170. Nakanishi, T., Kishikawa, M., Miyazaki, A., Shimizu, A., Ogawa, Y., Sakoda, S., Ohi, T., and Shoji, H. (1998) *J Neurosci Methods 81*, 41-4.

171. Schuppe-Koistinen, I., Moldeus, P., Bergmann, T., and Cotgreave, I. A. (1994) *Eur J Biochem 221*, 1033-1037.

172. Eaton, P., Byers, H. L., Leeds, N., Ward, M. A., and Shattock, M. J. (2002) *J Biol Chem 277*, 9806-9811.

173. Carballal, S., Radi, R., Kirk, M. C., Barnes, S., Freeman, B. A., and Alvarez, B. (2003) *Biochemistry 42*, 9906-14.

174. Halliwell, B. (1988) *Biochem Pharmacol 37*, 569-71.

175. Halliwell, B., and Gutteridge, J. M. (1990) *Arch Biochem Biophys 280*, 1-8.

176. Chen, Y. H., He, R. Q., Liu, Y., Liu, Y., and Xue, Z. G. (2000) *Biochem J 351*, 233-240.

177. Kurahashi, T., Miyazaki, A., Suwan, S., and Isobe, M. (2001) *J Am Chem Soc 123*, 9268-78.

178. Singh, R. J., Hogg, N., Joseph, J., and Kalyanaraman, B. (1996) *J Biol Chem 271*, 18596-603.

179. McLafferty, F. W., Turecek, F., and Choi, J. (1996) *Interpretation of Mass Spectra, 4th ed. University Science Books*.

180. Antonini, E., and Brunori, M. (1971) *Hemoglobin and Myoglobin in Their Reactions with Ligands*, North-Holland Pub. Co., Amsterdam,.

181. Djinovic, K., Gatti, G., Coda, A., Antolini, L., Pelosi, G., Desideri, A., Falconi, M., Marmocchi, F., Rotilio, G., and Bolognesi, M. (1992) *J Mol Biol 225*, 791-809.

182. Tainer, J. A., Getzoff, E. D., Beem, K. M., Richardson, J. S., and Richardson, D. C. (1982) *J Mol Biol 160*, 181-217.

183. Parge, H. E., Hallewell, R. A., and Tainer, J. A. (1992) *Proc Natl Acad Sci U S A 89*, 6109-13.

184. Briggs, R. G., and Fee, J. A. (1978) *Biochim Biophys Acta 537*, 100-9.

185. Calabrese, L., Federici, G., Bannister, W. H., Bannister, J. V., Rotilio, G., and Finazzi-Agro, A. (1975) *Eur J Biochem 56*, 305-309.

186. Ravichandran, V., Seres, T., Moriguchi, T., Thomas, J. A., and Johnston, R. B. (1994) *J Biol Chem 269*, 25010-25015.

187. Klatt, P., Pineda Molina, E., Perez-Sala, D., and Lamas, S. (2000) *Biochem J 349*, 567-78.

188. Applequist, S. E., Keyna, U., Calvin, M. R., Beck-Engeser, G. B., Raman, C., and Jack, H. M. (1995) *Gene 163*, 325-326.

189. Rivera-Nieves, J., Thompson, W. C., Levine, R. L., and Moss, J. (1999) *J Biol Chem 274*, 19525-19531.

190. Hirayama, K., Akashi, S., Furuya, M., and Fukuhara, K. (1990) *Biochem Biophys Res Commun 173*, 639-46.

191. Schuppe-Koistinen, I., Gerdes, R., Moldeus, P., and Cotgreave, I. A. (1994) *Arch Biochem Biophys 315*, 226-34.

192. Huang, K. P., and Huang, F. L. (2002) *Biochem Pharmacol 64*, 1049-1056.

193. Butler, A. R., and Williams, D. L. H. (1993) *Chem Soc Rev 22*, 233-241.

194. Allison, W. S. (1976) *Acc Chem Res 9*, 293-299.

195. Davis, F. A., Jenkins, L. A., and Billmers, R. L. (1986) *J Org Chem 51*, 1033-1040.

196. Davis, F. A., Jenkins, R. H. Jr., Rizvi, S. Q. A., and Yocklovich, S. G. (1981) *J Org Chem 46*.

197. Benitez, L. V., and Allison, W. S. (1974) *J Biol Chem 249*, 6234-43.

198. Reddy, S., Jones, A. D., Cross, C. E., Wong, P. S., and van der Vliet, A. (2000) *Biochem J 347*, 821-827.

199. Cappiello, M., Voltarelli, M., Cecconi, I., Vilardo, P. G., Dal Monte, M., Marini, I., Del Corso, A., Wilson, D. K., Quiocho, F. A., Petrash, J. M., and Mura, U. (1996) *J Biol Chem 271*, 33539-33544.

200. Jabusch, J. R. (1980) *Biochemistry 19*, 2310-2316.

201. Kajihara, J. (1988) *J Biochem 104*, 638-642.

202. Liu, H., Zhu, H., Eggers, D. K., Nersissian, A. M., Faull, K. F., Goto, J. J., Ai, J., Sanders-Loehr, J., Gralla, E. B., and Valentine, J. S. (2000) *Biochemistry 39*, 8125-32.

203. Yamazaki, Y., Takao, T., Murata, H., Kawaharada, Y., Sugiyama, T., and Shimonishi, Y. (1997) *Res Commun Biochem Cell Mol Biol 1*, 205-217.

204. Deng, H. X. (1993) *Science 261*, 1047-1051.

205. Ishii, T., Sunami, O., Nakajima, H., Nishio, H., Takeuchi, T., and Hata, F. (1999) *Biochem Pharmacol 58*, 133-143.

206. MacQuarrie, R. A., and Bernhard, S. A. (1971) *Biochemistry 10*, 2456-2466.

207. Parker, D. J., and Allison, W. S. (1969) *J Biol Chem 244*, 180-189.

208. Birkett, D. J. (1973) *Mol Pharmacol 9*, 209-218.

209. Marley, R., Patel, R. P., Orie, N., Ceaser, E., Darley-Usmar, V., and Moore, K. (2001) *Free Radic Biol Med 31*, 688-96.

210. Tanner, J. J., Hecht, R. M., and Krause, K. L. (1996) *Biochemistry 35*, 2597-2609.

211. Didierjean, C., Rahuel-Clermont, S., Vitoux, B., Dideberg, O., Branlant, G., and Aubry, A. (1997) *J Mol Biol 268*, 739-759.

212. Finley, J. W., Wheeler, E. L., and Witt, S. C. (1981) *J Agric Food Chem 29*, 404-407.

213. Roy, J., Minotti, S., Dong, L., Figlewicz, D. A., and Durham, H. D. (1998) *J Neurosci 18*, 9673-84.

214. Wilson, E. K. (March 8, 2004) *Chemical and Engineering News 82*, pp 39-44.